Dissertation

submitted to the
Combined Faculties
for the Natural Sciences and for Mathematics
of the Ruperto-Carola University of Heidelberg, Germany
for the degree of

Doctor of Natural Sciences

presented by

Katharina Beuke, Master of Science

born in Böblingen

Oral examination on April 29, 2016

TNF-induced

NF-κB Signal Transduction

in the Liver

Referees: Prof. Dr. Ursula Kummer
Prof. Dr. Thomas Höfer

"Il n’y a rien á craindre de la vie. Il y a tout á comprendre."

Nothing in life is to be feared, it is only to be understood.

Marie Curie

Summary

Gut-derived bacteria enter the liver via the portal vein where they induce an innate immune response leading to inflammation. Lipopolysaccharide, a part the baterial cell wall component endotoxin, functions as stimulus for toll-like receptors in non-parenchymal liver cells leading to secretion of diverse cytokines. Among these cytokines tumor necrosis factor (TNF) is one of the first to be produced. It binds to the TNF receptors of hepatocytes and activates NF-κB signalling. The transcription factor NF-κB enhances gene expressions of acute phase proteins. Its signalling primes hepatocytes for cell proliferation.

In this work, I have studied NF-κB signalling in hepatocytes in various ways, using computational models trained and validated with experimental data from primary murine cells. First, I extended an ODE model of canonical NF-κB signalling to include the experimentally validated influence of p38 MAPK signalling on this signalling pathway. Additionally, by including the receptor level to the model, I ensured an accurate description of dose response measurements for the main pathway components. This was especially important for the second part of this work, where I used the ODE intra-hepatocellular model to investigate the influence of different non-parenchymal cells on hepatocytes in the liver. By combining information on cell abundance and cell size, and experimental TNF secretion profiles in response to LPS with this ODE model, I was able to establish for the first time a computational model combing all liver cell types relevant to LPS-induced TNF secretion and intra-hepatocellular NF-κB signalling. I could show that liver resident macrophages and liver sinusoidal endothelial cells produce the most TNF in response to LPS. Furthermore, my simulations showed that not the final levels of TNF regulate the *in vivo* response, rather the initial cytokine increase defines how strongly NF-κB signalling is activated in hepatocytes. As a third part I converted the ODE model into a PDE model, which describes possible temporal and spatial aspects of single cell microscopy measurements. I was able to show that the relevant reaction parameters of the ODE model could be used for PDE simulations to describe experimental data on the localisation of fluorescently labeled NF-κB molecules after TNF stimulation. Furthermore, I could show that the dynamics observed on a population-based level were comparable to those observable on a single cell level.

These new insights into NF-κB signalling in the liver may change experimental procedures with respect to cytokine administration when analysing inflammation. Furthermore, the new multi-cellular model can serve as a basis for simulating the influence of non-parenchymal cells on hepatocytes under various experimental conditions.

Zusammenfassung

Darmstämmige Bakterien gelangen über die Vena partae hepatis (Leberpfortader) in die Leber. Dort aktiverien sie die unspezifische Immunantwort, welche zu Entzündungsprozessen führt. Lipopolysaccharide, Teile des Bakterienzellwandbestandteils Endotoxin, sind Stimuli für Toll-Like-Rezeptoren von nicht-parenchymalen Zellen und führen zur Sekretion von diversen Zytokinen. Unter diesen Zytokinen ist Tumornekrosefaktor (TNF) eines der ersten, welches produziert wird. Es bindet an TNF-Rezepotren von Hepatozyten und aktiviert die NF-κB-Signaltransduktion. Der Transkriptionsfaktor NF-κB aktiviert die Genexpression von Akutphaseproteinen, seine Signaltransduktion bereitet Hepatozyten auf die Zellproliferation vor.
In dieser Arbeit habe ich die NF-κB Signaltransduktion, unter Zuhilfenahme von computergestützen Modellen, die mit experimentellen Daten trainiert und validiert wurden, auf verschieden Arten studiert. Zuerst habe ich ein differentialgleichungsbasiertes Modell des kanonischen NF-κB-Signalweges erweitert, so dass es den experimentell validierten Einfluss der p38-MAPK-Signaltransduktion beinhaltet. Zusätzlich habe ich eine exakte Beschreibung von dosisabhängigen Messungen der Hauptbestandteile der NF-κB Signaltransduktion gewährleistet, in dem ich die Rezeptorebene mit eingebaut habe. Dies war besonders wichtig, da ich das ODE-Modell verwendet habe, um den Einfluss der nicht-parenchymalen Zellen auf Hepatozyten in der Leber zu analysieren. Indem ich Zellverteilungen und Zellgrößen mit TNF-Sekretionsprofilen als Antwort auf LPS-Stimulierung der nicht-parenchymalen Zellen und dieses ODE-Modell kombiniert habe, konnte ich zum ersten Mal ein computergestütztes Modell aller Zelltypen der Leber, die für die LPS induzierte TNF-Sekretion und die intrahepatozelluläre NF-κB-Signaltransduktion relevant sind, erstellen. Ich konnte zeigen, dass leberspezifische Makrophagen und Lebersinusiodalendothelzellen am meisten TNF als Antwort auf LPS produzieren. Darüber hinaus haben meine Simulationen gezeigt, dass nicht die finalen TNF-Konzentrationen, sondern der initiale TNF-Ansteig bestimmt, wie stark die Hepatozytenantwort ausfällt. Als dritten Teil dieser Arbeit habe ich das ODE-Modell zu einem partiellen-Differentailgleichungs- (PDE) Modell erweitert, das zeitliche und räumliche Aspekte der Mikroskopieeinzelzellmessungen beschreibt. Ich konnte zeigen, dass die relevanten Reaktionsparameter des ODE-Modells auch in PDE–Simulationen experimentelle Daten zur Lokalisation von fluoreszenzmarkiertem NF-κB gut beschreiben. Desweiteren konnte ich zeigen, dass die Dynamiken, die auf Populationsebene beschrieben wurden, mit denen auf Einzellebene vergleichbar waren. Diese neuen Einsichten zur NF-κB-Signaltransduktion in der Leber zeigen, dass die experimentellen Protokolle zur Zytokinadmistration bei der Untersuchung von Entzündungsprozessen überdacht werden sollten. Außerdem kann das neue multizelluläre Modell als Grundlage für Simulationen des Einflusses der nicht-parenchymal Zellen auf Hepatozyten unter diversen epxerimentellen Bedingungen genutzt werden.

Contents

1 Introduction

The liver is subject to many gut-derived bacteria and plays an important role as a front-line immunological organ in the innate and adaptive immune response [1]. On the microscopic scale, as one of the first events TNF-induced NF-κB signalling orchestrates the early innate immune response during bacterial infection-induced inflammation [2]. During my PhD I have chosen different systems biology approaches to study this signalling pathway in hepatocytes, the main liver cells, and how other liver cell types induce it during inflammation.
In the following introduction some biological and mathematical/computational background knowledge will be given. I will present the histological setup of the liver and the role of the different liver cells with emphasis on the innate immune response, the canonical NF-κB pathway and its main players, along with the JNK/p38/MAPK, IL-6/JAK/STAT and Hippo/YAP pathway. On the mathematical/computational side I will present the basics of describing biochemical reaction networks as compartmentalized, kinetic ODE models and as biochemical reaction-diffusion PDE models.

1.1 The Liver

The main functions of the liver in mammalians are: regulation of blood sugar, detoxification, and bile production. The hormones, insulin, adrenalin, and glucagon regulate the hepatic sugar uptake and release. Insulin produced by α cells in pancreatic islets induces glucose uptake by hepatocytes. There it is stored as glycogen and adrenalin or glucagon can trigger glycogen breakdown and release. During detoxification hepatocytes take up many drugs or metabolites which are insoluble in water. By bio-transformation or conjugation with hydroxyl groups these molecules are then made water-soluble [3].
Additionally, the liver is an important organ of the immune system. Its special micro-architecture facilitates its significant role in clearance of gut-derived bacteria delivered through the portal vein [1]. The main liver cells making up 60% of liver mass are hepatocytes (Table 1). These parenchymal cells form single cell thick plates with sinusoids on either side. The three major non-parenchymal cells in the liver are: liver resident macrophages or Kupffer cells (MCs) in the sinusoids, liver sinusoidal endothelial cells (LSECs) separating the sinuoids and the hepatocytic plates, and hepatic stellate cells (HSCs) in the space of Disse between the LSECs and hepatocytes (Figure 1.1). Each cell type produces cytokines and chemokines in response to cytokines and chemokines produced by the other cells which form a unique environment that at the same time ensures the correct differentiation of liver cells. For example, MCs are retained in the liver by cytokines and chemokines from LSECs. The cytokines and chemokines from MCs are necessary for LSECs to correctly from their fenestrae clusters, so called sieves, without a basal membrane, allowing most blood components except for larger cells to diffuse into the space of Disse [4].

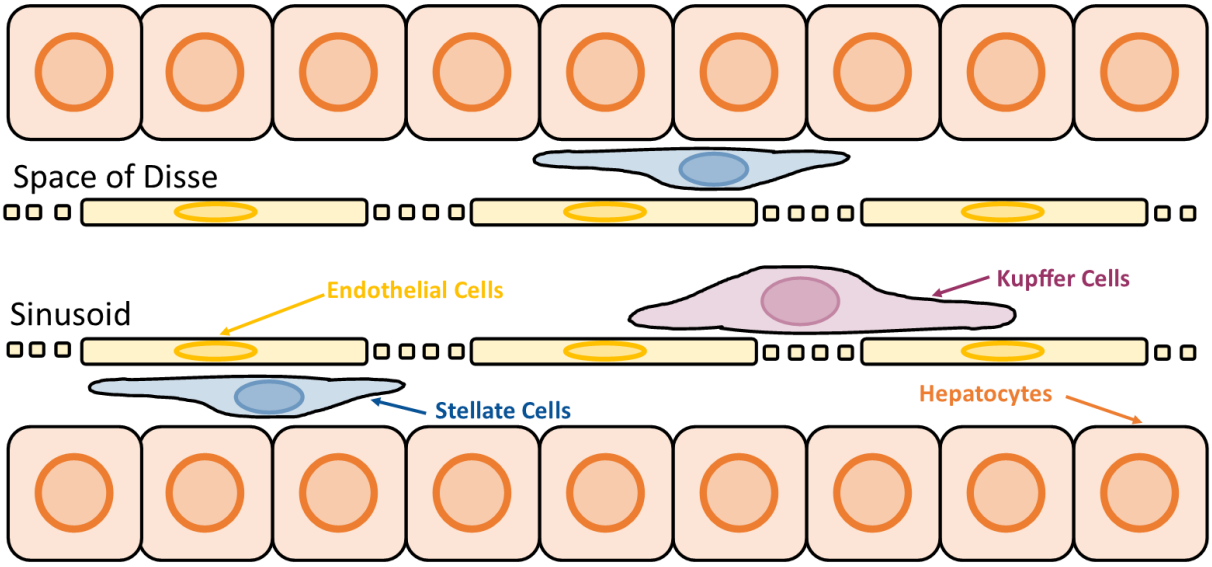

Figure 1.1: Graphical depiction of the liver micro anatomy showing the location of the different cell types in the liver.

Table 1: In 1977 Blouin *et al.* experimentally analysed the liver micro-anatomy with electron microscopy and determined the relative distributions of liver cells per liver volume and total liver cells [5]. (LSEC: liver sinusoidal endothelial cells, MC: liver resident macrophages, HSC hepatic stellate cells)

	Hepato-cytes	LSEC	MC	HSC	Space of Disse	Sinusoidal Lumen
% of total volume	77.8	2.8	2.1	1.4	4.9	10.6
% of total liver cells	60	19	15	5-8	–	–

1.1.1 Hepatocytes

Hepatocytes are the main liver cells with respect to both abundance and mass (Table 1). They fulfill all the main tasks of the liver. They are vital to regulating the blood sugar level, by taking up sugar from the blood, storing it as glycogen, and releasing it when needed. Furthermore, they produce bile fluid, and are vital to copper and iron metabolism, as well as detoxification. During inflammation they may play a role in pathogen clearance via endocytosis pathogen toxins [6, 7]. Hepatocytes express TLR4 receptors, which can be bound by LPS, however, they do not directly response with NF-κB signalling to LPS [8]. They produce many cytokines and chemokines and are responsive towards cytokines from non-parenchymal cells [9, 1].

1.1.2 Stellate Cells

Hepatic stellate cells (Ito cells or fat-storing cells, HSCs) are astral cells which reside outside of the sinusoidal lumen in the space of Disse. They form long projections reaching around hepatocytes. In the absence of liver damage or inflammation they are in a quiescent state, where their known functions are vitamin A and lipid storage. During inflammation or liver damage they proliferate and differentiate into myofibroblasts. They are the main producers of collagen in the liver and thus are strongly involved in liver cirrhosis [10].

1.1.3 Liver Resident Macrophages

Liver Resident Macrophages (Kupffer cells, MCs) are bone marrow derived macrophages which enter the liver via the portal vein. In contrast to other macrophages, which are non-resident and circulate through the body, MCs are trained to be resident by cytokines expressed by LSECs. They patrol the sinusoid and together with HSCs they can slow its blood flow, by essentially blocking the sinusoid. During inflammation their main function is phagocytosis of gut derived pathogens and initiation of both innate an adaptive immune responses, via cytokines and as anti-body presenting cells [11].

1.1.4 Sinusoidal Endothelial Cells

Liver Sinusoidal Endothelial Cells (LSECs) form the endothelial border between the sinusoid and hepatocytes. They do not form a basal membrane yet still contain large fenestrae clustered together in sieves which is a unique endothelial form found no where else in the body. Thus there is a small space between the LSECs and hepatocytes called space of Disse. The LSEC control the molecules entering the space of Disse through their fenestrae. Molecules of up to 120 nm can pass through the fenestrea and at the same

time molecules as small as 12 nm can hindered of passing. LSEC are antibody presenting cells and can phagocyte diverse pathogens [12, 13, 14].

1.2 The Canonical NF-κB Signalling Pathway

Signal transduction via NF-κB is the integration point for various cues and signals regarding cell fate. It plays an important role during infection, tissue regeneration after injuries, autoimmune diseases, and cancer [9, 15]. In these cases cellular decision making is a tremendously important event, as coming back from necrosis or apoptosis is essentially impossible for a cell. Similarly, proliferation requires resources and needs to be tightly controlled to avoid cancer. NF-κB activation alone cannot trigger any of the processes mentioned above. But its role in all of them is unique and usually it is one of the first steps in a tightly regulated set of steps leading up to them [16].

1.2.1 The Signalosome

The name NF-κB signalling comprises many individual pathways [15]. They can be activated by many different stimuli, such as viral RNA, DNA damage, components of the bacterial cell wall, cytokines, or chemokines [17]. These stimuli each act through different molecules and lead to different cell responses. The feature they have in common, is the activation of a NF-κB dimer by repressing a NF-κB inhibitor (IκB). The canonical NF-κB signalling can be activated by interleukin 1 alpha or beta (IL-1α or IL-1β) via IL-1R, TNF via TNFR1, and lipopolysaccharide (LPS) via TLR4 [15]. All four stimuli act through IκB kinase (IKK)β phosphorylating IκBα, whose subsequent ubiquination targets it for degradation. The NF-κB hetero dimer p50:p65 is freed and can than act as transcription factors in the nucleus. This work focuses on the TNF-induced canonical pathway, which has been studied in some detail and the exact steps in the signalling cascade are described below [].

TNF is a cytokine secreted by many cells. In its trimeric soluble form it can bind to TNF receptor (TNFR) 1 and induce the recruitment of several scaffolding proteins. First, TNFR-associated death domain protein (TRADD) binds to the death domain of the TNFR1 [18]. TRADD then recruits receptor-interacting serine/threonine-protein kinase (RIPK) 1 and together they recruit the scaffolding protein TNF receptor associated factor (TRAF) 2 [19, 20]. TRAF2 can than bind cellular inhibitor of apoptosis protein (cIAP) 1 and cIAP2 (also know as BRIC1 and BRIC2) which can ubiquinate RIPK1. Together these proteins form the so called complex I. (As apposed to the complex II consisting of Fas-associated death domain protein (FADD) and caspase 8, which induces cell death signalling.) RIPK1 is required for IKK activation, however, most probably as a scaffolding protein, as NF-κB signalling is intact in kinase deficient RIPK1 mutants [21]. RIPK1 facilitates TGFβ-activated kinase (TAK) 1 recruitment. TAK1 is bound to TAK1 associated binding protein (TAB) 2 and TAB3 in the TAK1 complex. Most probably RIPK1 recruits the IKK complex through NF-κB essential modifier (Nemo or IKKγ) together with TAK1 acting

through TAB2. Thus the RIPK1-induced close proximatey of TAK1 and IKK complexes leads to auto-trans-phosphorylation of TAK1 and IKK complexes and thus activation of the IKK complex [22]. IKKβ can then phosphorylate IκBα [23].

1.2.2 NF-κBs and IκBs

First discovered in 1986 [24], the nuclear factor κ light-chain-enhancer of B cells (NF-κB) family consists of five members p65 (or RelA), RelB, C-Rel, p50 (or in its uncleaved form p105), and p52 (or in its uncleaved form p100). All members contain the N-terminal Rel homology domain with which they can bind κB-sites in DNA and form homo- and heterodimers. RelB is the only NF-κB protein which cannot form homodimers. p65, RelB and C-Rel additionally contain a transcription activation domain with which they can bind to p300, CBP, histone deacteylases (HDACs), and other transcription factors to recruit the RNA-Polymerase II complex [25, 26].
Without stimulation a large property of the NF-κB is bound by inhibitors (IκBs). Just as there are several NF-κBs, there are several IκB family members: IκBα, IκBβ, IκBγ, IκBδ (IκBNS), IκBϵ, IκBζ, BCL-3, and the NF-κB precursor forms p100 (NF-κB1, precursor of p52) and p105 (NF-κB2, precursor of p50). They all contain ankyrin repeat domains and bind NF-κB dimers [22].
The canonical pathway describes mainly the NF-κB heterodimer p52:p65 bound to IκBα and how it is then freed. However, IκBϵ is among the genes which are activated by p65 and can help turn-off NF-κB signalling [27].

1.2.3 Inhibitors and Activators

The NF-κB pathway has many regulators and crosstalks to other pathways. Here, I would like to focus on A20 (or TNFAIP3) and phosphorylation of RelA. A20 is a (de-)ubiquitinase. It's role in NF-κB signalling is discussed vigorously in literature [28]. It functions mainly upstream of the IKK complex and inhibits its activation. In the TNF induced cannoncial pathway A20 most likely by ubiquitinating RIP1, thus inhibiting the interactions of RIP1 with TAK and IKK complexes. Furthermore, A20 is a target gene of NF-κB and its expression is induced by the canonical pathway, thus introducing an additional negative feed-back to the NF-κB pathway [28].
During TNF induced signalling the activated TAK complex also leads to phosphorylation and thus activation of JNK and p38 (or MAPK14) [9]. These kinases are involved in other pathways and allow crosstalk activated e.g. by other cytokines [29]. Additionally, p38 can enter the nucleus and activate the nuclear mitogen and stress activated kinase 1 (MSK1) [30]. MSK1 is a kinase for Ser276 of p65 [31, 32]. Phosphorylation of p65 at this site enhances its ability to induce chromatin remodeling by increasing its ability to recruit histone deacetylases (HDACs). p65 phosphorylation can in general increase its effectiveness as transcription factor. Other kinases which

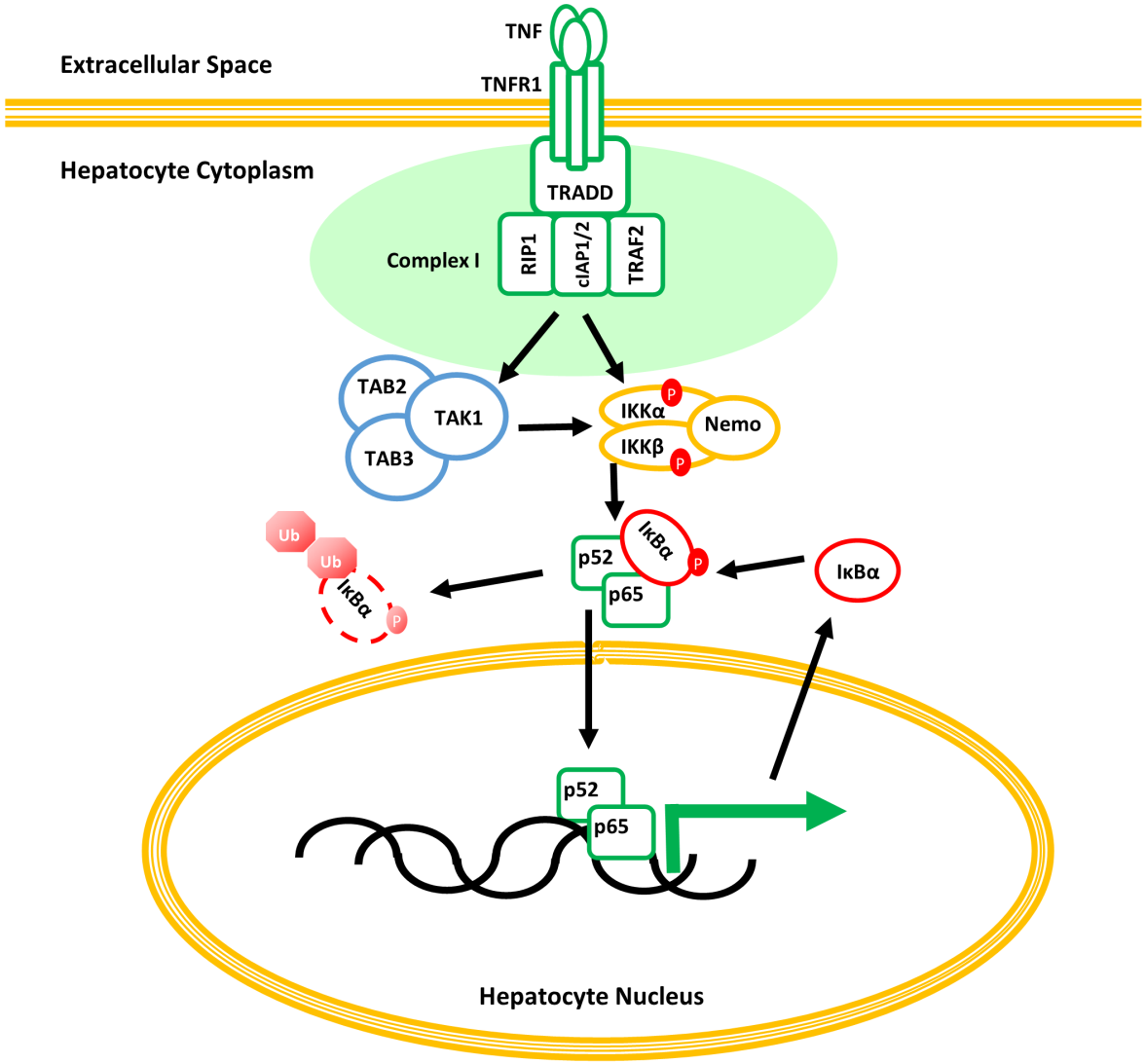

Figure 1.2: Graphical depiction of the signalosome assembling at the TNFR1 upon TNF binding and activation of the canonical NF-κB signalling.

can enhance p65's transcriptinal potential upon TNF stimulation are protein kinase C ζ (PKCζ) (Ser311) and casein kinase 2 (CK2) (Ser529) [33, 34, 35].

1.2.4 Possible Crosstalk with IL-6-induced STAT3 Signalling

NF-κB and STAT3 have been found to form protein complexes, if cells are co-stimulated with IL-6 and IL-1 [36]. IL-6 acts through two glycoproteins 130 (gp130) and IL-6 receptors which form a complex upon IL-6 binding. Janus kinases 1 (Jak1) associated to gp130 are thereby activated and phosphorylate gp130. Signal transducer and activator of transcription 1 and 3 (STAT1 and STAT3) can bind to the phosphorylated gp130 and are phosphorylated by Jak1. The phosphorylated STATs form homo- or heterodimers, which enter the nucleus and act as transcription factors. Among the target genes of STAT3 is suppresor of cytokine signalnig 3 (SOCS3), which inhibits STAT3 binding to gp130 [37]. IL-1-activated NF-κB can form a complex with STAT3 in the nucleus and may increase STAT3-induced gene expression [38].

1.2.5 Possible Crosstalk with Hippo/YAP Signalling

Hippo-YAP signalling is highly relevant to organ size control and thus may be linked to cell proliferation by NF-κB signalling. Yes-associated protein (YAP) over-expression in the liver leads to uncontrolled cell-division, which eventually leads to liver cancer. Mammalian STE20-like protein kinase 1/2 (MST1/2) can form a complex with its regulatory protein salvador homolog 1 or 45 kDa WW domain protein (Sav1) and phosphorylate. This activated complex can then phosphorylate large tumor suppressor homolog 1/2 LATS1/2 and Mps one binder kinase activator-like 1A/B (MOB1A/B). LATS1/2 then phosphorylates YAP and Transcriptional coactivator with PDZ-binding motif or Tafazzin (TAZ). In their phosphorylated form YAP and TAZ can no longer enter the nucleus and thus cannot bind to transcription factors such TEA domain family members 1-4 (TEAD1-4) and smad family protein 1-4 (SMAD1-4). Additionally, the phosphorylation of YAP/TAZ by LATS1/2 targets them for proteosomal degradation. The upstream receptors of the Hippo-YAP signalling in mammalina remain unclear. It is known that Merlin or neurofibromatosis type 2 (NF2) activates MST1/2 and thus YAP/TAZ phosphorylation, thereby interrupting the YAP/TAY interaction with TEAD family members [39, 40].

1.3 Mathematical Models in Biology

To analyze biochemical reaction networks different mathematical modeling techniques have been deployed. Here, I will present ODE based model and PDE models in general. The I give an overview of models developed to describe NF-κB signalling.

1.3.1 ODE Models

Ordinary differential equations (ODEs) are often used to describe population based dynamics in the field of biology such dynamics can be observed in experiments such as western immuno-blots to detect concentrations changes. Often the ODEs describe how species change over time. For modeling with ODEs to be a valid approach two aspects need to be considered. ODE models describe how species concentrations change with respect to one variable. In biology this variable is mostly time. Other variables such as space are not considered. Therefore, when applying ODEs in biology, we are assuming that diffusion happens on a much faster time scale than the biochemical reactions described by the model system and that thus the species are distributed homogeneously in the compartments modeled. Otherwise one would need to consider several variables and chose a PDE model system. The second aspect is that all biochemical reactions are ruled by Brownian motion of molecules and as such are random or stochastic processes. Thus the species concentrations should be relatively high and the population should behave as the averaged behavior of a stochastic simulated model.
The experimental techniques applied to measure intra-cellular protein and mRNA changes in hepatocytes applied in this work (western immuno-blot, ELISA, LUMINEX, and RT-qPCR) all measure the average population-based concentration changes. Thus, the ODE-model chosen is a valid representation.
The ODEs used to describe a species behavior depend on the biochemical reactions producing and degrading the species, and their rate laws. The reaction rate laws (e.g. constant flux, mass action, Michaelis-Menten, or Hill-kinetics) define the dynamics of reaction fluxes. If we consider the following simple reaction system:

$$\emptyset \rightarrow A \tag{1}$$
$$A \rightarrow B \tag{2}$$
$$B \rightarrow \emptyset \tag{3}$$

where reaction 1 follows the kinetics of a constant influx, reaction 2 is ezymatically catalyzed by a third species C, following Michaelis-Menten-kinetics and reaction 3 follows mass action kinetics, we can then describe the differential equations or the overall reaction fluxes for A and B:

$$\frac{dA}{dt} = +k_{influx} - \frac{k_{cat} * C * B}{K_M + B}$$
$$\frac{dB}{dt} = +\frac{k_{cat} * C * B}{K_M + B} - k_{deg}B.$$

These ODEs together with given initial conditions for model systems can be approximated and simulated by numerical integration with ODE solvers such as the LSODA [41]. LSODA can solve stiff ODEs and is implemented for the COPASI task time series. The sum of all degradation and production reactions fluxes of a species is called a species reaction flux.

1.3.2 PDE Models

As described above, in temporally dynamic ODE models of biochemical reactions used to describe the population-level experiments in this work the reaction fluxes (v) defined by reaction rate laws and species concentrations determine how the species concentration (c) changes over time (t): $\frac{dc}{dt} = v$.
To extend a temporally dynamic ODE model into a spatio-temporal PDE model the diffusion flux (J) change with respect to space (x) needs to be considered as well.
$\frac{\partial c}{\partial t} = v + \frac{\partial J}{\partial x}$ considering one space variable x.
With Fick's 1st law of diffusion ($J = -D\frac{\partial c}{\partial x}$) this can be transformed into the reaction diffusion equation: $\frac{\partial c}{\partial t} = v - D\frac{\partial^2 c}{\partial x^2}$ .Similar as for the ODE simulations a PDE solver needs initial conditions (i.e. the species concentration at t=0). Additionally, boundary conditions need to be defined to solve PDEs. These define what happens to the species at the boundaries of the space we are looking at. Two popular types of boundary conditions are Neumann and Dirichlet. Neumann conditions define the flux of a specie at a boundary, whereas a Dirichlet condition defines the value of a species concentration at a boundary [42]. For the models used in this work a Neumann condition was applied, as the boundaries are cell membranes which the modeled species should not be able to cross.

1.3.3 Model Parameters

In biological models most parameters cannot be measured and must therefore, be estimated from experimental data describing how model variable or combinations of model variables so called observables change. However, due to experimental limitations not all variables can be observed and thus not all parameters can be estimated equally well from experimental data. Some parameters may be structurally non-identifiable, with the given data the parameters cannot be derived. In other cases the parameters may be practically non-identifiable, e.g. due experimental errors the parameters cannot be derived. In both cases the best solution would be acquire new experimental data [43]. However, often this is not possible. In this case there are two options: reduce the model until all parameters can be identified with the current experimental data or work with a model in which not all parameters are identified. In both cases it can be helpful to figure out which parameters are identifiable and which are not.
There are several methods to define parameter identifiability. For example parameter sensitivity analysis describes how small parameter pertubations influence model characteristics. It can employed to define which parameters modify the target function of the parameter estimation. However, the results apply only locally to the parameter space and describe the effect of changing one parameter at a time. Sampling the parameter space and defining parameter sensitivities for several parameter value combinations, so called global sensitivity analysis gives a more complete picture [44]. An other example is the profile-likelyhood method. Each parameter value is scanned and while the other parameters are re-estimated, to describe the

parameter landscape in dependence of this parameter [45]. However, both methods are very cost intense with respect to computational time.

1.3.4 NF-κB Models in Literature

NF-κB signalling is a well studied system. The first mathematical description in form of an ODE-model was published in 2000 [46]. This work described NF-κ IκB complex association and dissociation and nuclear shutteling of NF-κB, IκB and the complex. In 2002 a model including IKK and TNF as stimulus, and differentiating between the different IκB forms IκBα, IκBβ, and IκBϵ appeared [47], showing that NF-κB-induced IκBα transcription is necessary to observe oscillatory dynamics of free NF-κB and the other two isoforms most likely stablize damped oscillations. 2004 models describing the IKK regulation with three types of IKK and A20 as its inhibitor followed [48, 49]. It was also shown that on single cell levels not all cells show an oscillatory behaviour [50]. The amount of cells that do oscillate depends on the cell type, and the oscillations dynamics define gene expression profiles [49]. Due to these cell to cell variabilities on a single cell level stochastic models quickly followed [51, 52] Later models focused on how stimulus administrations alters gene expression, on the molecular details of certain regulations, and on the roles of the diverse IκBs [53, 54, 55]. Many model analyses have been used to determine key regulatory parameters, such as sensitivity analysis and bifurcation analysis [56, 57, 58, 59].
During my master thesis I established a hepatocyte specific NF-κB model that included protein turn-over of all major NF-κB pathway constituents. It trained exclusively to experimental data obtained from primary murine hepaotcytes. Additionally, this model also included 2 forms of post-translational modifications of NF-κB monomer p65 and experimental measurements of these, as far as antibodies were available. Despite, its well-known influence on the ability of NF-κB to promote gene induction, phosphorylation of p65 was not included in previous models [9]. The role of cross-talks on these post-translational modifications was also not investigated so far. To describe NF-κB signalling as accurate as possible, the model should also be able to describe dose-response data, especially, as *in vivo* concentrations may change and cover broader ranges. Furthermore, the role of the TNF receptor in detecting TNF has been described in a mathematical model for granulomas containing macrophages and lymphocytes [60]. However, it has not been analysed in hepatocytes and it has never been combined with detailed NF-κB intracellular signalling. Next, other pathways are known or assumed to influence NF-κB signalling, such as p38-induced MAPK signalling, IL-6-induced STAT3 signalling, or Hippo-YAP signalling.
There are some models describing spatio-temporal NF-κB signalling. In 2012 a model describing a spherical three dimensional cell in was published. This model was not based on PDEs but rather based on ODEs using approximately 62000 compartments between which species could "diffuse" to allow spatial effects [61]. PDE-based models were published in 2011 and 2014 [62, 63]. These models use the same diffusion coefficients for all proteins

or all mRNA, and the volumes used for cytoplasm and nucleus differ from hepatocyte volumes. Both parameters have been shown to have strong influence on the outcome of spatial-temporal simulations [64, 62].

2 Material and Methods

2.1 Experimental Data

Hepatocyte data was kindly provided by the group of Kai Breuhahn (Institute of Pathology, University Hospital of Heidelberg, Germany). Federico Pinna measured relative protein concentrations for total p65, phospho-p65, total IκBα, phospho-IκBα, total p38, phospho-p38, total MSK1, phospho-MSK1, total JNK1, and phospho-JNK1 via immuno-blotting, relative protein changes for phospho-IKKβ with ELISA, relative mRNA concentrations for IκBα and A20 via reverse transcription quantitative PCR, and microarray data for primary murine hepatocytes. Michaela Bissinger acquired images of florescently labeled RelA in single HLF cells. HLF cells are a hepato-cellular-carcinoma cell line and measured relative protein changes as described above HCC Hep56 and Hepa1-6.
Dose response TNF secretion profiles were measured via LUMINEX: by Frank Schildberg in Percy Knolle's laboratory (Institute of Molecular Immunology and Experimental Oncology, München Rechts der Isar, Technische Universität München, German) for liver resident endothelial cells, by Ute Albrecht in Johannes Bode's laboratory (Clinic for Gastroenterology, Heinrich-Heine-University of Düsseldorf, Germany) for Kupffer cells, and by Roman Liebe in Steven Dooeleys' laboratory (Molecular Hepatology, Department of Medicine II, Medical Faculty at Mannheim, Heidelberg University, Germany) for hepatic stellate cells.
All experimental data is listed in the Appendix Tables A.4 - A.17.

2.2 Data Processing

The experimental data was preprossed as described in the results section with the help of the software R [65]. Optimization of parameters in R was carried out using the R-built-in functions optimize and optim for single parameters and multiple parameters respectively. The default algorithm as used in this work for the optim method is Nelder-Mead. The optimize method uses a combination of golden section search and successive parabolic interpolation.

2.3 ODE Simulations

The software COPASI was used to modify and simulate the ODE-model, as well as estimate its parameters. For time course simulations a specially compiled version of COPASI was used, with the additional option of starting the time-course simulations from the results of steady-state simulations. For time-course simulations the implemented LSODA solver was used. For parameter estimations the implemented particle swarm algorithm, genetic algorithm SR and Levenberg-Marquardt algorithm were used. For steady

state simulations a combination of damped Newton method and forward and backward integration is used.[66]
All parameter simulations and parameter estimations were carried out with model ensembles of models with 30 parameter sets. The modifications of the models and scheduling of different tasks was carried out with Java language bindings for COPASI.

2.4 Automated Analysis of Protein-Protein-Interactions from STRING-DB

Protein-Protein Interactions for NF-κ and Hippo-YAP pathway components were extracted from the STRING database. Together with experimental data from microarrays, kindly provided by the group of Kai Breuhahn and statistically analyzed by the group of Fabian Theis (Institute of Computational Biology, Helmholtz Zentrum München, Germany), this information was analyzed with PHP-scripts written by Martin Zauser, a bachelor student in our lab, under my guidance.

2.5 PDE Simulations

For PDE simulations software calling on the DUNE Package [67, 68, 69] was used. The results were visualized and analyzed with the software PKV-Viewer, the images were exported and combined to videos. Frank Bergmann programmed an export of SBML files from COPASI to a graphical user interface program (Edit Spatial). In this program I defined diffusion coefficients, the size and shape of the compartments, the grid size on which the PDEs were simulated, and the time intervals between simulation outputs. If files describing the compartments spatial form were used, the grid size needed to match the file size (e.g. 64 x 64 gridding, 64 x 64 image-file). These files were in DMP-format. For later program versions an additional event file could be created, this contained information on which species to modify at a given time point, how to modify it, and whether to create output before the time point of the event. This program then automatically extended the ODE model into a PDE model. The time course simulations where then run with DUNE. For modifying the reaction parameters and the diffusion coefficients I later modified the file containing the model information itself (".conf-file").

2.6 Analysis of Single Cell Fluorescent Microscopy Images

The images provided by Michaela Bissinger were analysed with the help of CellProfiler [70]. Nuclei were detected and defined as primary objects. Cells were defined as secondary objects with then nuclei as the priming center to find cells. Cytoplasm was defined as a ternary object by subtraction of nuclei area from cell area. The red fluorescent intensity of all images was

measured. The resulting CSV tables were read into R and analyzed. For more details see the CellProfiler and R scripts on the supplementary DVD.

3 Results

To study NF-κB signalling I chose three levels of investigation. First, I concentrated on the intracellular hepatocyte response on a population based level. I investigated crosstalks with other pathways and extended an ODE-based model established during my master thesis to describe TNF-induced dose-response signalling in primary hepatocytes. As a second level, I looked at hepatocytes within the context of other liver cell types. Based on secretion data from non-parenchymal liver cells I simulated the different TNF profiles hepatocytes would see during inflammation *in vivo* and simulated the response in hepatocytes based on the intracellular NF-κB model. Third, I investigated individual hepatocytes; I converted the ODE-model into a PDE model and simulated the PDE model using the parameterisation for reaction kinetics from of the ODE model trained on population based experiments. The results were compared to microscopy images of single cells from hepatocellular carcinoma cell lines stably transfected with red fluorescent protein-tagged p65 (p65-RFP).
In order to enlarge and investigate the ODE model I needed to run several parameter estimations against a diverse set of experimental data. Therefore, this chapter begins with two sections describing data preprocessing to deal with experimental errors in semi-quantitative data and the reduction of the parameters to estimate during parameter estimation based on parameter identifiability information derived from the fisher information matrix.

3.1 Data Processing for Population Based Measurements

The data used for the ODE-based hepatocyte model was semi-quantitative western blot, ELISA or quantitative real time PCR data from primary murine hepatocytes. As no recombinant proteins were added to the western blot or ELISA samples and absolute quantification with PCR is difficult, theses samples quantitatively display the changes in concentrations over time. However, no information on the absolute concentrations is given.
In biology many researchers normalize this kind of data to the first time point (t_0) or the control. Often they even combine both in a single sample. This lays a strong emphasis on this first data point. If this first data point was also known to have the least error, this would be a valid approach. However, in the described experimental setups the error is distributed over all data points, therefore this may not be the best method.
In this work, the data error is assumed to be spread randomly and additive within one replicate or data series and to arise from pipetting and other sample treatments. Between the replica the error is assumed to be multiplicative, originating from e.g. different protein expression profiles within animals. Therefore, a multiplicative scaling factor is introduced for aligning the data series to one another.

An arbitrary biological replicate is chosen as base for normalization (x_0). All other data series (x_{1-n}) are multiplied with a scaling factor (k_{1-n}) which are

then optimized in such a way that the difference between all data series is minimized. The resulting target function (T.F.) reads as follows:

$$\begin{aligned} T.F. = &(x_0 - k_1 * x_1) + (x_0 - k_2 * x_2) + \cdots + (x_0 * k_n * x_n) \\ &+ (k_1 * x_1 - k_2 * x_2) + \cdots + (k_1 * x_1 - k_n * x_n) \\ &+ \ldots (k_{n-1} * x_{n-1} - k_n * x_n). \end{aligned} \tag{4}$$

The resulting scaled data series still show the same relative changes between the values from a single time series as before, however, the differences between the different time series is minimal. In figure 3.1 the data normalized to t_0 and with optimized scaling factors is shown exemplary for the Western immunoblot data measuring p-p65 concentration over time for 10 ng/ml TNF as stimulus.
The resulting data series still represent only the relative changes in concentration and contain no information on the absolute values. In the model, species are represented with absolute concentrations. Some absolute concentrations can be found in literature for some of the species in the model, for others an additional scaling factor (k_{model}) in the model is needed to map the scaled data series to species in the model:

$$X_{obs} = k_{model} * X_{sim}. \tag{5}$$

As the initial concentrations are assumed to be steady state values, which mainly depend on the reaction parameters of the model, the initial values can be calculated prior to time series simulations. Using the average initial value of all data replicates the scaling factor (k_{model}) can then also be calculated by adapting formula 5.
Therefore in the parameter estimations both the initial values of species and the parameters are changed, as the initial values are directly depend on the parameter values. The concentrations of TNF measured with LUMINEX from the non-parenchymal cells are absolute protein measurements. Therefore, they neither have a scaling factor in the model, nor are they normalized.

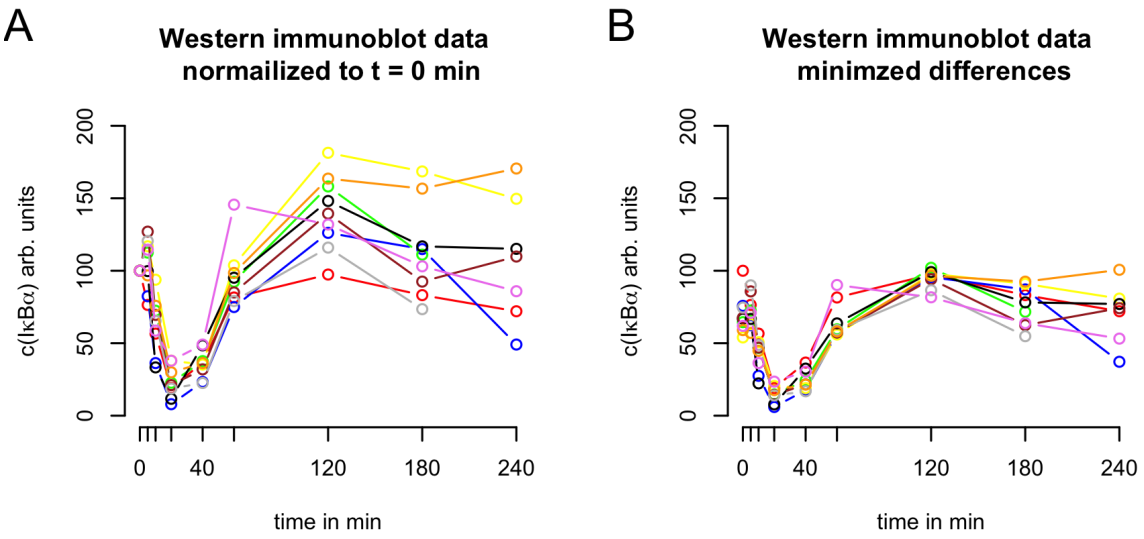

Figure 3.1: Plotted time series of Western immunoblots measurements of IκBα (A) normalized to the first time point, (B) normalized by minimizing the differences between replicates with a multiplicative scaling factor.

3.2 Using the FIM to Reduce the Dimensions of the Parameter Estimation

For enlarging the ODE-based NF-κB model many parameter estimations were necessary. As the ODE-models contained many parameters and reactions taking place on diverse time scales, parameter estimation was time intensive. Additionally, since I chose model ensembles to deal with parameter uncertainty, I needed several parameter sets, which required several runs of parameter estimations. Model ensembles are several parameter sets, for an identical model topology and reaction kinetics, which each describe the experimental data equally well [71, 72]l. If the model contains uncertainties, these parameter sets included parameters which spread over broad value ranges. Thus they should represent diverse possible parameterisations given the experimental data an the model topology. For validation, all parameter sets of the model ensembles should describe the validation data and for prediction, only observations which are true for all models are considered. In order to make running parameter estimations for model ensembles feasible, I looked for ways tor reduce the amount of parameters I needed to fit, without reducing the model itself, nor inhibiting the parameters from distributing widely along the parameter space. Therefore, I employed the the Fisher Information Matrix (FIM) or Fisher Information. FIM is a statistical method to measure the uncertainty of model parameters. In Computational Biology or Systems Biology it has rarely been applied. However, intermediate sized models such as those used and developed in this work contain many parameters which are difficult to identify. Different strategies have evolved to define these non-identifiabilities [45, 73, 74].
The method I developed in this work was aimed at reducing the computational cost of the parameter estimation for the ODE-based NF-κB hepatocyte model. The calculation of the FIM was already implemented in COPASI as part of the parameter estimation results. Therefore, no further computing was required to receive the FIM. The general idea of the approach was to reduce the parameter estimation problem by eliminating parameters which are practically non-identifiable, but using model ensembles allowing different parameter values for the other estimated parameters. Thus the computational cost of the parameter estimation was reduced, without losing the flexibility of an intermediate sized model containing parameters which are derived from typical biological specifications such as K_m or k_{cat} values for enzymatic reactions following Michaelis-Menten kinetics.
After an initial parameter estimation starting from random start values within biologically reasonable ranges for the model parameters and using a global optimization algorithm such as the Particle Swarm algorithm followed by a local optimization for example with the Levenberg-Marquardt algorithm to find parameter values, I employed the FIM to define parameters that have little to no influence on the models behavior and are thus ill defined or non-identifiable. The FIM describes the sensitivities of two parameters on the objective function. However, it is important to note that the FIM is dependent on the parameterization and a different parameter set for the model may have a different FIM. The FIM is an approximation of the Hessian of the

parameter estimation target function. Thus, it is an intrinsic characteristic of the model and its parameterization.
Eigenvalues of the FIM describe dimensions of the model with respect to the parameter estimation target function. Large eigenvalues describe well defined dimensions, small eigenvalues describe ill defined dimensions [73, 74]. The eigenvectors describe how the parameters contribute to the dimensions described by the corresponding eigenvalues. If a parameter is exclusively involved in ill defined dimensions, it is practically non-identifiable. If a parameter is involved in ill and well defined dimensions, it may be structurally non-identifiable, or taking part in a combination of structural and practical non-identifiablity. In the case of practical non-identifiability the parameter can be omitted from the parameter estimation, without further analysis. If there are structural non-identifiabilities in the model, it is necessary to have a closer look at the eigenvectors and the model structure. Parameters which are structurally non-identifiable, can compensate each other changes. The question is, how is this observable in the FIM? Unfortunately, it is not necessarily observable. However, in most cases by clustering the absolute values of the eigenvector entries, eigenvectors or parameters with similar participation in dimensions of the parameter landscape can be found. This is not a proof, but rather an indication for ill defined parameters and when combining it with knowledge about the model topology, these ill defined model parameters can be determined.
As a simple example, the TNF-induced JNK phosphorylation (as depicted in the NF-κB model in Figure 3.4) can be analyzed. Here, I fitted all parameters of the TNF degradation, the JNK phosphorylation, and dephosphorylation reactions (k(TNF degradation), k(JNK basal phosphorylation), k_{kat}(JNK phosphorylation), K_M(JNK phosphorylation), k(JNK dephosphorylation)). The total amount of JNK is assumed to be 1 μM. The data is normalized as described in section 3.1. The scaling factor for the initial state is determined by the absolute value of the mean of all data points at 0 min and the steady-state value of phospho-JNK. The experimental data shows, that phospho-JNK exists to a certain extent before the induction with TNF. It is assumed that this initial state corresponds to the steady state of the system. This initial state is thus defined by the ratio of basal phosphorylation and the de-phosphorylation of JNK. The initial increase in phospho-JNK after TNF administration depends mainly on the parameters of the active phosphorylation reaction. However, as the K_M value depends on the JNK concentration, this value is also somewhat correlated to the basal phosphorylation and degradation. The decrease in phospho-JNK then depends on JNK dephosphorylation and on the v_{max} of JNK phosphorylation, which is defined as the product of TNF and the k_{cat} value of the JNK phsophorylation. Thus all parameters are interlaced.

When looking at the FIM for various parameterizations of this model it becomes clear, that there are at least two very small and one small eigenvalues. Figure 3.2 shows the FIM eigenvalues and clustered eigenvectors. For the parameterization chosen here the K_M value of JNK phosphorylation is mainly involved in the very small eigenvalues, thus is practically non-identifiable and it can immediately be omitted from the parameter estima-

Eigenvalues	kcat_JNK_phosphorylation	k TNF_degradation	Km_active_phosphorylation	k_basal_phosphorylation	k_dephosphorylation
2.98E-009	0.015584	0.049985	0.998628	0.000461	0.001108
1.29E-004	0.477566	0.876914	0.051332	0.016933	0.005475
3.44E-002	0.022454	0.020529	0.000163	0.670148	0.741604
0.877913	0.876767	0.475443	0.01006	0.068205	0.021923
12.0668	0.049632	0.045332	0.002579	0.738893	0.670457

Figure 3.2: Matrix showing all eigenvalues and absolute values of the eigenvector entries after clustering. Entries with values higher than 0.001, 0.01, or 0.1 are colored in light, medium, and dark blue, respectively.

tion. The k_{kcat}(JNK phosphorylation) and the k(JNK basal phosphorylation) cluster together, as do the k(TNF degradation) and k(JNK dephosphorylation). The latter two are mainly involved in the larger eigenvalues, therefore these are left in the parameter estimation. The others are involved in all eigenvalues and are most likely combined in a form of practical and structural ill-identifiability. Here, it makes sense to chose one parameter to omit from further parameter estimations. To compare if the omitting the two parameters (K_M JNK phosphorylation, k_{kcat} JNK phosphorylation) simplifies the parameter estimation task, parameter estimations with Levenberg-Marqaurdt algorithm from random start values (parameter boarders indicated in Appendix) were repeated 200 times with all parameters and with only three parameters, after reducing the parameters estimated. When all parameters were tried to be estimated the global minimum was found only 148 times and the parameter estimations ran on average for 7457 s CPU time, whereas for the second case it was found for all 200 estimates and the parameter estimations ran on average for 290 s CPU time (Appendix Tables A.22, A.23).
The parameters estimated for the final intra-hepatocellular model were chosen with this approach. As described in the scheme 3.3 an initial guess of the parameters was obtained for all unknown parameters with the particle swarm algorithm starting from randomized values, followed by an optimization with the Levenberg-Marquardt algorithm to ensure a local minimum. Then for each parameter set of the model ensemble parameters were omitted based on their FIM entries, the FIM eigenvalues and eigenvectors. Subsequently parameter estimation was repeated, again first using the particle swarm algorithm then the Levenberg-Marquardt algorithm. The resulting parameters are listed in the Appendix Table A.20.

In summary, I was able to drastically reduce the cost of parameter estimation for the NF-κB model in hepatocytes by eliminating ill defined parameters from the parameter estimation I identified with the help of the FIM. At the same time I employed model ensembles that covered broad ranges of parameter space and only features all parameter sets of the model ensemble had in common were considered as model predictions.

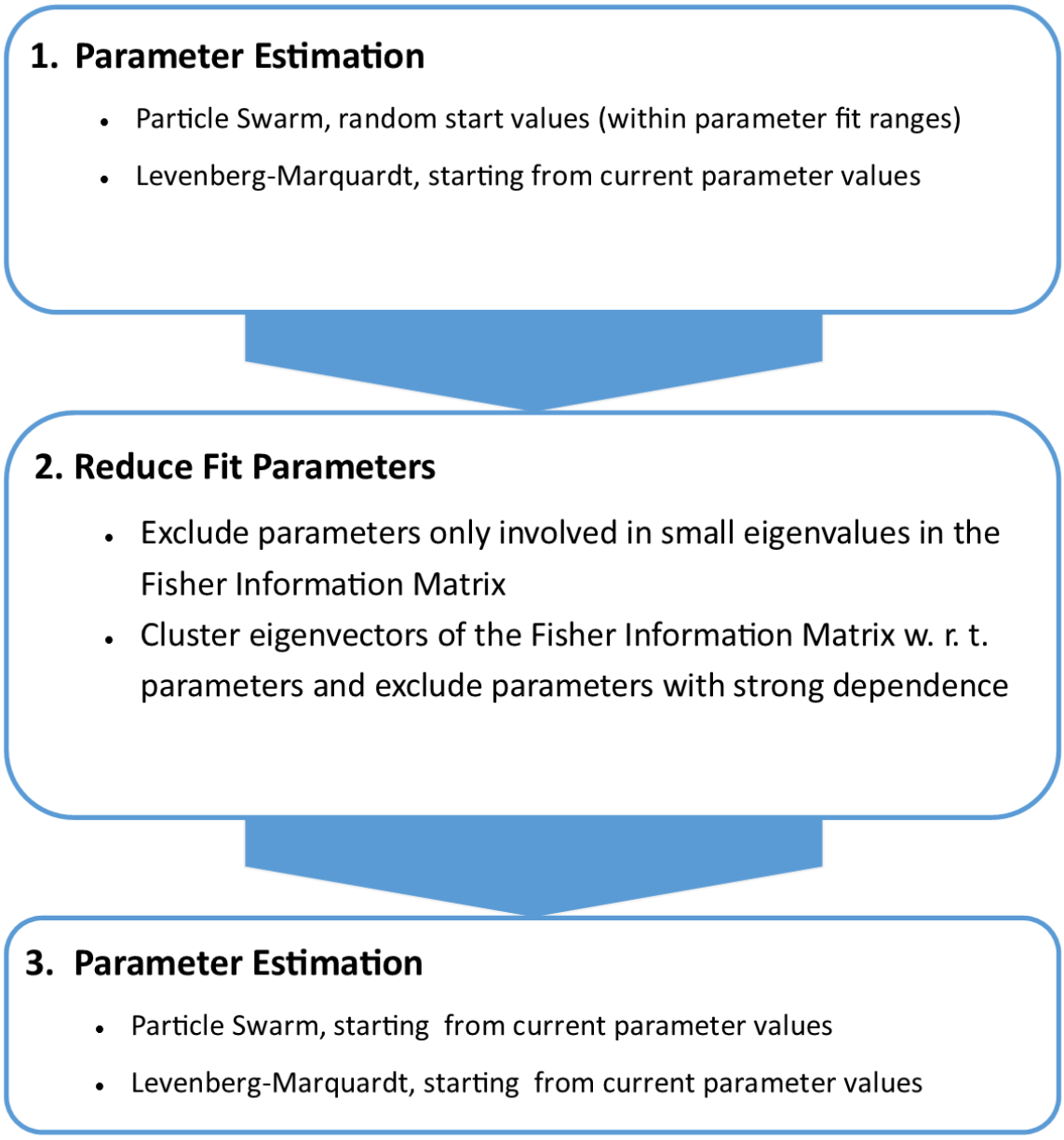

Figure 3.3: Scheme for employing the FIM to reduce fit parameters. In stead of Particle Swarm or Levenberg-Marquardt algorithms other global and local parameter estimation algorithms could be employed.

3.3 Analyzing and Enlarging the ODE-based NF-κB Model

In previous work during my master thesis I established an ODE-based NF-κB model, which described protein turnover for all model species in detail [59]. In the following sections the extension of that work is described and further analysed. Most of these results will be submitted to Hepatology.

3.3.1 Hippo-YAP

NF-κB signalling controls cell proliferation and apoptosis [23]. The Hippo-YAP pathway is import for organ size control and regulates the organ growth in dependence of cell-cell contacts [75]. The assumption that the two pathways are somehow correlated and share some sort of crosstalk is thus obvious. Trying to find a connection between TNF-induced NFκB signalling and Hippo-YAP signalling lead to a bioinformatics based approach.
Under my guidance Martin Zauser a Bachelor student created PHP scripts accessing STRING [76]. STRING is a database on protein-protein-interactions describing seven different categories of interactions (neighborhood, fusion, occurence, coexpression, experiments, database, and textminig). The results used in this work, were interactions found with experiments or in databases, as the other categories are not reliable indicators for protein interactions in eukaryotes. For the analysis I created two lists of genes encoding proteins involved in the signalling cascades (TNF/NF-κB pathway and Hippo/YAP pathway) derived from literature research. Martin then extracted the identifiers for these proteins from the PDB database [77], STRING database and Kegg database [78]. Next he searched for each of these genes in all entries for mus musculus and homo sapiens in STRING and within these entries he then searched for connections to the other pathway (e.g. for all entries for p65/RelA he searched for connections to genes of the Hippo/YAP pathway). If connections were found, they were verified with literature research. Additionally, the search was repeated for second level connections, connections where a protein from the NF-κB pathway interacted with a protein that also interacted with protein from the Hippo/YAP pathway. With this method CK2 was found as a possible link. CK2 can phosphorylate p65 and E-cadherin. E-cadherin in turn can lead to modulations of the subcellular localisation of YAP [79]. Additionally, it was found that Smad1 and YAP may form a complex and that TAK1 may phosphorylate Smad1.
Furthermore, microarray results from hepatocytes stimulated with TNF and from hepatocytes in which YAP was over-expressed where analyzed. First, Martin analyzed, if members of the according other pathway showed altered expression patterns in the microarrays. Next he analyzed, if among the genes up- or down-regulated in response to TNF any interacted with members of the Hippo-YAP pathway according to the STRING entries found and vice versa for genes induced by YAP over-expression and members of the TNF/NF-κB pathway.
The results from this study showed an up-regulation of IκBα, A20 and cIAP1/2 by Hippo/YAP signalling in the microarray. However this could not be vali-

dated experimentally. mRNA measurements with RT qPCR in the same cells showed no significant changes in the IκBα mRNA or A20 mRNA concentrations.
Modified expression of cIAP1/2 and interactions between YAP, Smad1 and TAK1 were not investigated further experimentally. Together with our collaborations, we decided that it was not very likely these connections would have an effect on canonical NF-κB signalling or Hippo/YAP signalling. As there were no further direct crosstalks found, I did not extend the NF-κB model with Hippo/YAP signalling. (Appendix Figure A.1 show the connections found.)

3.3.2 p38-MAPK

In my previous work on this project the hypothesis of p38 (MAPK14) signalling being induced by TNF and leading to further activation of a nuclear kinase which additionally phosphorylated p65 at serine 276 was formulated [59]. This hypothesis was verified with experimental data by Federico Pinna. There are several steps between TNF-induction and the phosphorylation of p38 and JNK1. For extending the model topology the simplest solution well describing the data was chosen, which was a direct activation of p38 and JNK phosphorylation by TNF or in later model version TNF bound to TNFR1. To describe the phosphorylation of p38 in the model an enzyme driven phosphorylation activated by TNF, a basal phosphorylation and a dephosphorylation reaction were added to topology published in 2012 [59], together with a phosphorylation of MSK1 catalyzed by p-p38 and dephosphorylation. A parameter estimation for the parameters of this new model part was executed without altering any of the other parameters in the 30 parameter sets. The parameter estimation for the p38/JNK/MSK1 branch resulted in a model ensemble which described the data published equally well as the original model and also described the new MAPK data well. See figure 3.4 for the new model topology and the new plots, the ODEs and parameters for the final model topology are summarized in the Appendix Tables **??** - A.18. All parameters of the p38/JNK/MSK1 module were identifiable except for the K_M values of the active phosphorylation reactions. The parameter algorithms tried to minimize these, which indicates that the active phosphorylation reactions were running at v_{max}. Subsequently the K_M were set to small values.

3.3.3 NF-κB Dose Response in Hepatocytes

Previous work was carried out for TNF concentrations of 10 ng/ml. However, the predictive power of the model is much higher, if it can also describe dose response data. *In vivo* hepatocytes are exposed to TNF over a broad range of concentrations and the systems fine tuned response to these different concentrations are important for an appropriate cellular response to different scenarios. Western Immunoblots of total IκBα, p-IκBα, total p65 and p-p65 for TNF doses of 0.1, 1.0, 10, 20, and 50 ng/ml were measured by Federico Pinna.

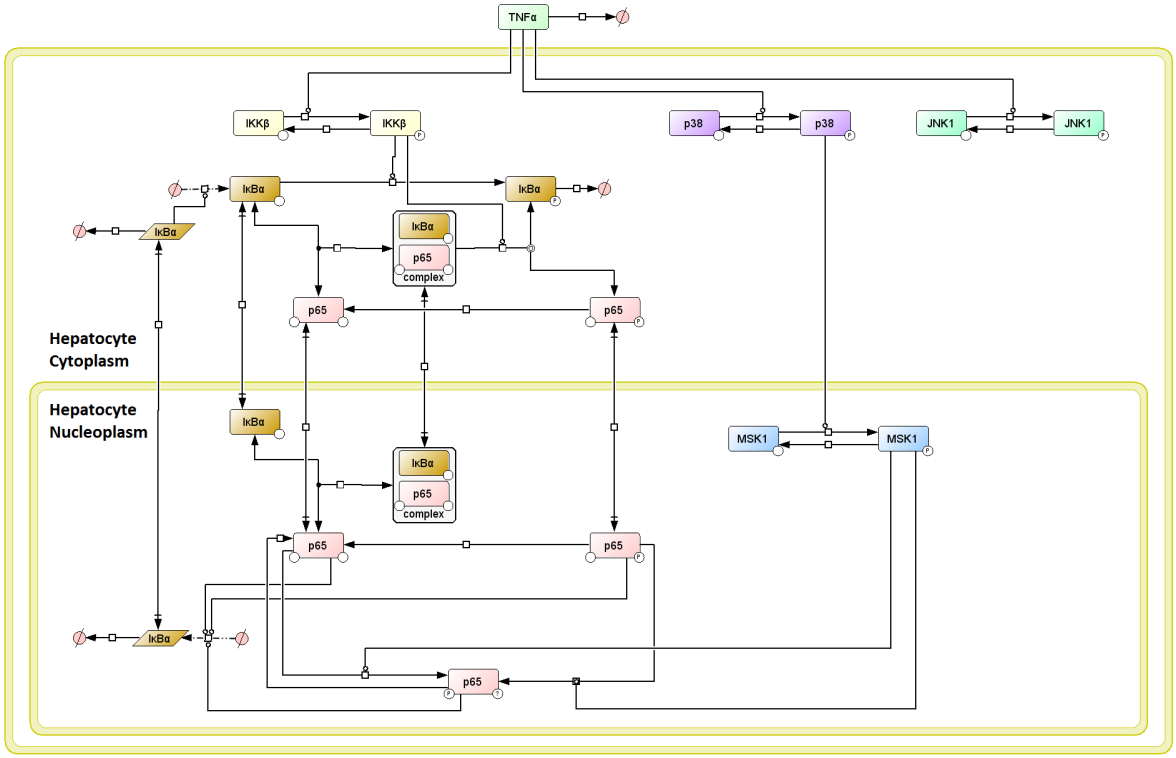

Figure 3.4: (A) Model topology including the new p38/JNK/MSK1 module. (B) Plots of model simulations (solid lines, n=30) and experimental data from the publication, as well as new measured p-p38, p-JNK, p-MSK1 experimental data (symbols, n=3) after estimating parameters for the p38/JNK/MSK1 model branch. Experimental data was measured by Federico Pinna, Appendix Table A.4.

As a first approach the model was not fitted to the data, but simply used to predict the time courses for the indicated TNF concentrations (see figure 3.5). The parameter sets do capture many features of the dose-response data. They show a saturation effect for high doses and that for low doses the amplitude height and width are changed.
However, the saturation is observed for lower concentrations in the experimental data than most model ensemble simulations predict and the experimental data show a stronger response to low data then the simulations of the model ensembles.

To improve the models description of the protein dose response data and the mRNA data for 10 ng/ml TNF several model versions were tested. First, a simple re-parameterization of the model was applied. Second, the active IKKβ phosphorylation reactions kinetic currently described as a simple enzyme catalyzed reaction was changed to a Hill-Kinetic. Third, an inhibition of the active IKKβ phosphorylation by an arbitrary molecule induced by TNF was included. Fourth, a combination of the Hill-kinetic and the inhibition of the active IKKβ were included. None of the above improved the results satisfactorily (data not shown). Finally, the TNF receptor 1 (TNFR1) was added to the model topology (see figure 3.6). TNFR1 synthesis and degradation were

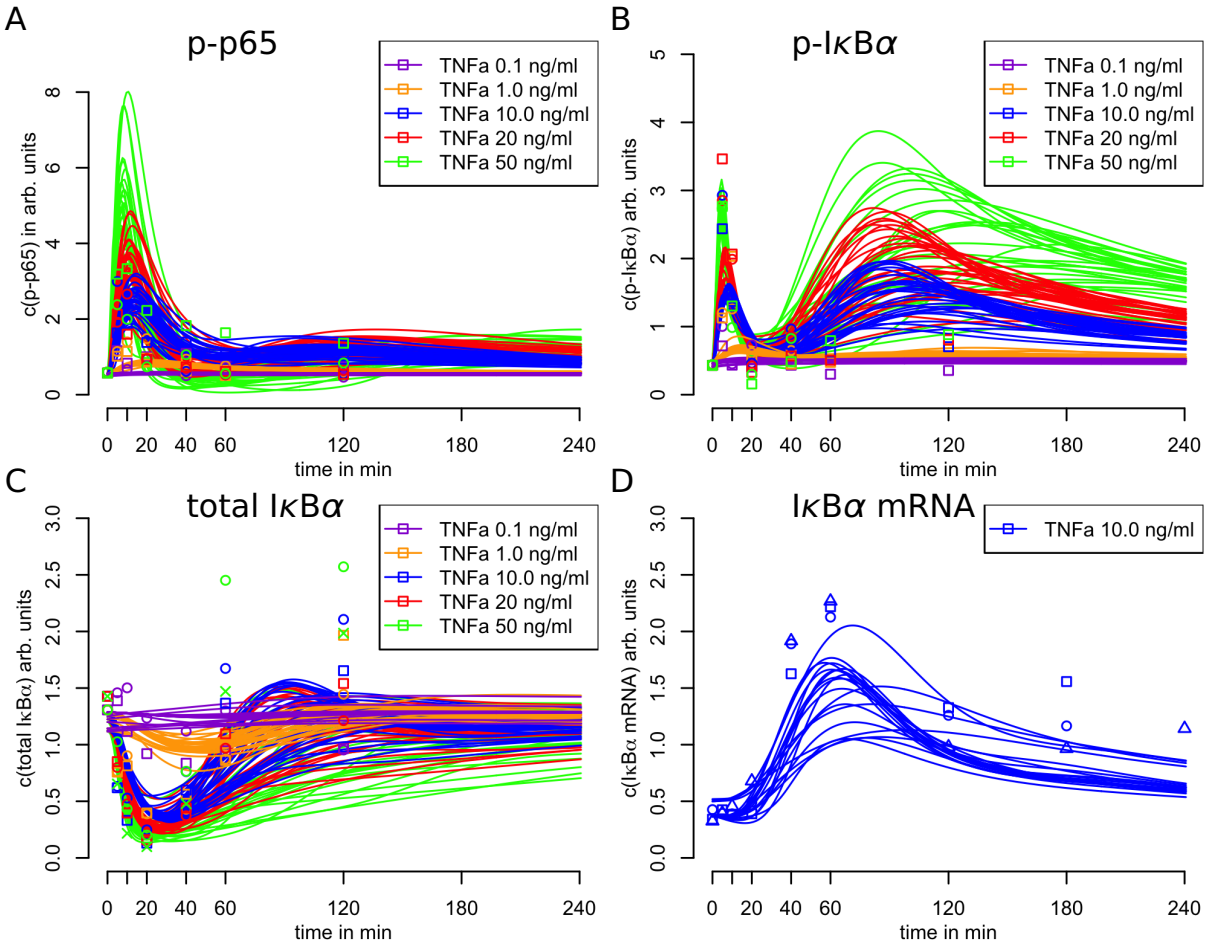

Figure 3.5: Plots of model simulations (solid lines, n=30) and experimental data (symbols, n=2) for dose response data with c(TNF)={0.1 ng/ml, 1 ng/m, 10 ng/ml, 20 ng/ml, 50 ng/ml} and the previously measured mRNA trajectory for c(TNF)=10 ng/ml predictions of the model without further parameter or model topology modifications. Experimental data was measured by Federico Pinna, Appendix Talbe A.5.

assumed to be negligble for the time span investigated. Receptor numbers measured for hepatocytes are between 1500 - 2900 [80], therefore the concentration of total TNFR1 was set to be 0.0068 μM. By including the receptor with a specific receptor number the extracellular volume and particle number of TNF in this volume became relevant. Before, the TNF concentration multiplied with an additional parameter freely chosen was used in the reactions, making the relative concentration changes, not absolute numbers relevant for the kinetics. Therefore, the extracellular volume was adjusted to account for the experimental conditions of 800 000 cells in 3 ml medium and the TNF concentration was simulated in molar concentrations instead of mass concentrations. Literature values were taken from a computational model on the TNF TNFR1 signalling in granulocytes [81], the estimated parameters were re-estimated using the original values as starting points and for setting the parameter estimation boundaries. After parameterization of the new model the simulations of the time courses of the protein concentration changes for the dose response data were drastically improved (see

Figure 3.7).

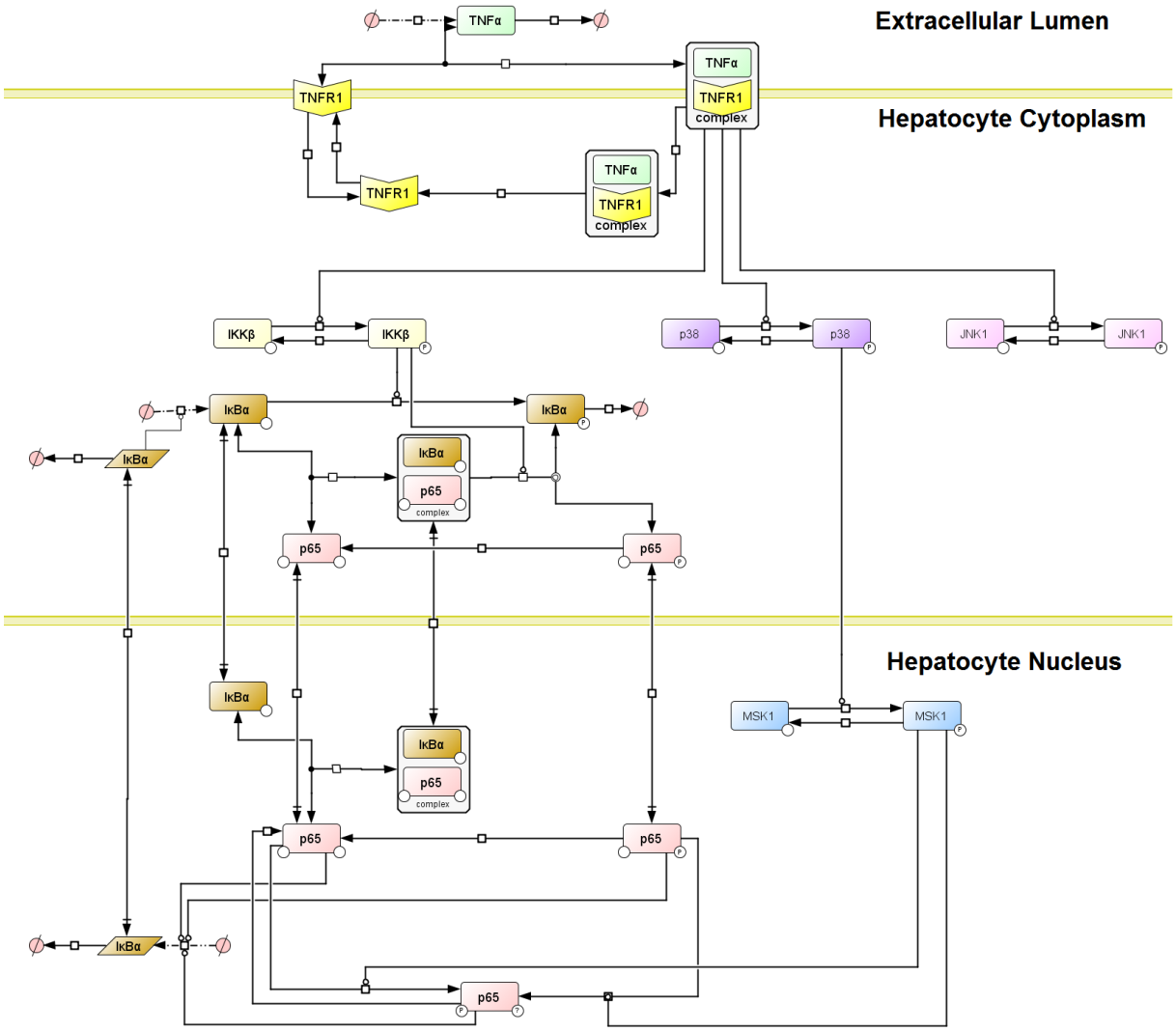

Figure 3.6: Model topology including the receptor TNFR1.

Describing the mRNA remained a challenge. By increasing the weight of the mRNA data in the target function, the model could be forced to describe the mRNA data. However, this led to a strong deviation in simulations from experimental measurements of the protein time courses. mRNA transcription and translation are both complex processes and mathematical model have been published, which describe them in much more detail [82, 83]. However, I aimed to find a mathematical description that could describe the mRNA levels without including much details. Again here two approaches were applied, to resolve this problem. First, the equation describing the transcription initiation of the IκBα mRNA was described with a Michaelis-Menten kinetic. Previously, this mechanism had been suggested to be important in the NF-κB system [84]. However, in my work the system became very unstable and a steady-state was no longer found (data not shown). Second, the mass action kinetics for the IκBα translation were replaced by

a Michaelis-Menten kinetic. After re-parameterization a good description of the protein and mRNA data was found. Figure 3.7 shows the new plots of the model with both TNFR1 and the changed kinetics for the mRNA translation.

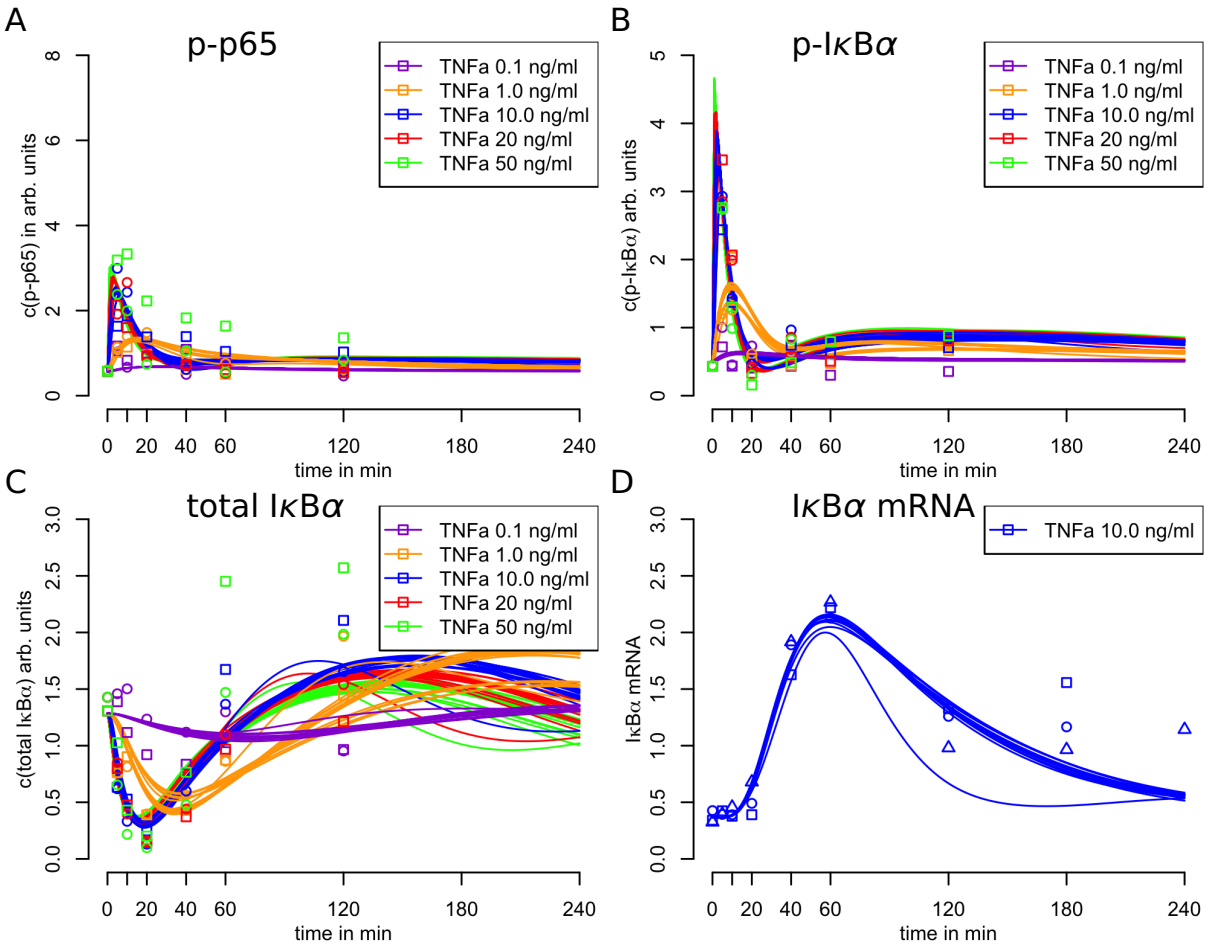

Figure 3.7: Plots of model simulations (solid lines, n=30) and experimental data (symbols, n=2) for dose response data with c(TNF)={0.1 ng/ml, 1 ng/m, 10 ng/ml, 20 ng/ml, 50 ng/ml} and the previously measured mRNA trajectory for c(TNF)=10 ng/ml simulations of the model after model topology modifications and parameter estimation. Experimental data was measured by Federico Pinna.

This model could also be validated with dose response measurements of the IκBα mRNA. The model accurately described the mRNA time course dynamics for all concentrations, without any further modifications (Figure 3.8).

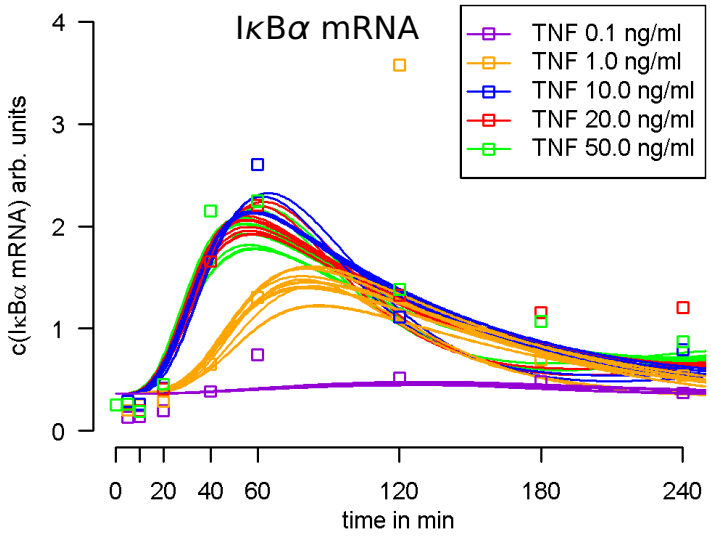

Figure 3.8: Plots of model simulations (solid lines, n=30) and experimental data (symbols, n=1) for dose response mRNA data with c(TNF)={0.1 ng/ml, 1 ng/m, 10 ng/ml, 20 ng/ml, 50 ng/ml}. The model describes all data without further adjustments. Experimental data was measured by Federico Pinna.

3.3.4 Hepatocarcinoma Cell lines

Under my supervision Nicolas Huber wrote his bachelor thesis on "Model-based comparison of TNFα/NF-κB signalling between primary hepatocytes and hepatocellular carcinoma cell lines Hep56 and Hepa1-6". In this thesis he used the model presented here, which I generated for and trained on experimental data from primary murine cells, to describe experimental data from murine heptocellular carcinoma cell lines.
The aim of these investigations was to establish which changes were needed to describe the carcinoma cell lines. If the NF-κB pathway signalling had been found to be altered beyond different protein expressions, for example if the binding affinity between IKKβ and the IκBα:NFκB complex was altered, which have been reflected in the K_M of the phosphorylation reaction, then this would have indicated a possible mutation in the carcinoma cell lines. However, only changes in the protein levels were needed, indicating that the protein transcription or translation profile varied. This was most likely not due to a mutation, but simply due to a different state of the carcinoma cells compared to the primary cells.

3.4 Multi-Scale Model of NF-κB in the Liver

In order to analyze the hepatocytes response to LPS-induced TNF secretion I integrated the input-output descriptions of the non-parenchymal cells TNF secretion profiles into the ODE model by using the average cell sizes, assuming that these cells are distributed rather homogeneously in the liver. Thus the final integrative model describes all cell types relative to a single hepatocyte. This approach gives an estimate of the upper limit of TNF concentrations that can arise locally *in vivo*.

3.4.1 Cell Type Specific Volumes

The cell populations' abundance in the liver have been determined by Blouin et al. in 1977[5]. Table 1 summarizes these numbers. Using the volume of a single hepatocyte the average size and adjacent extra cellular volume for all liver cell types can be determined. Below this is done exemplarily for the upper volume limit of LSECs.

$$\begin{aligned} V_{single\ LSEC} &= V_{single\ Heps} * \frac{V_{all\ LSEC}}{n_{all\ LSEC}} * \frac{n_{all\ Heps}}{V_{all\ Heps}} \\ &= 13\ pl * \frac{77.8\%}{2.8\%} * \frac{19\%}{60\%} \\ &= 1.5\ pl \end{aligned}$$

In Table 2 the volumes of all cell types and their adjacent extra cellular volumes are summarized. It is important to note that the average extra cellular volume adjacent to cell varies for the different cell types. Figure 3.9 shows this difference for hepatocytes and LSECs. Since there are less LSECs

than hepatocytes, (there are 3.16 hepatocytes per 1 LSEC, see Table 3) the average extra cellular volume per LSEC is 3.16 times larger than the extra cellular volume per hepatocyte.

Table 2: Average volumes per liver cell type.

	Heps	LSEC	Kupffer Cells	Stellate Cells
cell volume	3 - 13 pl[85, 86]	0.3 - 1.5 pl	0.3 - 1.4 pl	0.4 - 2.8 pl
Space of Disse per cell	0.19 - 0.82 pl	0.60 - 2.61 pl	(0.7 - 3.27 pl)	1.4 - 9.8 pl
Sinusoid Lumen per cell	0.41 - 1.77 pl	1.13 - 5.68 pl	1.51 - 7.0 pl	(3.03 - 21.2 pl)
total extracellular volume per cell	0.60 - 2.59 pl	1.73 - 8.29 pl	2.21 - 10.27 pl	4.43 - 31.0 pl

Figure 3.9: Simplified scheme of the liver anatomy. Cubical hepatocytes (orange) are in contact with Space of Disse which is lined by long stretched endothelial cells (yellow), separating the hepatocytes from the sinusoid. Right side: Space of Disse a hepatocyte is in contact with. Left side: Space of Disse an endothelial cell is in contact with.

Table 3: Comparison of cell abundance and size for non-parenchymal cells with hepatocytes as reference.

	LSEC	Kupffer Cells	Stellate Cells
hepatocytes per cell	3.16	4	12 - 7.5
times smaller than hepatocytes	8.7	9.26	4.6 - 7.41

3.4.2 Non-Parenchymal Cells' Responses to LPS

Primary bone marrow derived macrophages, liver sinusoidal endothelial cells, and hepatic stellate cells were isolated from mice and cultured *in vitro* by Ute Albrecht, Frank Alexander Schildberg, and Roman Liebe, respectively. For each of these cell types LPS-induced TNF secretion profiles were measured for a defined number of cells *in vitro*. Using the ratios in numbers and in volume of non-parenchymal and parenchymal cells (Table 2, 3), and the moleculare weight of the soluble TNF trimer 52 kDa [87] these profiles could be translated into *in vivo* concentration profiles (Figure 3.10).

All non-parenchymal cells secrete TNF. However, the LPS induction of TNF secretion by macrophages (MCs) and liver sinusoidal endothelial cells (LSECs) is clearly observable. The stellate cells (HSCs) show a mostly constant level

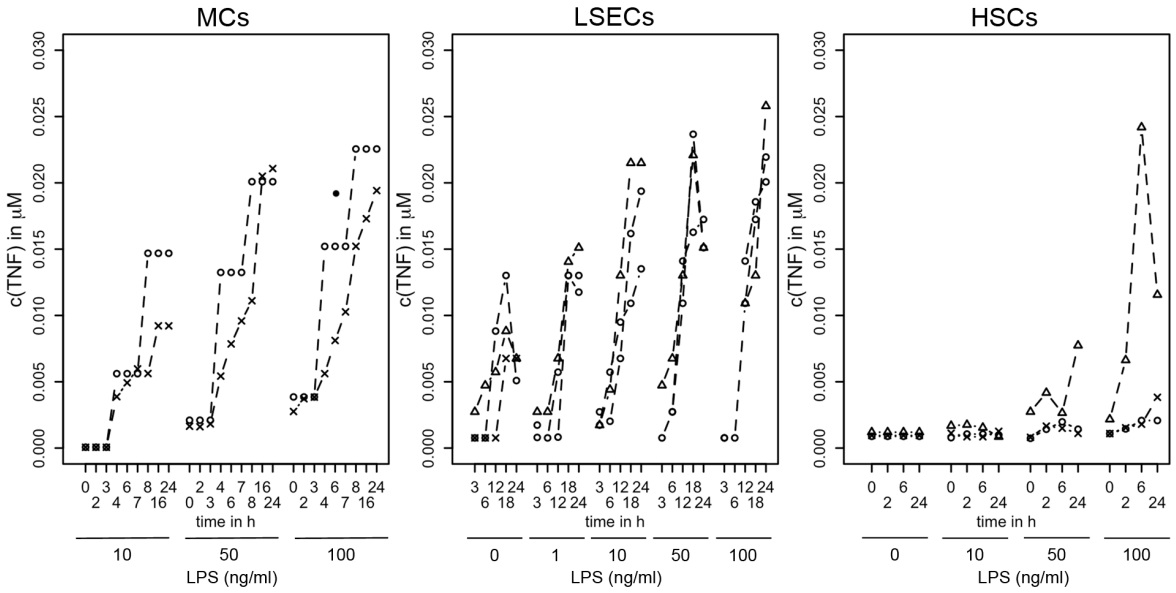

Figure 3.10: Secretion profiles of LPS-induced TNF secretion from non-parenchymal cells. (B) Recalculated profiles accounting for cell abundance in the liver to estimate *in vivo* TNF concentration profiles. Experimental data was measured by Ute Albrecht (MCs), Frank A. Schildberg (LSECs), and Robert Liebe (HSCs).

of TNF secretion and due to their low abundance in the liver, the estimated *in vivo* concentration is comparable to the basal level of the TNF secreted by MCs or LSECs. The non-parenchymal cells were subject to stress, from cell isolation and experimental treatment. Thus, these basal TNF levels are likely to be caused form these experimental procedures. Therefore, I set the TNF concentration to be zero in the absence of LPS, to mimic the *in vivo* situation and the stellate cell profiles were not included into the further investigations.

3.4.3 Hepatocellular Response to Non-Parenchymal Cells' Secretion Profiles

Additionally to the compartmentalisation further assumptions were necessary to calculate the LPS-induced TNF/NF-κB signalling:

1. The diffusion of TNF happens on a faster time scale than the modelled biochemical processes. (Proteins diffuse within seconds through LSECs [12], the measured and simulated protein and mRNA concentration changes take place within minutes to hours.)

2. TNF can diffuse freely between the sinusoidal lumen and the Space of Disse through LSEC fenestrae, as was illustrated for albumin (diameter 34 nm) [12]. (Assuming that TNF is of globular shape and by using the formula from Erickson, the cytokine diameter was estimated to be 5 nm [88].)

3. TNF is approximately homogeneously distributed. (This follows directly from 1. and 2.).

The secretion profiles of the calculated molar TNF concentrations from MCs and LSECs were described by a small ODE-system which was added as an input to the *in vitro* hepatocellular model. The extracellular volume was adjusted to match the *in vivo* volumes described in this integrative liver model (Figure 3.11).
The model ensemble with its 30 parameter sets was used to simulate the intra-hepatocellular response to TNF secreted by MCs and LSECs individually and combined after LPS induction for 0.1, 1, 5, and 10 ng/ml (Figure 3.12). These simulation results revealed that TNF concentrations are dependent on the LPS concentration the non-parenchymal cells are stimulated with. Furthermore, TNF concentrations reached locally *in vivo* are much higher than the concentrations used for training the *in vitro* hepatocellular model. However, the intra-hepatocelluar response in the simulations of the integrative model is not as strong as the *in vitro* response (i.e. the amplitude height of phospho-p65 and phospho-IκBα is lower, the decrease of IκBα less pronounced). At first this seems paradox. However, when taking into account the small extra-cellular volumes *in vivo* and the large medium volume *in vitro*, as well as the dynamics of the TNF secretion in the integrative liver model and the intra-hepatocellular response this can be perfectly explained.

The TNFR1 particle number and the dynamics of its shuttling to and from the extra-cellular membrane to intracellular vesicles define, how much TNF can be detected by the hepatocytes. In the *in vitro* experiments a single dose of TNF is administered to the hepatocytes. Due to the large medium volume the TNF particle number is much higher in the medium than in the extra-cellular volume in the simulations of the integrative model (*in vitro* experiments: 10 ng/ml TNF = 0.000193 μM TNF = 440800 TNF particles / hepatocyte, integrative model simulations: MCs and LSECs combined TNF secretion: 5 ng/ml LPS, 0.049 μM TNF = 7640 TNF particles / hepatocyte). Additionally these TNF particles can immediately bind to all available TNFR1 particles. In the integrative model TNF is secreted gradually, thus the TNFR1:TNF complexes form gradually. When looking at the amount of time it takes for the intra-heptaocellular response to be triggered, it becomes clear that this response takes place long before the maximal TNF levels are reached (Figure 3.13, for 5 ng/ml LPS stimulations phospho-p65 peaks after 30 minutes, maximal TNF concentrations are reached after 10 hours). Thus the final TNF levels cannot be decisive for the strength of the intra-hepatocellular response. Rather it is the initial increase in TNF levels that defines this response. MCs showed a weaker initial TNF secretion than LSECs, when both secreted TNF, its levels increased the fasted. However, secretion velocity is limited for cells. Therefore, once the non-parenchymal cells have reached the maximal speed at which they can secrete TNF higher LPS dosages cannot increase the TNF increase and thus cannot increase the intra-hepatocellular response. Therefore, LPS doses higher than 5 pg/ml do not invoke a stronger intra-hepatocellular response.

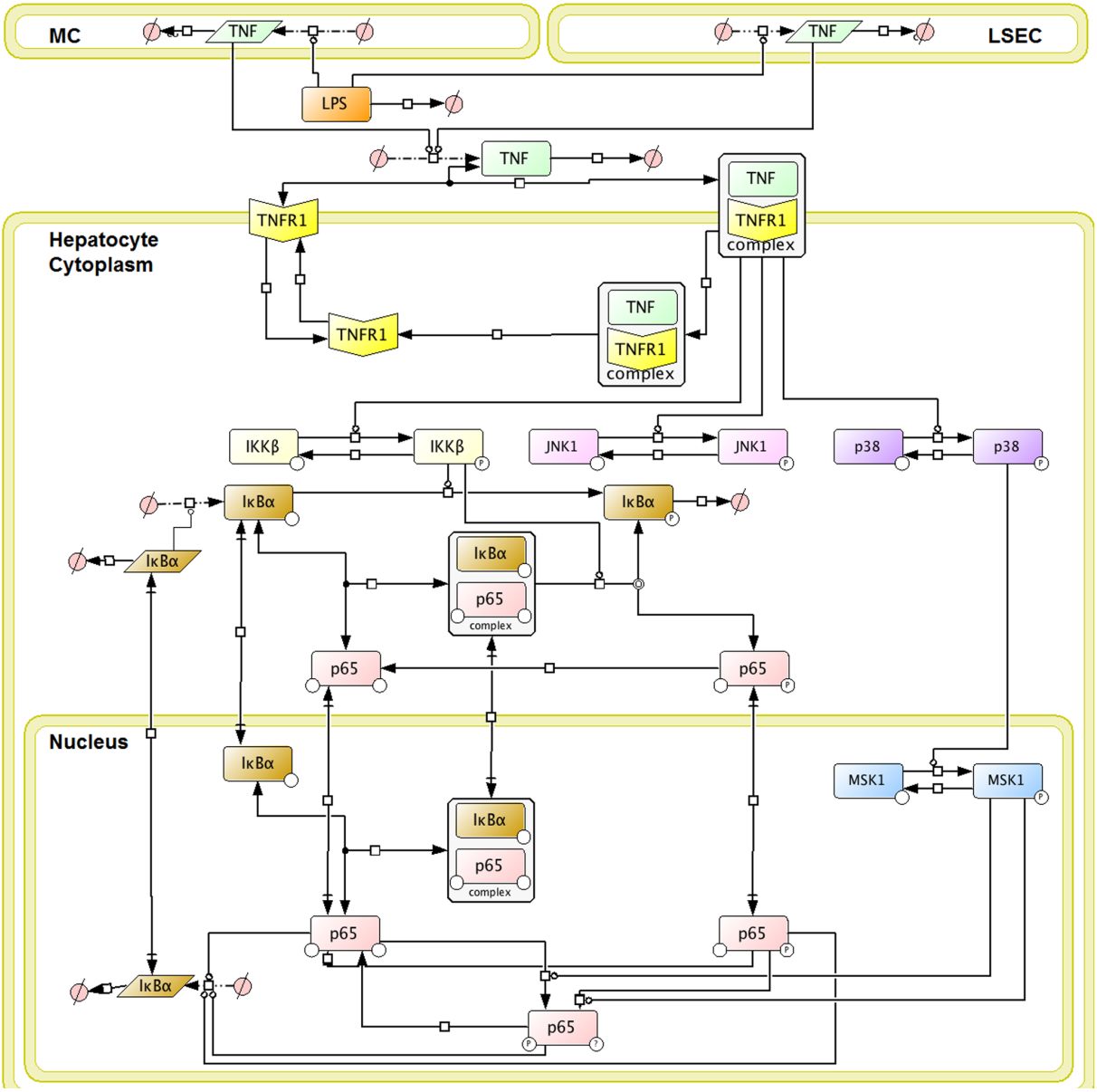

Figure 3.11: Model Topology of the integrative NF-κB liver model. LPS induces non-parenchymal TNF synthesis, TNF induces parenchymal NF-κB signalling.

In general the dynamics of the intra-hepatocellular response depend on the LPS stimulus and resulting initial TNF increase. For very low stimulus concentrations (0.1, 1 ng/ml LPS) the intra-hepatocellular response shows broader and lower phospho-p65 and phospho-IκBα peaks. The IκBα expression is less strongly induced than for high LPS concentrations (>5 ng/ml). However, as described above, for these higher LPS concentrations the steepness of the initial TNF increase cannot be increased further and thus the intra-hepatocellular response can also not be increased further.
In summary, TNF secreted by LSECs or MCs individually in response to low dosages of LPS (0.1 and 1 ng/ml) was sufficient to induce a partial intra-hepatocellular response. However, the highest intra-hepatocellular response was invoked when LSECs and MCs secreted TNF simultaneously in response to doses higher than 5 ng/ml LPS. These high LPS concentrations induced concentrations of more than 240 ng/ml TNF secreted by LSECs or MCs individually.
Although the maximal intra-hepatocellular response simulated for the integrative model was not as strong as the response provoked by *in vitro* experiments, this response could not be increased by stimulating the non-parenchymal cells with more LPS. This can explained by the cytokine secretion dynamics of cells which differs strongly from stimulating cells with a single high dose, as done according to current *in vitro* experimental procedures.

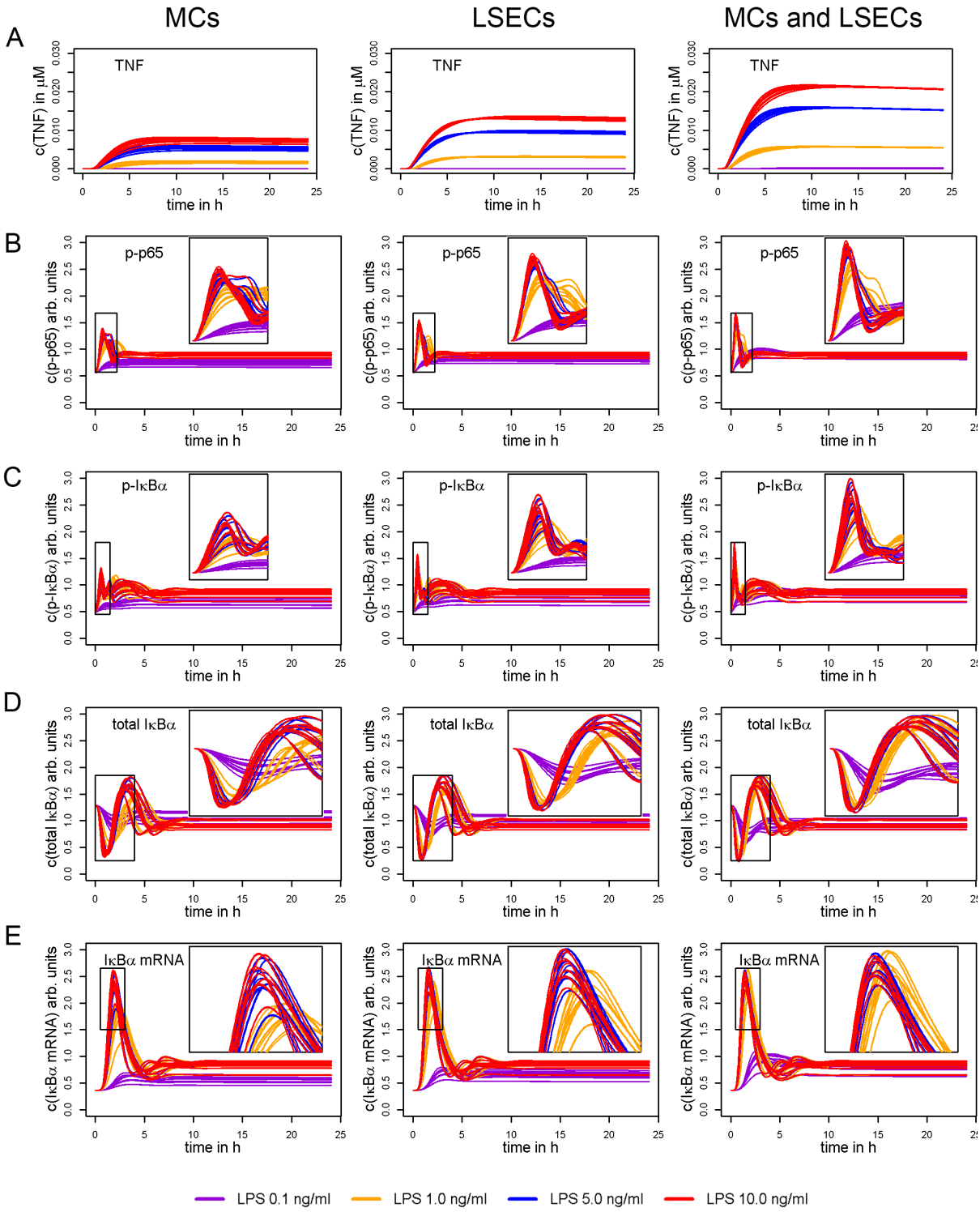

Figure 3.12: Integrative liver model predictions. Upon LPS-induction with various LPS concentrations the simulated response of the non-parenchymal cells individually and combined in form secreted TNF is shown in A. Subsequently NF-κB signalling in hepatocytes is induced, B - E show concentration changes of phospho-p65, phopho-IκBα, IκBα, and IκBα mRNA.

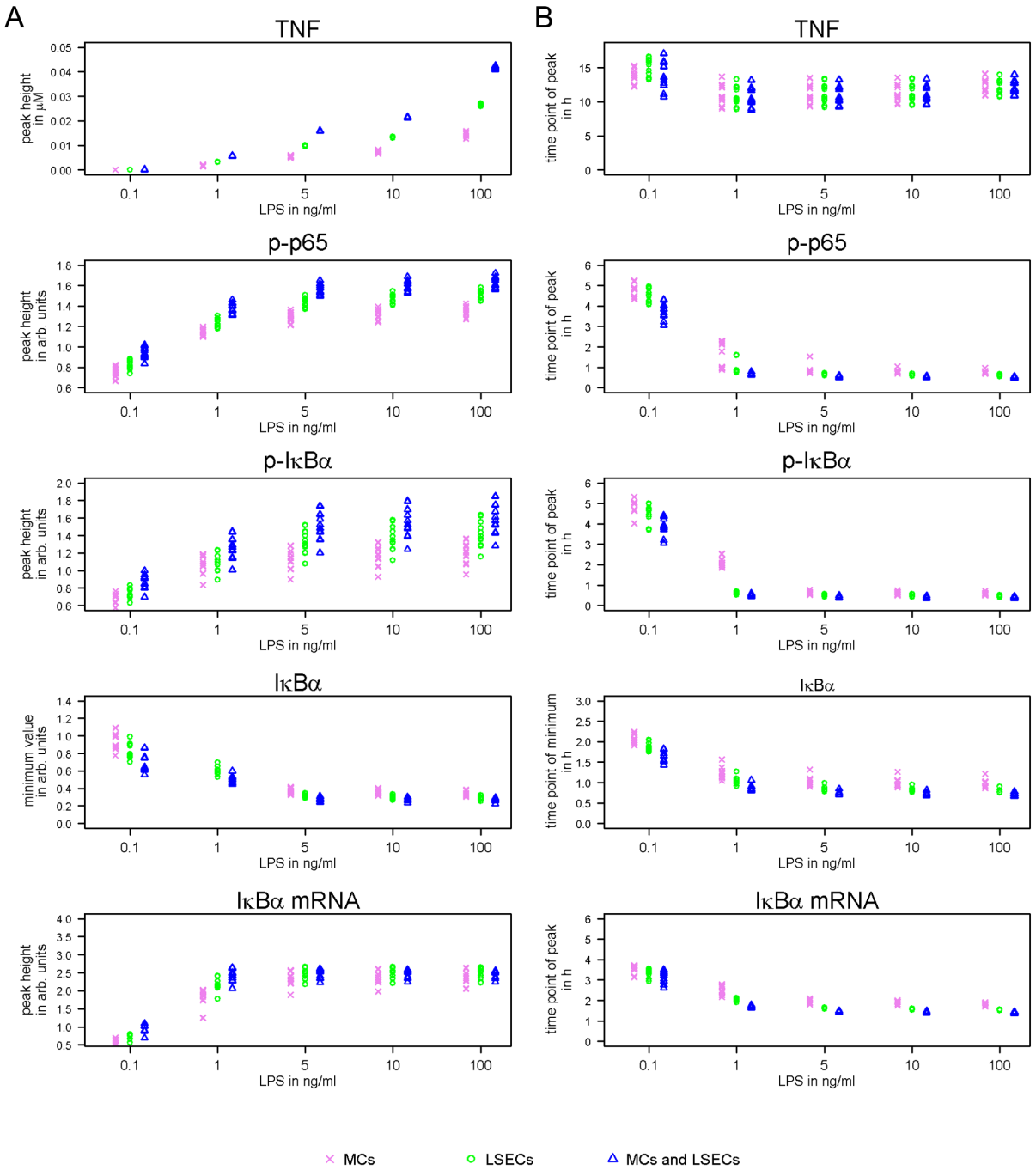

Figure 3.13: Characteristics of the integrative liver model predictions. Panel A shows the strength of characteristics in the simulations, panel B shows the time points of these events for different LPS dosages.

3.5 Spatial Model

On the single cell level, I wanted to look at spatial and temporal effects of TNF on the NF-κB pathway. For this our collaborators established human hepatocarcinoma cell lines with first transiently and later stably transfected red fluorescent protein (RFP) tagged p65. Images of these cells after TNF stimulation were recorded with a fluorescence microscope and I quantitatively analyzed the RelA localization based on the red fluorescence intensity in these images. At the same time I converted a reduced NF-κB ODE model into a PDE model taking into account both time and x and y positions of species concentrations. Finally, I extended for the final intra-hepatocellular ODE model of NF-κB signalling into a PDE model and redid the simulations.

3.5.1 Single Cell Analysis

The experimental data, the spatial model should describe, were fluorescent images of hepatocyte carcinoma cell lines expressing p65/RelA tagged with RFP (p65-RFP, RelAdsRed). For the establishment of the experimental set-up our collaborators (Michaela Bissinger) provided us with different image types and we analyzed these. Based on the feedback we could give on these results, the experiments were adopted.
The first sets of experiments were performed in HLF cells, later HLE cells were used. HLF is a human hepatic carcinoma cell line which shows fibroblast like behavior, HLE is a human hepatic carcinoma cell line which shows eptihelial like behaviour [89].

First, p65-RFP was transfected transiently in the cells before each experiment. Thus the amount of red-fluorescent RelA varied between individual cells. Some cells had a very strong red-fluorescent signal, here, the transfection was successful. The cells took up the vector with the gene encoding for p65-RFP and expressed it at high levels. Some cells didn't show any red-fluorescent signal, these cells most likely did not take up any vector. A third group of cells only showed a weak red-fluorescent signal, these cells most likely took up the vector but for some reason did not express p65-RFP in a strong manner. The very first images of cells were additionally colored with a plasma membrane specific fluorescent protein: CellMask. This dye specifically integrates into the plasma membrane. However, it was not possible to analyze these pictures in an automated way. The background signal was equally strong as the signal from some of the cells, making automated cell detection not feasible. Therefore, I decided to analyze these images manually based on the bright field recordings. Thus, I established a semi-automated script using CellProfiler. Cells borders were outlined manually, Hoechst stained nuclei were detected automatically. The program then measured the area and RelA intensity in the cells and nuclei. A student assistant completed these analyses under my guidance. The manual analysis of a single time series following up to 10 cells took six hours.

Later, the experimental set-up was changed. The cells were stained with

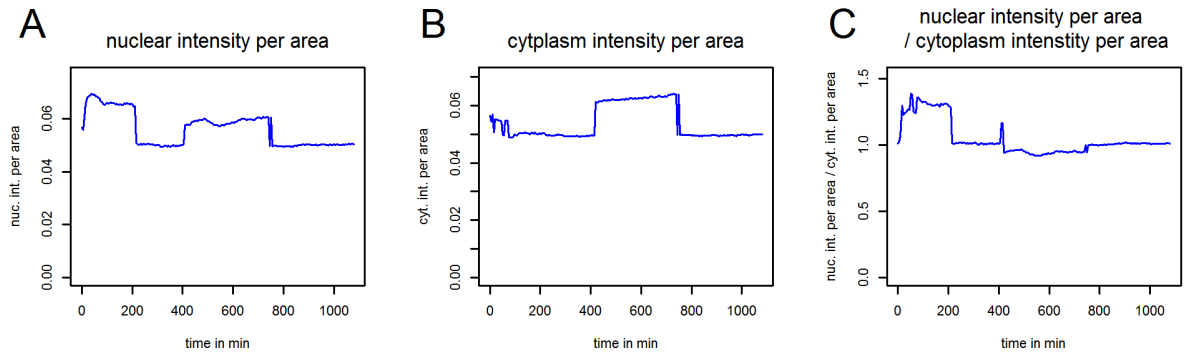

Figure 3.14: Time course showing how the distribution of p65-RFP between the nucleus and the cytoplasm changes over time in HLE cells. A p65-RFP nuclear intensity, B p65-RFP cytoplasm intensity, C ratio of p65-RFP nuclear intensity normalized per area and p65-RFP cytoplasm intensity normalized per area.

CellTracker a cytoplasm specific stain fluorescing green. This than allowed a fully automated CellProfiler analysis of the images. The green fluorescent signal from CellTracker was used to identify the cells. A threshold was set automatically. In some cases this was not successful, then manually a threshold was set for each image set. Pixels with intensity of above the threshold, and grouped together to form objects with a radius larger than 10 pixels and smaller than 50 pixels were defined as cells. In a second channel the blue light emitted from Hoechst stained nuclei was recorded. An automatic threshold for pixel intensity was calculated from within CellProfiler, and objects with a radius between 5 and 30 pixels were defined as nuclei. The cell area without the nuclei was defined as cytoplasm. For cells, nuclei, and cytoplasm the p65-RFP fluorescence intensity was detected and the area was calculated. An exemplary CellProfiler Script can be found in the Appendix.

CellProfiler writes the analysis results into large tables which than need further processing. For this I loaded the tables into R and resorted the data. For each cell I then created time-course profiles depicting the changes in RFP intensity. Figure 3.14 shows an exemplary cell profile.

3.5.2 From ODEs to PDEs

As described in the introduction PDEs describe biochemical reaction and diffusion processes. Essentially, they can be divided into the biochemical reaction flux vector which is similar to the ODEs in a biochemical reaction model and the diffusion fluxes. As simulating the final PDE model took up to several days, it would not have been feasible to try to do parameter estimation for the parameters of the PDE model. Therefore, the paramteres of the reaction flux vector were taken from the parameters estimated from population based data with the ODE system. For the diffusion flux the diffu-

sion coefficients for each species are needed. A literature research did not yield any measured values for the species of the NF-κB system. Therefore, the Young-Carroad-Bell method was used to calculate estimates of the diffusion coefficients based on the molecular weights of the species [90]. The formula was derived for spherical molecules in aqueous solutions. It yields rough estimates for proteins moving within in the cytoplasm. Table 4 lists the molecular weights and the estimated diffusion coefficients. mRNA diffusion was measured to be between 108 $\mu m^2/h$ and 2160 $\mu m^2/h$ [91], I set the diffusion coefficient to 140 $\mu m^2/h$ in the PDE model.

Table 4: Diffusion coefficients for the NF-κB pathway. The diffusion coefficients were calculated with Young-Carroad-Bell Method.[90]

Molecule	Moleculare Weigth in Da (= g/mol)	Diff. Coef. in cm^2/s	Diff. Coef. in $\mu m^2/h$
p65 / RelA	60212	4.05235E-10	146
p50	47508	5.13598E-10	185
IκBα	35071	6.95732E-10	251
P_*i* (PO_3)	79	3.08861E-07	111190
NFκB	107720	2.26513E-10	82
P-IκBα	35239	6.92415E-10	249
NFκB:IκBα complex	142801	1.70867E-10	82
P-p65	60291	4.04704E-10	145
PP-p65	60370	4.04174E-10	145
P-(p65)NFκB	127799	1.90925E-10	82
PP-(p65)NFκB	127878	1.90807E-10	82
IKKβ	86564	2.81872E-10	101
P-IKKβ	96643	2.52476E-10	91
IKKα	84640	2.8828E-10	104
IKK*gamma*	48198	5.06245E-10	182
IKK-complex	219402	1.11211E-10	40
MSK1	89865	2.71518E-10	98
P-MSK1	89944	2.7128E-10	98
p38	41293	5.90899E-10	213
P-p38	41384	5.896E-10	212
JNK1	48296	5.05218E-10	182
P-JNK1	48357	5.04581E-10	182
TNFR1	50495	1.611E-10	58
TNF	25644	4.685E-10	170
TNF:TNFR1 complex	76139	1.199E-10	43

Furthermore, in spatial models the geometry of the cell plays an important role. As the Diffusion coefficients were calculated in $\mu m^2/h$, the dimensions of the cells should be in μm, as well. Hepatocytes have an almost cubic form with a side length $20 - 30 \mu m$ [92]. Therefore, I chose a 20 x 30 rectangle with rounded corners as the shape for the cytoplasm. Primary hepatocytes often have two nuclei, however the cell lines we used mainly showed one nucleus, therefore I only included one nucleus. I used the formula of a sphere and the volume of the nuclei (0.8 pl) used in the ODE model to calculate the radius of the nucleus (5.7 μm). For the nuclear geometry I then included a circle with this radius.
As currently, the exact simulation of species crossing into different compartments for the dune package is not available, we chose to estimate the crossing of molecules from one compartment into the next by having overlapping regions of the nucleus and the cytoplasm. Only in these regions the transport processes, transforming e.g. cytoplasmic p65 into nuclear p65, could take place 3.15.
The exact PDE solutions for the species concentrations are calculated on a grid, in between the grid knots the concentrations are interpolated from the grid positions. This plays an important role in defining the geometry. Especially the circular overlap region should have the a continuous thickness, or to be more precise a continuous amount of knots. Otherwise artificial spatial effects may occur.

Figure 3.15: Spatial distribution of the compartments in the PDE simulations on a 64 x 64 grid. The green area is defined as cytoplasm, the white area is defined as nucleus and the blue area is defined as both cytoplasm and nucleus.

3.5.3 PDE Model Simulation

As solving PDEs is a much complexer problem than solving ODEs, initially a reduced version of the ODE model was used to reduce the computational costs of the PDE simulations (see figure 3.16). After the reduced model could roughly reproduce the experimental single cell images, the final intrahepatocellular NF-κB ODE model was also extended to a PDE model. The insights gained from extending the reduced version could then be transferred to the extended model. The aim of this study was to reproduce the experimental data qualitatively in the simulations.

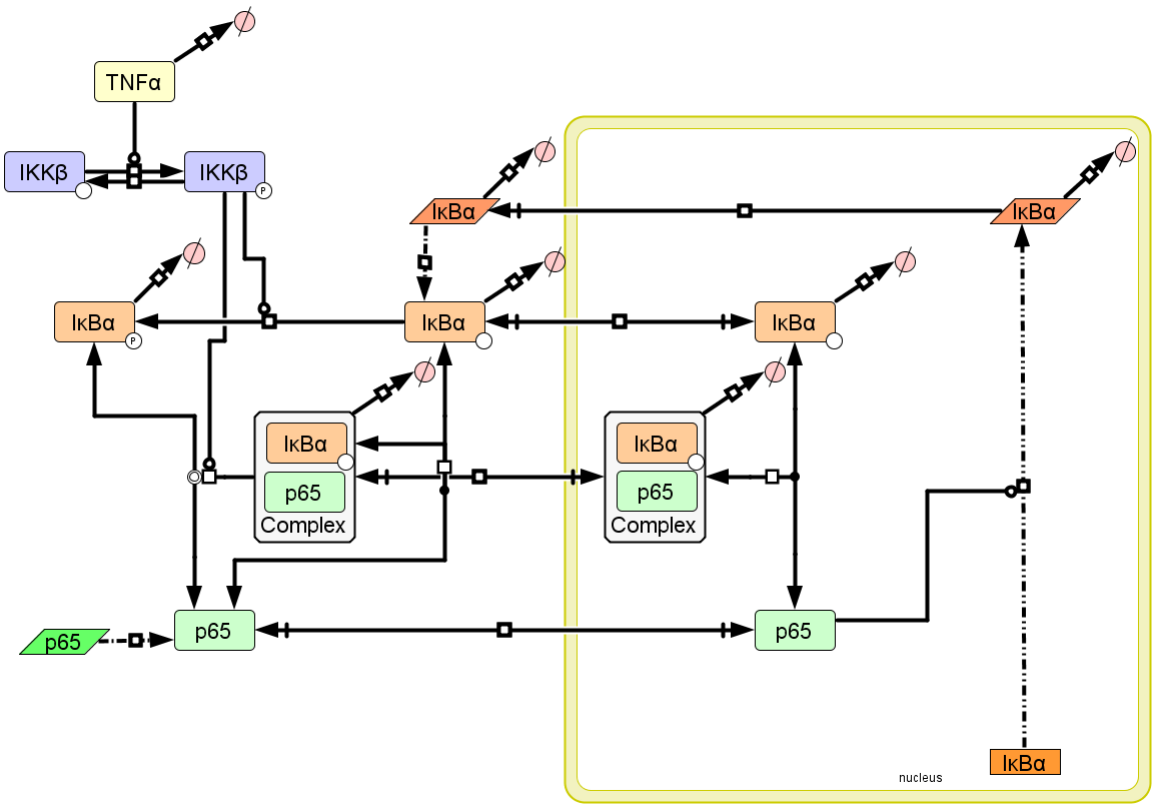

Figure 3.16: Model topology of the reduced NF-κB model for PDE-simulations. The boxes mark the p65 species observed in experimental single cell microscopy images.

To ensure the reduced ODE model was transferred correctly into a PDE model, I ran a simulation of the model using very high (1 000 $\mu m^2/s$) diffusion coefficients and I defined the area of the nucleus and cytoplasm to be identical. In this simulation the diffusion took place on a much faster time scale than the biochemical reactions. Therefore, the total species concentration changes in a compartment should behave as in the ODE model. Figure3.17 shows the simulation results. The PDE simulations match the ODE simulations.

Next the diffusion coefficients calculated from the formulas as described above were used. These simulations indicated a different problem. As shown in Figure **??** the simulations did not show the expected behavior.

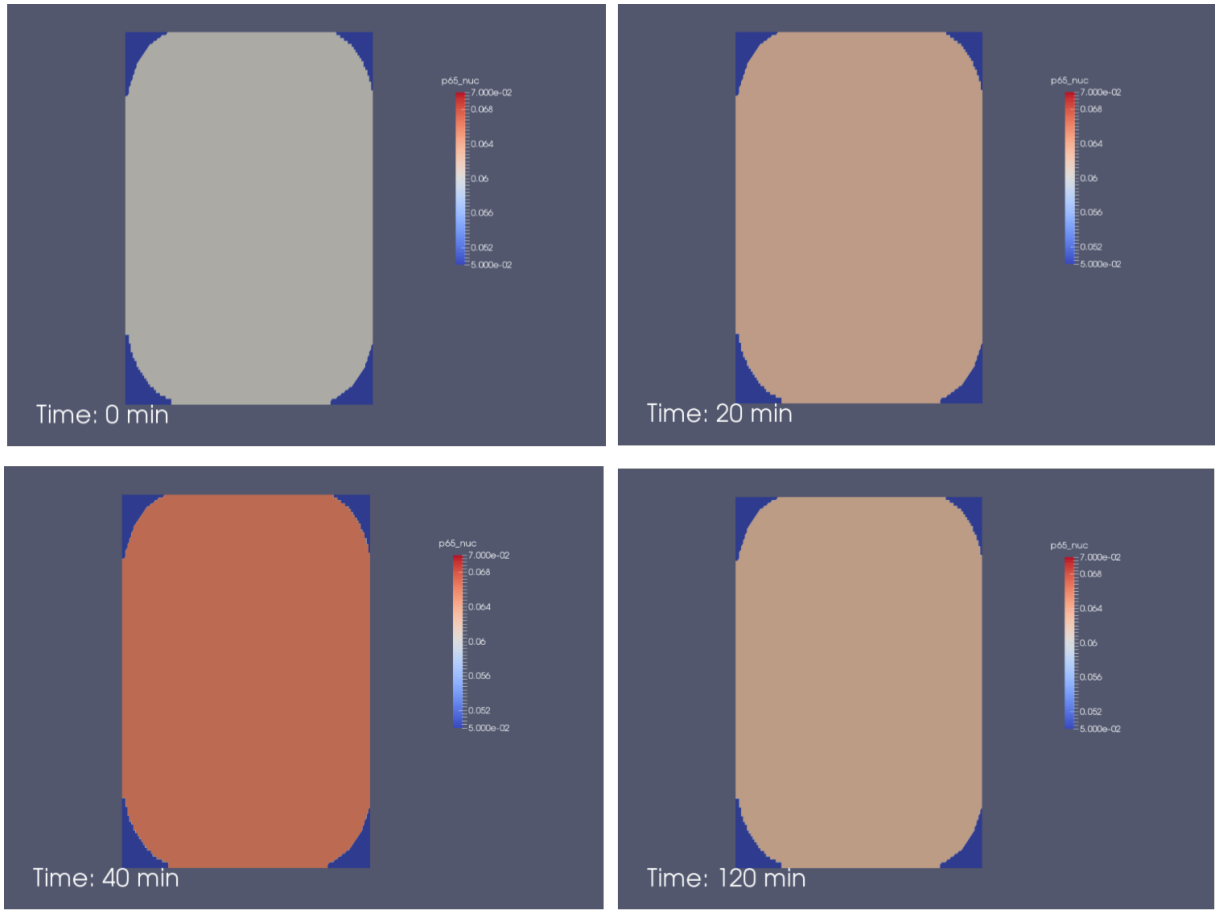

Figure 3.17: Simulations of the reduced reduced PDE model with very high diffusion coefficients to show the ODE model and PDE model show the same general dynamics. p65 local concentrations in PDE simulations are shown at time points 0, 20, 40, and 120 min.

We were observing two things happening at the same time, in the overlap region between nucleus and cytoplasm the concentrations of all species shuttling between nucleus and cytoplasm was increasing strongly, additionally, the TNF induced concentrations changes were taking place. The initial concentrations of species from the ODE model are average concentrations for all areas of cytoplasm or nucleus. In the PDE model the species are not distributed equally, because there is an on going exchange between the nucleus and cytoplasm. Thus the model was not in a steady-state when simulating TNF addition in the beginning of the simulations. Therefore, I decided to simulate the addition of TNF after 48 h. This allowed the model to find a steady-state given the geometrical conditions.
Additionally, the aggregation of the species in the overlap region was very high. Most species did not leave the overlap region again. The initial transport rates from the ODE model, describe diffusion and the transport process. In the PDE model, this needs to be separated further. The diffusion processes are described by the diffusion vectors. The reaction processes of the transport only should be described in the reaction flux vector. As all species modeled can cross the nuclear membrane rather quickly, I increased the transport rates from the ODE model by a factor of 100 for the PDE simulations. The translocation of p65 from the cytoplasm into the nucleus is much slower in the PDE simulations than in the ODE simulations. Most likely the diffusion coefficients are too slow. Therefore, I simulated how increasing the diffusion coefficients by factor 2, 5, 10, 40 and 100 altered the results. (Figure 3.18 shows the simulation results for diffustion factors increased by factor 40.)

The simulations show that increasing the diffusion coefficients by factor 100 leads to dynamics that are similar to the observed dynamics in the single cell microscopy images for 65-RFP localisation. After XXX minutes the concentration in the nucleus peaks followed by a shift of p65 concentration back to the cytoplasm. It does not re-enter the nucleus. Similarly the microscopy images show that in most cells p65-RFP is in the nucleus after 20 minutes and after approximately 4 hours it is back in the cytoplasm .
Next the complete NF-κB intra-hepatocellular model was extended to a PDE model. However, in PDE models only species in the same compartment can react. There I needed to add import and export reactions of p38 and phospho-p38 to this model. As the dephosphorylation reaction is independent of the TNF-TNFR1-complex it also can take in the nucleus, however, phosphorylation reaction cannot (Figure 3.19).

For this extended model only simulations were run with adjusted transport rates and increased diffusion coefficients (factor 40). Figure 3.20 shows the results form the final simulations together with images from the single cell microscopy experiment. When comparing these to the p65-RFP single cell microscopy images, it can be seen, that the model nicely reproduces the dynamics of these experiments.

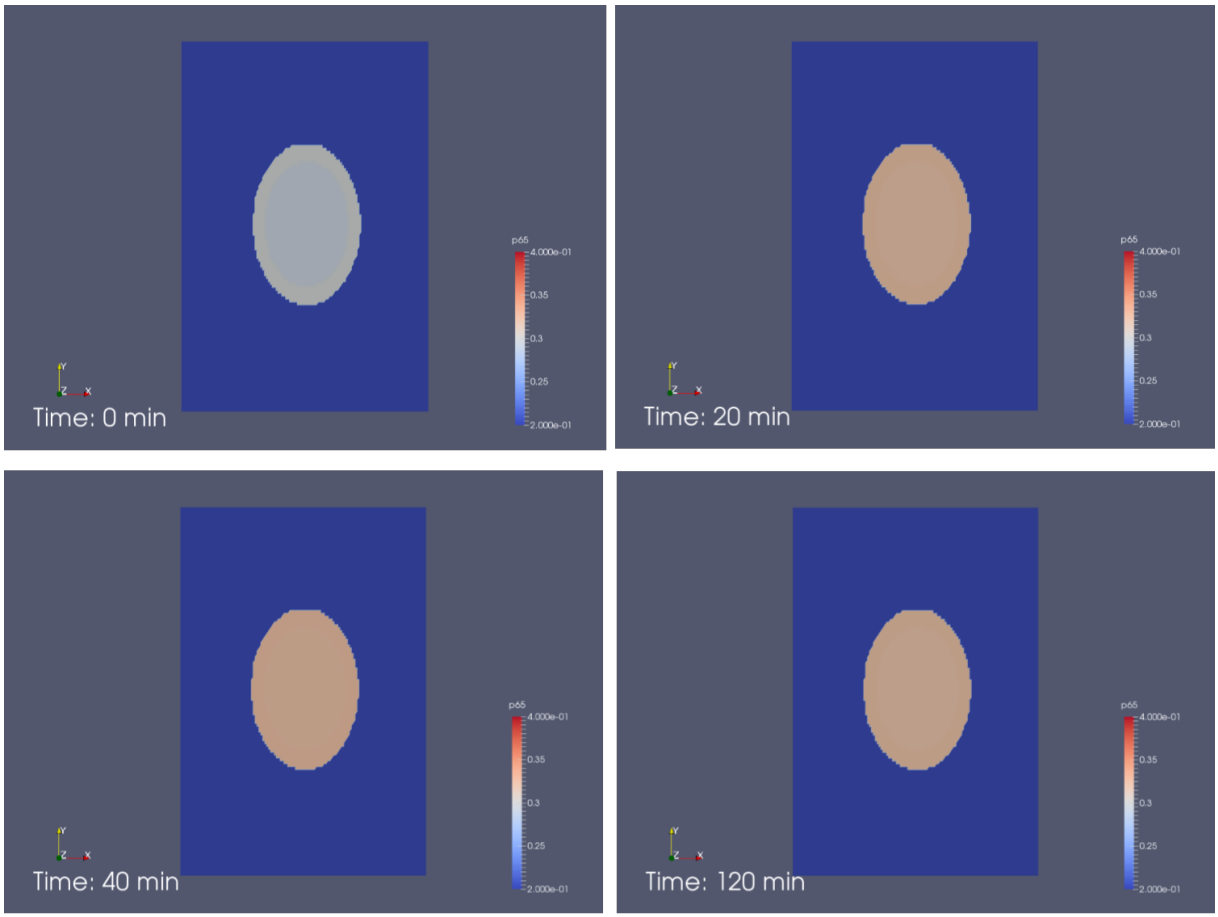

Figure 3.18: Simulations of the reduced PDE model with adjusted transport rates and TNF stimulation after the steady state is reached. p65 local concentrations in PDE simulaitons with diffusion coefficients increased by factor 40 are shown at time points 0, 20, 40, and 120 min. Inner circle is the nucleus, outer area is the cytoplasm.

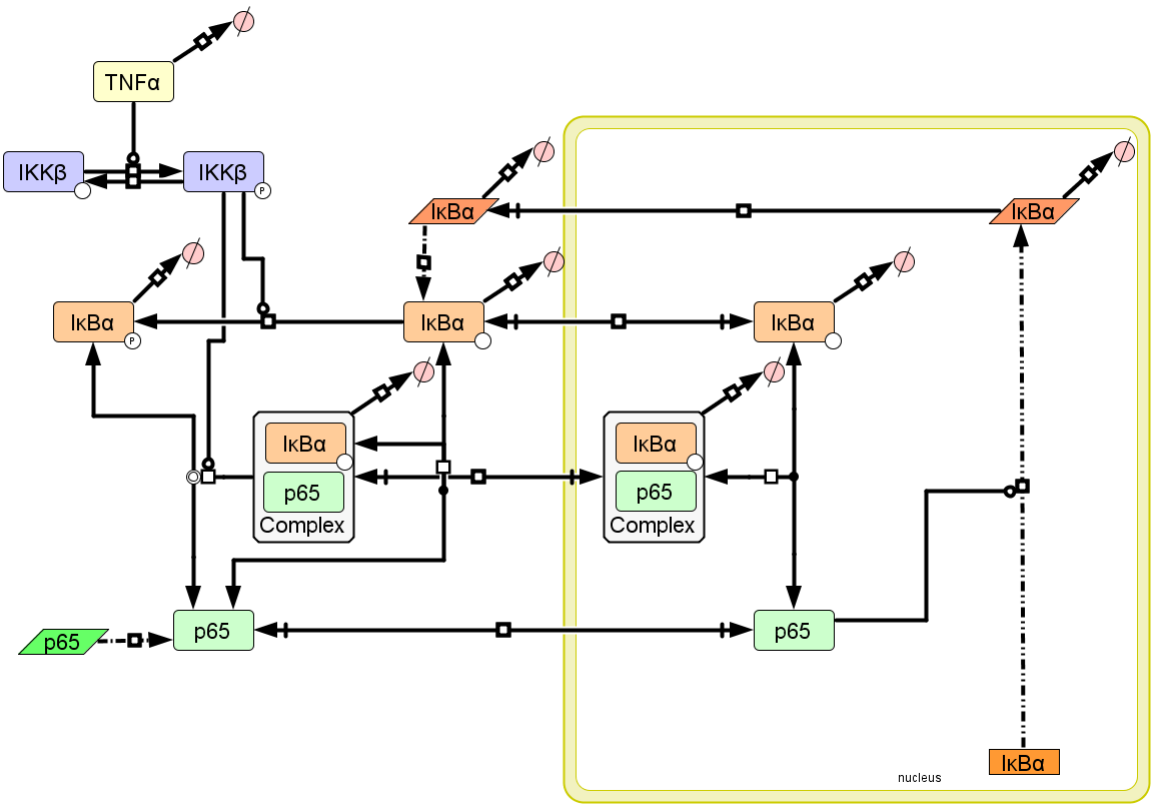

Figure 3.19: Model topology of the complete NF-κB model for PDE-simulations. The boxes mark the p65 species observed in experimental single cell microscopy images.

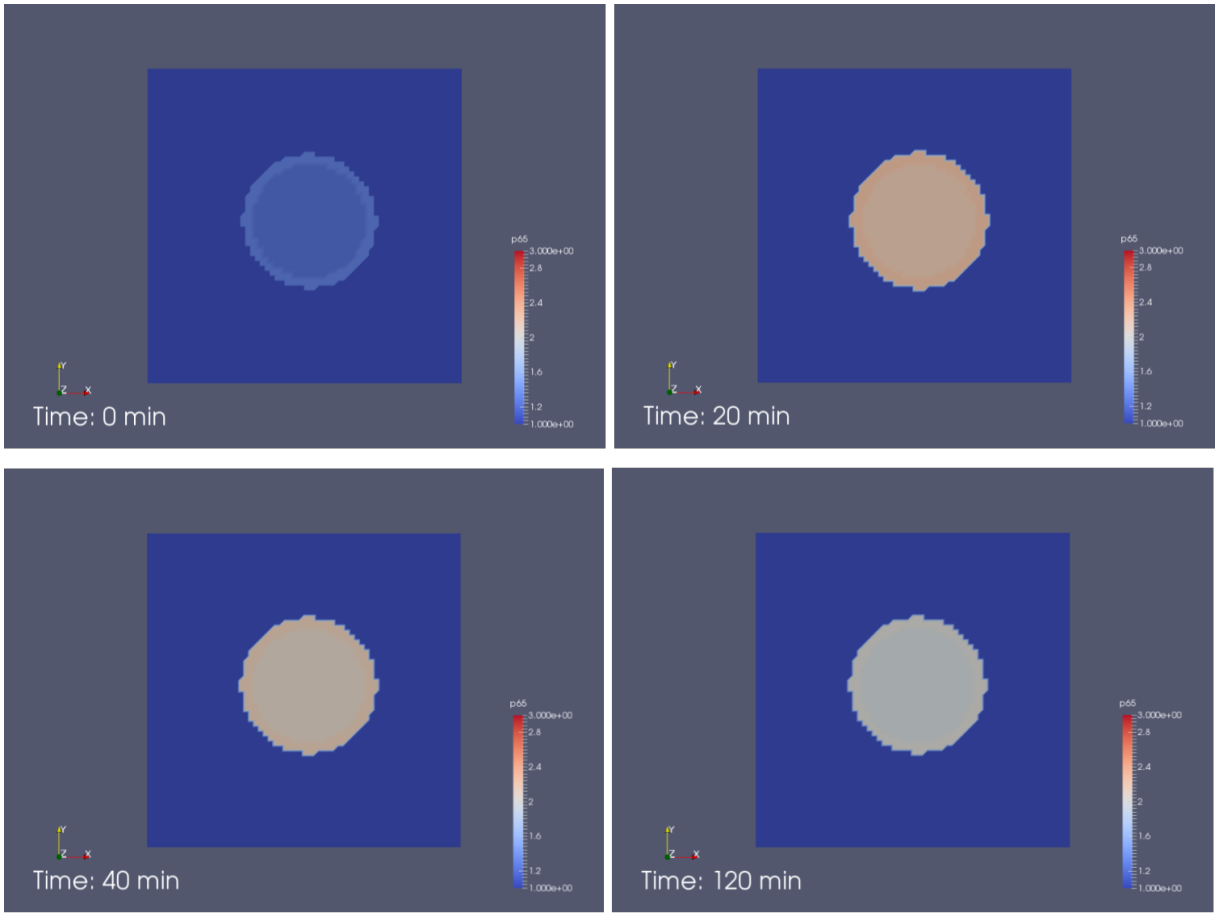

Figure 3.20: Simulations of the complete PDE model (left column) and images form the single cell microscopy experiments (right column). In the PDE model transport rates and diffusion coefficients were adjusted. TNF addition was simulated after the steady state is reached. p65 local concentrations for 0, 20, 40, 120 min are shown. A complete simulation video can be found on the supplementary DVD.

4 Discussion

NF-κB signalling is involved in cancer development and in inflammation, making it an important system to understand [93]. The details of its crosstalks, which become even more important during these complex processes with several cytokines and other stimuli activating cells, are far from being well understood [94]. With the population-based ODE-model the crosstalk to p38-MAPK signalling could be established as a feature of primary NF-κB signalling in primary hepatocytes.
Furthermore, the local cytokine concentrations that arise during inflammation were formerly unknown, as experimental procedures hinder their determination. By simulating, this situation with a model trained to describe quantitative time resolved data from diverse primary liver cell types we now have an estimate of the upper limit of concentrations occurring locally, which are surprisingly high (240 ng/ml TNF).
Third, the single cell analysis of HCCs has revealed that in these cells NF-κB does not oscillate without a stimulus addition, providing an important difference in hepatocyte specific NF-κB signalling and that of other cell types such as SK-N-AS. I have established a PDE model describing these dynamics and the NF-κB signalling pathway in detail in spatio-temporal resolution.

4.1 Crosstalks in NF-κB Signalling in Hepatocytes

Inflammation in the liver and the innate immune response are complex processes involving many cell types and cell-cell-communications via cytokines and chemokines [1]. During early LPS-induced inflammation TNF and interleukins, such as IL-1α, IL-1β, IL-6 are among the first cytokines produced by non-parenchymal liver cells [36]. TNF, IL-1, and IL-6-induced signalling results in acute phase protein production in hepaotcytes. TNF, IL-1α and IL-1β can act as stimuli to the cannonical NF-κappaαB pathway by binding to TNFR and IL-1 receptor (IL-1R) [95, 15]. IL-6 induces the JAK/STAT pathway [96, 97]. There are several cross links between these pathways e.g. via MAPK p38 [36].
Adiitionally, it has been suggested that NF-κB enhances STAT3 signalling transduciton, by complex formation of p65 and STAT3 [98, 38]. Many of the NF-κB and STAT3 target genes overlap, supporting this hypothesis [99]. To further investigate this cross-talk experiments with co-stimulation and stimulation with the individual cytokines could be done followed by cross-link chromatin immuno precipitaion (XChIP) assays [100]. Then one could investigate, if p65 and STAT3 are bound to genes simultaneously. Additionally, a comparison of micro-arrays of co-stimulated and cells stimulated with the individual cytokines could be compared. Micro-array results could then be further confirmed by RT-qPCR analysis.
In the conserved NF-κB pathway as described in the introduction the stimulus leads to an activation of IKKβ, which phosphorylates IκBα, thus targeting it for degradation and freeing NF-κB which can act as transcription factor in the nucleus for diverse genes. The modifications described by the

crosstalk to p38/MSK1 signalling do not alter this pathway, but the additional phosphorylation of p65 at serine 276 increases the NF-κB affinity for certain genes [101]. Here, I was able to validate the prediction made in my master thesis, that a second form of phosphorylated NF-κB is necessary to describe TNF-induced NF-κB signalling. Our experimental collaborators measured the concentration changes in phosphorylated p38 and MSK1. When substituting the unspecified placeholder reactions in the original model with p38 phosphorylation and MSK1 phosphorylation reactions that lead to NF-κB signalling and fitting only the parameters of these steps to the newly measured data, the model was able to capture all the prior data proving this a valid replacement for the original placeholder reactions. In summary the model predictions lead to new experimental measurements and brought new understanding of the systems regulation.
As it remains unclear how hepatocytes keep their ability to proliferate even as mature cells. It be would interesting to find out, if this phosphorylation of p65 and the according gene transcription profiles are relevant to this process. Future experiments could involve blocking this post-translational modification or analyzing, if other stimuli activating hepatocellular NF-κB signalling induce it as well.
Furthermore, p38 is involved in cancer development in some cases, most likely its activation has an inhibitory effect on cancer formation[102]. Thus including it in the model in this early stage allows further investigations to take the role of this crosstalk into account.
For a furhter analysis of crosstalks the role of IL-1 in hepatocyte NF-κB signlaing should be investigated. Hepatocytes express IL-1R [103], therefore a next step could be to extend the model, so that it describes IL-1-induced NF-κB signalling as well as TNF-induction and to compare the effects of the different stimuli on the NF-κB pathway. An ODE-based model describing IL-1R-induced signalling has been published [104]. The receptor and IL-1 interactions could easily be included in my model and used to analyze experimental data. This would especially be interesting, when combined with the integrative model and cytokine expression profiles form non-parenchymal cells for IL-1α and IL-1β secretion. Most likely the NF-κB-induction will induced stronger during inflammation when both cytokines are expressed.

4.2 Extending the *in vitro* Model to Capture Dose Responsiveness

The *in vivo* concentration of TNF varies, therefore, it is important to describe and understand TNF-induced NF-κB signalling not just for a single concentration but for a concentration range. The original *in vitro* hepatocyte model was trained with experimental data from primary hepatocytes stimulated with 10 ng/ml TNF only. However, varying the dose (0.1, 1, 10, 20, 50 ng/ml TNF) showed that the system has a strong saturation for higher stimuli (20, 50 ng/ml) and remains responsive even for the lowest dosage (0.1 ng/ml). The model as it was originally set up was not able to describe this data in full detail (even after re-parameterization), thus its topology and reaction

kinetics needed to be changed. Choosing the levels of detail to include in a model is an important decisions. My goal was to keep the model as accurate as possible with respect to knowledge from literature research and our collaborators experiments on biochemical reactions taking place and at the same time keep the model simple enough to understand and learn about the systems characteristics from the model.
Other models publised include three states of IKKβ, an activated, an inactivated, and an unactivated state [48]. Thus, I decided to try different model versions to see which described the data best. A model including IKKβ and an arbitrary TNF-induced post-translational modification inhibiting IKKβ activation did not describe the data sufficiently. This was not a proof that this does not take place in hepatocytes, it may very well take place, but including it in the model did not help with analyzing the dose responsive dynamics the system shows. However, including TNF receptor 1 (TNFR1) and modeling TNF uptake in the cell did work to describe the dose responsiveness of the protein measurements. Therefore, this model version was chosen for further simulations.
This is the first NF-κB model to include details on the signalling itself and the receptor level. Previous models included either the receptors level [81], or the details on the intra-cellular signalling [55]. The receptor number in this case turned out to be a crucial parameter in the model, as the number of receptors at the cell surface defines how much TNF can be detected by a cell at a specific point in time and how much TNF is needed to provoke NF-κB signalling in hepatocytes. It directly relates TNF concentrations in the medium or extracellular volume to the intracellular hepatocyte species concentrations. Especially, when simulating the TNF secretion from non-parenchymal cells this became of particular importance. Including the receptors as a part of the model additionally makes it feasible to use this model without further adaptations in pharmaco-kinetic/pharmaco-dynamic modeling [105].

4.2.1 Model Parameterization

The ODE-models of NF-κB signalling presented here have many parameters which cannot all be estimated accurately from the available experimental data. Therefore, I have used model ensembles. These are ensembles of several parameterizations of the same model topology that describe the experimental data equally well. As the parameter sets cover large ranges of the parameter space for the ill defined parameters it is likely that behaviour exhibited by all parameter sets in a model ensemble will be inherent to the true (unknown) parameterization, as it is independent of these ill-defined parameters. Therefore, the model ensembles allow predictions despite parameter non-identifiability.
Nevertheless, the parameter estimation can be rendered difficult, as parameter dependencies can lead to flat planes in target functions. In this particular work, it took up to a week to estimate all parameters of the *in vitro* hepatocyte model. Therefore, I reduced the complexity of the parameter estimation problem by excluding parameters based on their identifiabil-

ity. Using the Fisher Information Matrix to identify parameter identifiability is efficient with respect to computational cost, as it is already calculated in COPASI for each parameter estimation. Whereas, computing parameter sensitivities or the target function landscape with respect to every parameter on the other hand is rather computational cost intensive [45, 106, 107]. However, it is possible that the FIM does not reveal all parameter dependencies. Here the correlation matrix, the inverse of the FIM could be used instead [74]. However, in this work it proved sufficient to reduce only some of the parameters in the parameter estimation to reduce time for running the parameter estimation by more than factor two. Therefore, employing the FIM was a timely efficient and in the resulting model ensembles all parameter sets described the experimental data very well.
Experimental data used for parameter estimation contains unknown errors. To deal with these errors, some groups work with sophisticated error models, they calculate before running a parameter estimation on the experimental data [108], others include the error models as model parameters into the parameter estimation and estimate them together with the model parameters [59], others ignore it. For this work originally a multiplicative error as parameter was included to the model. As the model grew bigger over time, the parameter estimation problem grew bigger as well. At some point, it became too time consuming trying to estimate parameters and errors simultaneously for the model. Therefore, I have tried to combine data normalization and thus indirect error estimation, by using other parameters to describe the error. The solution I have found works for this specific type of model with the data available very well: a signal transduction model, which is assumed to be in a steady-state before stimulus addition, optimized against semi-quantitative data, describing relative concentration changes.
Calculating the scaling factor from the average initial experimental value and the steady state value may introduce an error, as the averaged initial experimental value may not represent the best initial value for the time-series simulation. Using the median instead of mean initial experimental values or estimating the scaling factor in the model together with the other parameters could overcome this potential problem. However, in this work the parameter estimation resulted in good fits without any of further modification and the reduced computational time made the chosen approach the best solution for this particular problem.

4.3 Modeling Liver Micro-Anatomy

The liver is a complex organ, with several cell types and different levels of anatomical structures. As described in the introduction in details, the lobules form larger lobes that than form the liver. It would not have been feasible to try to describe these anatomical structures in detail in this work. Luckily, on a micro-anatomical level liver lobules have a homologue distribution of cells and extra cellular structures. Hepatocytes form one to two cells thick layers around a sinusoid. The sinusoid is lined by liver resident endothelial cells (LSEC) which form so called fenestrae through which most blood

components can enter the Space of Disse between the LSEC and the hepatocytes. Within the sinusoids of one liver zone liver resident macrophages so called Kupffer Cells are distributed homogeneously. They can control the blood flow through the sinusoid, which is slow (270-410 μm/s [109]) compared to flow through other vessels (1500 μm/s [110]).
All these attributes of the liver make it feasible to assume that by compartmentalising the liver into small sections until looking at the immediate surroundings of a single hepatocyte, we can still describe the average behavior of all hepatocytes in the liver would show, if they were at an inflammatory core. Thus the average volumes of sinusoidal lumen and Space of Disse adjacent to a single liver cell were used to calculate the secretion profiles of TNF in response to LPS and the hepatocyte response to these estimated *in vivo* concentrations of TNF.

4.3.1 TNF Amounts in the Liver Versus in vitro

The TNF secretion levels from the non-parenchymal cells were measured per single cell. Yet in the liver these cells are not equally abundant. Thus the influence of the HSCs was weak compared to the influence of MCs or LSECs. Furthermore, the HSCs cytokine secretion was not increased by LPS addition, but remained constant. Thus, the HSCs were not included in the integrative liver model. If they had been included, the hepatocytes would have had to remain responsive to TNF despite a constitutive TNF level. With the model as it was trained, this would not have been explicable. It is unlikely that constitutive TNF levels are secreted by all non-parenchymal cells *in vivo*. Rather the constitutive TNF levels measured for all non-parenchymal cells *in vitro* are due to experimental procedures such as cell isolation and cultivation, which exert stress to the cells. Otherwise *in vivo* the hepatocytes would have to shut off the signalling response to low TNF levels until a certain threshold was reached, which could not be observed *in vitro*. This would require a more complex system then is currently known and would be more costly with respect to biosynthesis of cytokines and signalling molecules than simply not producing TNF under non-inflammatory or non-cancerous conditions. Therefore, it is biologically feasible to assume that no TNF is secreted from non-parenchymal cells *in vivo* in the absence of stimuli such as LPS. However, for the further analysis of my simulation results, it should be considered that HSCs might additionally increase the TNF levels during inflammation, despite that no induction was observed in the experiments presented here.

4.4 NF-κB Signalling in the Liver

MCs and LSECs secreting TNF simultaneously invoke the greatest hepatocyte response, although the *in vitro* experiments and model show a greater hepatocellular response in NF-κB signalling would be possible. The TNF values simulated can arise in the center of inflammation. 5 pg/ml LPS stimulation lead to more than 240 ng/ml TNF. Thus, they would only occur locally

and the average values measured for the entire liver as an organ would be much lower. Therefore it is not surprising that these values are above the measured TNF serum concentrations *in vivo* (5-43 ng/ml TNF [111, 112]).
In the *in vitro* experiments TNF was added in a fixed concentration to the medium. This set-up differs strongly from the *in vivo* processes. Here, TNF is secreted gradually from non-parenchymal cells, this secretion takes some time and does not result in a sudden exposure of hepatocytes to a very high dose of TNF, furthermore, the extracellular volume into which the non-parenchymal cells secrete TNF is several orders of magnitudes smaller than the *in vitro* volume of the medium into which the TNF is added in the *in vitro* experiments. Therefore, the *in vitro* concentration of TNF is much smaller than the *in vivo* concentrations, yet the *in vitro* particle numbers of TNF are much higher than the 440800 *in vivo* particle numbers (TNF *in vivo*: 240 ng/ml = 7640 particles, TNF *in vitro*: 10 ng/ml = 440800 particles). There are 2300 TNFR1 particles per hepatocyte, thus the amount of receptors which can bind free TNF is limited. In the *in vitro* experiments TNF can immediately bind to all available TNFR1s as there is immediately enough TNF available. In the *in vivo* simulations TNF becomes available gradually and thus only some of the TNFR1 receptors are bound at first. These are then internalized and TNF is internally degraded until the receptors are free again and can be recycled to the outer cell membrane. However, for the NF-κB signalling response the intact TNF:TNFR1 complex on the membrane is decisive and not the internalized, partly degraded forms. Thus, the NF-κB response in the *in vitro* experiments is much stronger than in the *in vivo* simulations, because secretion velocity of the non-parenchymal cells is limited and lead to limited TNF particles available in the first few hours.
This is an important result and new insight, as it shows that the mode of cytokine administration has a strong influence on the NF-κB response. Therefore, it may be worth wile to reconsider the way cytokines are administered in *in vitro* experiments, when investigating inflammation. It would make sense to use a pump to slowly increase the TNF levels, mimicking the TNF secretion profiles of non-parenchymal cells. Furthermore, the volumes of the medium could be reduced strongly to mimic the smaller extracellular *in vivo* volumes. Alternatively co-culture experiments with non-parenchymal cells and parenchymal cells would also help validate these results. However, these would most likely not be feasible with primary cells and thus it would be necessary to ensure that the TNF secretion in the non-parenchymal cell line and the NF-κB signalling in the hepatocyte cell line are not altered. Furthermore additional cytokines or chemokines produced by the non-parenchymal cells such as IL-1 may alter the NF-κB signalling. Therefore the model could be extended in a way that it includes responses to these cytokines as well.
Our results show that MCs and LSECs combined can invoke the largest response. However, TNF secreted by either cell type individually is more than sufficient to invoke a intra-hepatocellular response, even for very low dosages of LPS. As described above, the secretion velocity is the decisive parameter for the hepatocellular reaction strength. MCs secrete TNF slower than LSECs thus they invoke a less strong response. The secretion veloc-

ity can only be altered within certain ranges. Adding very high LPS concentrations thus cannot increase the TNF secretion velocity of the non-parenchymal cells beyond a certain speed and therefore, cannot lead to a stronger a hepatocyte response. However, by increasing the number or abundance of non-parenchymal cells in the liver, more cells could secrete TNF, TNF levels could increase faster, and this would lead to a stronger hepatocellular response.

4.5 Linking NF-κB Signalling During Inflammation to Cancer

Unresolved chronic inflammation in the liver leads to liver fibrosis which in turn leads to hepatocellular carcinomas [113]. The role of NF-κB signalling in hepatocytes can vary. Depending on the surrounding conditions permanently active NF-κB signalling can enhance or inhibit hepatocellular carcinoma formation [16]. Therefore, it is especially important to investigate NF-κB signalling in hepatocytes in a setting as close as possible to *in vivo* conditions. For the work presented here, I had the opportunity to work with experimental results from primary murine cells. Therefore, this model has the is different from many models of NF-κB signalling that exist [54, 47]. As these were all dervied from experimental data from carcinoma cell lines, where a potential modification of NF-κB signalling cannot be ruled out [114, 115].
However, under my guidance, Nicolas Huber was able to show that the differences in NF-κB signalling of investigated hepatocellular carcinoma cell lines (Hep56 and Hepa1-6) and hepatocytes can be explained by differential protein expression levels. This was an important step as not all experiments for this work could be carried out in primary cells. For the final single cell analysis protocol stably transfected cell lines were used. However, as parameter estimation for the PDE model is not feasible a pre-requisite to model this data was that the human hepatocellular carcinoma line on a population level follows the same dynamics as the primary murine hepatocytes the ODE model was trained against.
Additionally, under my guidance, Martin Zauser tried to link NF-κB siganling with the Hippo-YAP signalling. The Hippo-YAP pathway is known to be cruical to organ size control [39] and NF-κB signalling is a mayor player in cell fate decisions [116]. Although organ size control and cell fate should be linked, we were not able to find a connection between the NF-κB and the Hippo-YAP pathway. Our results indicate that most likely these pathways are co-regulated. To further understand how priming cells for proliferation by NF-κB signalling and organ size control are interlinked a more complete picture of other signaltransduction processes is necessary.

4.6 Single Cell Investigations and PDE Modeling

Single cell dynamics may not be identical to population-based dynamics. This is especially interesting as these effects may affect the way cells response to different stimuli administrations [54]. Other groups have observed that on the single cell level there are stochastic effects in the NF-κB pathway [117]. Some cells oscillate without stimulus and the amount of cells that oscillate depends on the cell types investigated. For example 30 % of HeLa cells and 70% of SK-N-AS cell oscilllate [49]. The cells are oscillating asynchronously in the absence of a stimulus and synchronous temporarily after stimulus addition. Thus, the average behavior measured in population-level experiments shows no oscillations without a stimulus.
In our experiments we found that HLE and HLF cells do not oscillate in the absence of TNF. Rather all p65 is in the cytoplasm and enters the nucleus only once in some cells twice upon TNF stimulation. This is a difference of NF-κB signalling in hepatocytes compared to other cell types. Thus the population-level experiments and the single cell experiments should have similar dynamics. However, in the single cell experiments we see that NF-κB remains longer in the nucleus (p65 has returned back to the cytoplasm after 180 min) than in the population experiments (p65 has returned back to the cytoplasm after 60 min). For the population-level experiments I had only one replicate of the experiment from hepatocytes. Therefore, I cannot completely rule out an experimental error in the data or a difference between dynamics in primary hepatocytes and HLE cells. On the other hand, the ODE model predictions are in good agreement with this experiment. Therefore, the difference may arise from the experimental set-up for measuring the nuclear fraction of p65. It may be that over-expression of p65 in the stably transfected HLE cells is the reason for the delayed return of p65 to the cytoplasm. If there is more NF-κB the IκBα concentration could also be up regulated and thus it may simply take longer until enough IκBα is reproduced and the system can return to its steady-state. An alternative explanation may be that the red fluorescent protein tagged to p65 may slow the nuclear export of the complex. Or the red fluorescent tag could reduce the transcription activator strength of p65.
In the PDE model changes were also necessary to describe the experiments qualitatively. It would not have been feasible to re-estimate the parameters for the biochemical-reactions, therefore, I was lucky that the single cell dynamics showed the same qualitative behaviour as the population-based dynamics. Otherwise, I would have needed to reparameterize the model so that it would be able to describe oscillations. Here, I used the parameters of biochemical-reactions estimated for the ODE-model [118]. However, the transcription rates of the ODE-model could not be used in the PDE model. In the PDE model as it is currently implemented the nuclear transport of molecules poses as problem. Currently there is no mathematically exact solution to this problem available in DUNE. Therefore, I decided to work with an overlap region.This region is defined as both nucleus and cytoplasm at the same time. This is not an accurate solution, however, it does approximate a membrane. In this region a nuclear species can become a cytoplasmic

species for example nuclear p65 can turned into cytoplasmic p65. The aspect of diffusion is already included in the PDE model, as a species needs to cross the overlap region to have crossed the membrane. Therefore, I considered only molecules in the cytoplasm out side of the overlap region as true cytoplasmic molecules. Essentially I need to ignore the species in the overlap region, as these are species in the membrane.
In the currently published spatio-temperal models of NF-κB signalling the diffusion factor for all proteins is assumed to be the same, although there are differences in the protein sizes (IκBα weighs approximately six times less than the IKK complex) and these will affect the diffusion coefficients [62, 63, 61, 64, 119]. My PDE model is the first to consider different diffusion coefficients for each species based on their molecular weight.
Further investigations in the PDE model could involve changing the ratio of nucleus to cytoplasm and changing the cell shape. In oscillating regimes of the model this has an influence on the oscillations[62]. However, these results were based on a 2D PDE where it was assumed that active IKK only appears at the outer edge of the cytoplasm. In *in vitro* experiments TNF is added the medium which has contact to the upper side of the cell and would thus be available to all parts of the cytoplasm of a 2D PDE model. Therefore the effect of the nuclear and cytoplasm size and shape should be reconsidered in a 3D PDE model describing the TNF addition and IKK activation more accurately. Furthermore, it would be worthwhile to simulate the cell in 3D and include the medium as an additional compartment on upper side of the cell and at same time limiting the area in which receptor complexes with TNFR1 and IKK can form to be close to the upper membrane. Furthermore it would be good to measure the diffusion coefficients of the main species in the NF-κB pathway with fluorescent recovery after photobleaching (FRAP) [120].
Additionally, the amount of cells which are responsive to TNF vary depending on the TNF dose, thus the average population level peak height is not the result of cells showing a less pronounced change in NF-κ localisation but rather the result of less cells being activated by TNF [117]. The PDE model to describe the single cell data was created based on the ODE model. The parameters for the biochemical reactions remained the same, a part from the transport reactions. If the population-based dynamics were the result of single cells acting differently, however canceling out each others effects in the population-based measurements this would have posed a great problem. However, in our data this was not the case, therefore and as parameter estimation for the PDE model was not feasible due to its large computational costs, it was valid to keep the parameters from the ODE model.
The diffusion coefficients of the individual species were unknown. They were calculated with a formula derived for spherical molecules in water was taken as an approximations. Cytoplasm and nucleoplasm are aqueous solutions, however, as the concept of molecular crowding illustrates there are more than just water molecules in cells. Additionally there are motor proteins moving cells a long cytoskeletal molecules such as myosines moving a long actin filaments. Some signalling molecules are mobile, such as NF-κB or its inhibitor, however, the signalsome or the recruited IKK-complex are less

mobile and rather rest in one place as soon as they are recruited. Therefore assuming spherical molecules moving in water is a very rough approximation. Our results showed that to describe the single cell measurements these estimated diffusion coefficients needed to be increase by a factor of 100.
The single cell data showed no spatial effects. All effects observed could be easily described with the compartmentalized ODE model. However, they did show that the hepatocellular carcinoma cell lines did not oscillate as apposed to other cell lines such as SK-N-AS, were the cells oscillated asynchronously in the absence of a stimulus and were synchronized when treated with e.g. TNF. These synchronized oscillations were then observable on a population-based level. The absence of these asynchronous oscillations still remains unclear. It may be that these cells are simply in a different state that the other so far investigated cells. An alternative explanation could be that most cells secrete TNF as a result of NF-κB signalling, however, hepatocytes do not. Maybe the secreted TNF acts autocrinely in other cell lines and this is the reason for the asynchronous oscillations.The current model would suggest that the cells are indifferent states. It is capable of oscillating in the absence of TNF, if the steady-state ratio of IκBα to p65 is changed. However a prolonged exposure to TNF would not lead to continuous oscillations. This could be validated by inhibiting TNF secretion in cell lines oscillating in the absence of a stimulus. If these cells continued to oscillate they would be in a different state than the hepatocellular cell lines analyzed here.

4.7 Concluding Remarks

In this work NF-κB signalling in hepatocytes was first investigated with population based measurements, describing its dose responsiveness and crosstalks to other pathways, such as MAPK and Hippo/YAP. It was found that the MAP-kinase p38 can induce NF-κB post-translational modification via MSK1, which is essential to accurately describe all kinetic data available for hepatocyte NF-κB signalling. Furthermore, NF-κB and Hippo/YAP signalling most likely share upstream co-regulation. The established hepatocyte ODE model was further used to validate, if NF-κB signalling is altered beyond varied protein expression in the hepato-caricinoma cell lines Hep56 and Hepa1-6. It could be shown, that altering the concentrations of proteins is sufficient for the ODE model to describe all kinetic data for both cell lines. The hepatocyte ODE model was used to described the effects of different non-parenchymal cells on hepatocytes in an integrative model of parenchymal and non-parenchymal cells. This model is the first to describe these different cell types of the liver. The results from these investigations show that TNF administration is decisive for the hepatocytes dynamic response and that the current experimental procedures, with a single high dose TNF administration are not in good correlation to the *in vivo* gradual TNF secretion from non-parenchymal secretion, thus the current *in vitro* measurements may not be good models of *in vivo* reactions. As a last step the ODE model was converted into a PDE model. Using microscopy images from newly established cell lines expression p65-RFP as reference it can be concluded that

the PDE simulations of the NF-κB model compare well to the TNF-induced p65 translocation.
Taking together these findings give new insight on regulation of NF-κB signalling in hepatocytes, the role of different non-parenchymal cells during inflammation, the high impact of cytokine administration on signalling and lead to the question if NF-κB oscillations in other cells arises from intrinsic factors or from autocrine or paracrine cytokine secretion.

Acknowledgments

I would like to thank Professor Doctor Ursula Kummer for her unlimited support and her great guidance and Professor Doctor Thomas Höfer for his valuable insight. Many thanks to Doctor Sven Sahle for the fruitful discussions and creative input, to Doctor Christoph Zimmer for providing an open ear to any kind of problem and a mathematical angle to a biologists ideas, to Doctor Frank Bergmann for his immediate solutions to any (un-)thinkable software problems, and to the entire Kummer group for all the funny and supportive lunch and coffee breaks, the open doors, and the great support. I would especially like to thank Doctor Kai Breuhahn, Doctor Federico Pinna, and Michaela Bissinger for a great collaboration open to new ideas and for providing me with more data than I could have ever dreamt of. Many thanks to my family and friends for their love an support.
I could not have done this without the help of each and every one of you.

References

[1] Craig N Jenne and Paul Kubes. Immune surveillance by the liver. *Nat Immunol*, 14(10):996–1006, Oct 2013.

[2] Masahito Nagaki and Hisataka Moriwaki. Implication of cytokines: Roles of tumor necrosis factor-α in liver injury. *Hepatology Research*, 38:S19–S28, 2008.

[3] R. Lüllmann-Rauch. *Taschenlehrbuch Histologie*. Thieme, 2006.

[4] *The Liver: Biology and Pathobiolgy*. John Wiley & Sons, Ltd, 2009.

[5] A Blouin, R P Bolender, and E R Weibel. Distribution of organelles and membranes between hepatocytes and nonhepatocytes in the rat liver parenchyma. a stereological study. *J Cell Biol*, 72(2):441–55, Feb 1977.

[6] Melanie J. Scott and Timothy R. Billiar. β2-integrin-induced p38 mapk activation is a key mediator in the cd14/tlr4/md2-dependent uptake of lipopolysaccharide by hepatocytes. *Journal of Biological Chemistry*, 283(43):29433–29446, 2008.

[7] Meihong Deng, Melanie J Scott, Patricia Loughran, Gregory Gibson, Chhinder Sodhi, Simon Watkins, David Hackam, and Timothy R Billiar. Lipopolysaccharide clearance, bacterial clearance, and systemic inflammatory responses are regulated by cell type-specific functions of tlr4 during sepsis. *J Immunol*, 190(10):5152–60, May 2013.

[8] Robert F Schwabe, Ekihiro Seki, and David A Brenner. Toll-like receptor signaling in the liver. *Gastroenterology*, 130(6):1886–900, May 2006.

[9] Andy Wullaert, Geert van Loo, Karen Heyninck, and Rudi Beyaert. Hepatic tumor necrosis factor signaling and nuclear factor-κb: effects on liver homeostasis and beyond. *Endocr Rev*, 28(4):365–86, Jun 2007.

[10] Marcos Rojkind and Karina Reyes-gordillo. *Hepatic Stellate Cells*. John Wiley & Sons, Ltd, 2009.

[11] Christian Ehlting, Natalia Ronkina, Oliver Böhmer, Ute Albrecht, Konrad A Bode, Karl S Lang, Alexey Kotlyarov, Danuta Radzioch, Matthias Gaestel, Dieter Häussinger, and Johannes G Bode. Distinct functions of the mitogen-activated protein kinase-activated protein (mapkap) kinases mk2 and mk3: Mk2 mediates lipopolysaccharide-induced signal transducers and activators of transcription 3 (stat3) activation by preventing negative regulatory effects of mk3. *J Biol Chem*, 286(27):24113–24, Jul 2011.

[12] Robin Fraser, Victoria C Cogger, Bruce Dobbs, Hamish Jamieson, Alessandra Warren, Sarah N. Hilmer, and David G. Le Couteur. The liver sieve and atherosclerosis. *Pathology*, 44(3):181–186, 2008.

[13] Eddie Wisse, Filip Braet, Luo Dianzhong, Ronald De Zanger, Danny Jans, Evelyne Crabbe, and An Vermoesen. Structure and function of sinusoidal lining cells in the liver. *Toxicologic Pathology*, 24(1):100–111, 1996.

[14] Laurie D. Deleve. *The Hepatic Sinusoidal Endothelial Cell: Morphology, Function, and Pathobiology*. John Wiley & Sons, Ltd, 2009.

[15] Bastian Hoesel and Johannes A. Schmid. The complexity of nf-κb signaling in inflammation and cancer. *Molecular Cancer*, 12(1):1–15, 2013.

[16] Tom Luedde and Robert F Schwabe. Nf-κb in the liver—linking injury, fibrosis and hepatocellular carcinoma. *Nature reviews. Gastroenterology & hepatology*, 8(2):108–118, 02 2011.

[17] Giuseppina Bonizzi and Michael Karin. The two nf-κb activation pathways and their role in innate and adaptive immunity. *Trends in Immunology*, 25(6):280 – 288, 2004.

[18] Hailing Hsu, Jessie Xiong, and David V. Goeddel. The {TNF}, receptor 1-associated protein {TRADD}, signals cell death and nf-κb activation. *Cell*, 81(4):495 – 504, 1995.

[19] Hailing Hsu, Hong-Bing Shu, Ming-Gui Pan, and David V Goeddel. Tradd-traf2 and tradd-fadd interactions define two distinct {TNF}, receptor 1 signal transduction pathways. *Cell*, 84(2):299 – 308, 1996.

[20] Gioacchino Natoli, Antonio Costanzo, Angelo Ianni, Dennis J. Templeton, James R. Woodgett, Clara Balsano, and Massimo Levrero. Activation of sapk/jnk by tnf receptor 1 through a noncytotoxic traf2-dependent pathway. *Science*, 275(5297):200–203, 1997.

[21] Thomas H. Lee, Jennifer Shank, Nicole Cusson, and Michelle A. Kelliher. The kinase activity of rip1 is not required for tumor necrosis factor-α-induced iκb kinase or p38 map kinase activation or for the ubiquitination of rip1 by traf2. *Journal of Biological Chemistry*, 279(32):33185–33191, 2004.

[22] Matthew S. Hayden and Sankar Ghosh. Regulation of nf-κb by {TNF}, family cytokines. *Seminars in Immunology*, 26(3):253 – 266, 2014. The {TNF}, family - challenges ahead.

[23] Petrus J. W. Naudé, Johan A. den Boer, Paul G. M. Luiten, and Ulrich L. M. Eisel. Tumor necrosis factor receptor cross-talk. *FEBS Journal*, 278(6):888–898, 2011.

[24] Ranjan Sen and David Baltimore. Multiple nuclear factors interact with the immunoglobulin enhancer sequences. *Cell*, 46(5):705 – 716, 1986.

[25] Grigory Ryzhakov, Ana Teixeira, David Saliba, Katrina Blazek, Tatsushi Muta, Jiannis Ragoussis, and Irina A. Udalova. Cross-species analysis reveals evolving and conserved features of the nuclear factor κb (nf-κb) proteins. *Journal of Biological Chemistry*, 288(16):11546–11554, 2013.

[26] Dev Bhatt and Sankar Ghosh. Regulation of the nf-κb-mediated transcription of inflammatory genes. *Frontiers in Immunology*, 5(71), 2014.

[27] Vincent Feng-Sheng Shih, Rachel Tsui, Andrew Caldwell, and Alexander Hoffmann. A single nfκb system for both canonical and non-canonical signaling. *Cell research*, 21(1):86–102, January 2011.

[28] Leen Catrysse, Lars Vereecke, Rudi Beyaert, and Geert van Loo. A20 in inflammation and autoimmunity. *Trends in immunology*, 35(1):22 – 31, January 2014.

[29] Marie Cargnello and Philippe P. Roux. Activation and function of the mapks and their substrates, the mapk-activated protein kinases. *Microbiology and Molecular Biology Reviews*, 75(1):50–83, 2011.

[30] Eirini Kefaloyianni, Catherine Gaitanaki, and Isidoros Beis. Erk1/2 and p38-mapk signalling pathways, through msk1, are involved in nf-κb transactivation during oxidative stress in skeletal myoblasts. *Cellular Signalling*, 18(12):2238 – 2251, 2006.

[31] Linda Vermeulen, Gert De Wilde, Petra Van Damme, Wim Vanden Berghe, and Guy Haegeman. Transcriptional activation of the nf-κb p65 subunit by mitogen- and stress-activated protein kinase-1 (msk1). *The EMBO Journal*, 22(6):1313–1324, 2003.

[32] Chien-Huang Lin, Chung-Hung Shih, and Bing-Chang Chen. Thrombin-induced il-8/cxcl8 release is mediated by ck2, msk1, and nf-κb pathways in human lung epithelial cells. *European Journal of Pharmacology*, 767:135 – 143, 2015.

[33] Angeles Duran, Marìa T. Diaz-Meco, and Jorge Moscat. Essential role of rela ser311 phosphorylation by ζpkc in nf-κb transcriptional activation. *The EMBO Journal*, 22(15):3910–3918, 2003.

[34] Patrick Viatour, Marie-Paule Merville, Vincent Bours, and Alain Chariot. Phosphorylation of nf-kappab and ikappab proteins: implications in cancer and inflammation. *Trends in biochemical sciences*, 30(1):43–52, January 2005.

[35] Harald Wajant and Peter Scheurich. Tnfr1-induced activation of the classical nf-κb pathway. *FEBS Journal*, 278(6):862–876, 2011.

[36] Johannes G. Bode, Ute Albrecht, Dieter HÃd'ussinger, Peter C. Heinrich, and Fred Schaper. Hepatic acute phase proteins - regulation by il-6- and il-1-type cytokines involving {STAT3}, and its crosstalk with nf-κb-dependent signaling. *European Journal of Cell Biology*, 91(6-7):496 – 505, 2012. Molecular mechanisms of cytokin-mediated inflammatory processes: Signal transduction and pathophysiological consequences.

[37] Peter C. HEINRICH, Iris BEHRMANN, Gerhard MÜLLER-NEWEN, Fred SCHAPER, and Lutz GRAEVE. Interleukin-6-type cytokine signalling through the gp130/jak/stat pathway. *Biochemical Journal*, 334(2):297–314, 1998.

[38] S. Lafarge, H. Hamzeh-Cognasse, Y. Richard, B. Pozzetto, M. CognÃl', F. Cognasse, and O. Garraud. Complexes between nuclear factor-κb p65 and signal transducer and activator of transcription 3 are key actors in inducing activation-induced cytidine deaminase expression and immunoglobulin a production in cd40l plus interleukin-10-treated human blood b cells. *Clinical & Experimental Immunology*, 166(2):171–183, 2011.

[39] Stefano Piccolo, Sirio Dupont, and Michelangelo Cordenonsi. The biology of yap/taz: Hippo signaling and beyond. *Physiological Reviews*, 94(4):1287–1312, 2014.

[40] Carsten Gram Hansen, Toshiro Moroishi, and Kun-Liang Guan. Yap and taz: a nexus for hippo signaling and beyond. *Trends in Cell Biology*, 25(9):499–513, 2016/02/23 XXXX.

[41] Linda Petzold. Automatic selection of methods for solving stiff and nonstiff systems of ordinary differential equations. *SIAM Journal on Scientific and Statistical Computing*, 4(1):136–148, 1983.

[42] Christopher P. Fall, Eric S. Marland, and John M. Wagner. *Computational Cell Biology*. Springer, Berlin, February 2002.

[43] Jeremy Gunawardena. *Models in Systems Biology: The Parameter Problem and the Meanings of Robustness*, pages 19–47. John Wiley & Sons, Inc., 2010.

[44] Z. Zi. Sensitivity analysis approaches applied to systems biology models. *Systems Biology, IET*, 5(6):336–346, Nov 2011.

[45] Andreas Raue, Johan Karlsson, Maria Pia Saccomani, Mats Jirstrand, and Jens Timmer. Comparison of approaches for parameter identifiability analysis of biological systems. *Bioinformatics*, 30(10):1440–1448, 2014.

[46] Franco Carlotti, Steven K. Dower, and Eva E. Qwarnstrom. Dynamic shuttling of nuclear factor κb between the nucleus and cytoplasm as a consequence of inhibitor dissociation. *Journal of Biological Chemistry*, 275(52):41028–41034, 2000.

[47] Alexander Hoffmann, Andre Levchenko, Martin L Scott, and David Baltimore. The iκb-nf-κb signaling module: temporal control and selective gene activation. *Science*, 298(5596):1241–5, Nov 2002.

[48] Tomasz Lipniacki, Pawel Paszek, Allan R. Brasier, Bruce Luxon, and Marek Kimmel. Mathematical model of nf-κb regulatory module. *Journal of Theoretical Biology*, 228(2):195 – 215, 2004.

[49] D. E. Nelson, A. E. C. Ihekwaba, M. Elliott, J. R. Johnson, C. A. Gibney, B. E. Foreman, G. Nelson, V. See, C. A. Horton, D. G. Spiller, S. W. Edwards, H. P. McDowell, J. F. Unitt, E. Sullivan, R. Grimley, N. Benson, D. Broomhead, D. B. Kell, and M. R. H. White. Oscillations in nf-κb signaling control the dynamics of gene expression. *Science*, 306(5696):704–708, 2004.

[50] Bing Tian, David E. Nowak, and Allan R. Brasier. A tnf-induced gene expression program under oscillatory nf-κb control. *BMC Genomics*, 6(1):1–18, 2005.

[51] F. Hayot and C. Jayaprakash. - oscillations and cell-to-cell variability. *Journal of Theoretical Biology*, 240(4):583 – 591, 2006.

[52] Tomasz Lipniacki, Pawel Paszek, Allan R. Brasier, Bruce A. Luxon, and Marek Kimmel. Stochastic regulation in early immune response. *Biophysical Journal*, 90(3):725 – 742, 2006.

[53] Ellen L O'Dea, Derren Barken, Raechel Q Peralta, Kim T Tran, Shannon L Werner, Jeffrey D Kearns, Andre Levchenko, and Alexander Hoffmann. A homeostatic model of iκb metabolism to control constitutive nf-κb activity. *Molecular Systems Biology*, 3(1):n/a–n/a, 2007.

[54] Louise Ashall, Caroline A Horton, David E Nelson, Pawel Paszek, Claire V Harper, Kate Sillitoe, Sheila Ryan, David G Spiller, John F Unitt, David S Broomhead, Douglas B Kell, David A Rand, Violaine Sée, and Michael R H White. Pulsatile stimulation determines timing and specificity of nf-κb-dependent transcription. *Science*, 324(5924):242–6, Apr 2009.

[55] Raymond Cheong, Alexander Hoffmann, and Andre Levchenko. Understanding nf-κb signaling via mathematical modeling. *Molecular Systems Biology*, 4(192), 2008.

[56] Janina Mothes, Dorothea Busse, Bente Kofahl, and Jana Wolf. Sources of dynamic variability in nf-κb signal transduction: A mechanistic model. *BioEssays*, 37(4):452–462, 2015.

[57] Yunjiao Wang, Pawel Paszek, Caroline A Horton, Douglas B Kell, Michael Rh White, David S Broomhead, and Mark R Muldoon. Interactions among oscillatory pathways in nf-kappa b signaling. *BMC Syst Biol*, 5:23, 2011.

[58] Jaewook Joo, Steve Plimpton, Shawn Martin, Laura Swiller, and Jean-Loup Faulon. Sensitivity analysis of a computational model of the ikk-nf-κb-iκbα-a20 signal transduction network. *Annals of the New York Academy of Sciences*, 1115(1):221–239, 2007.

[59] Federico Pinna, Sven Sahle, Katharina Beuke, Michaela Bissinger, Selcan Tuncay, Lorenz A D'Alessandro, Ralph Gauges, Andreas Raue, Jens Timmer, Ursula Klingmüller, Peter Schirmacher, Ursula Kummer, and Kai Breuhahn. A systems biology study on nfκb signaling in primary mouse hepatocytes. *Front Physiol*, 3:466, 2012.

[60] Mohammad Fallahi-Sichani, Matthew A. Schaller, Denise E. Kirschner, Steven L. Kunkel, and Jennifer J. Linderman. Identification of key processes that control tumor necrosis factor availability in a tuberculosis granuloma. *PLoS Comput Biol*, 6(5):e1000778, 05 2010.

[61] Daisuke Ohshima, Jun-ichiro Inoue, and Kazuhisa Ichikawa. Roles of spatial parameters on the oscillation of nuclear nf-κb: Computer simulations of a 3d spherical cell. *PLoS ONE*, 7(10):e46911, 10 2012.

[62] Alan J. Terry and Mark A.J. Chaplain. Spatio-temporal modelling of the intracellular signalling pathway: The roles of diffusion, active transport, and cell geometry. *Journal of Theoretical Biology*, 290:7 – 26, 2011.

[63] Alan J. Terry. A minimal spatio-temporal model of the nf- κb signalling pathway exhibits a range of behaviours. *Bulletin of Mathematical Biology*, 76(10):2363–2388, 2014.

[64] Daisuke Ohshima and Kazuhisa Ichikawa. Regulation of nuclear nf-κb oscillation by a diffusion coefficient and its biological implications. *PLoS ONE*, 9(10):e109895, 10 2014.

[65] Ross Ihaka and Robert Gentleman. R: A language for data analysis and graphics. *Journal of Computational and Graphical Statistics*, 5(3):299–314, 1996.

[66] Stefan Hoops, Sven Sahle, Ralph Gauges, Christine Lee, Jürgen Pahle, Natalia Simus, Mudita Singhal, Liang Xu, Pedro Mendes, and Ursula Kummer. COPASI, – a COmplex PAthway SImulator. *Bioinformatics*, 22(24):3067–74, Dec 2006.

[67] Markus Blatt and Peter Bastian. The iterative solver template library. In gström Bo Kå, Erik Elmroth, Jack Dongarra, and Jerzy Waśniewski, editors, *Applied Parallel Computing. State of the Art in Scientific Computing*, volume 4699 of *Lecture Notes in Computer Science*, pages 666–675. Springer, 2007.

[68] P. Bastian, M. Blatt, A. Dedner, C. Engwer, R. Klöfkorn, M. Ohlberger, and O. Sander. A Generic Grid Interface for Parallel and Adaptive Scientific Computing. Part I,: Abstract Framework. *Computing*, 82(2–3):103–119, 2008.

[69] A. Dedner, R. Klöfkorn, M. Nolte, and M. Ohlberger. A Generic Interface for Parallel and Adaptive Scientific Computing: Abstraction Principles and the DUNE-FEM Module. *Computing*, 90(3–4):165–196, 2010.

[70] Anne Carpenter, Thouis Jones, Michael Lamprecht, Colin Clarke, In Kang, Ola Friman, David Guertin, Joo Chang, Robert Lindquist, Jason Moffat, Polina Golland, and David Sabatini. Cellprofiler: image analysis software for identifying and quantifying cell phenotypes. *Genome Biology*, 7(10):R100, 2006.

[71] Deyan Luan, Fania Szlam, Kenichi A. Tanaka, Philip S. Barie, and Jeffrey D. Varner. Ensembles of uncertain mathematical models can identify network response to therapeutic interventions. *Mol. BioSyst.*, 6:2272–2286, 2010.

[72] Jaewook Joo, Steven J. Plimpton, and Jean-Loup Faulon. Statistical ensemble analysis for simulating extrinsic noise-driven response in nf-κb signaling networks. *BMC Systems Biology*, 7(1):1–18, 2013.

[73] Bryan C Daniels, Yan-Jiun Chen, James P Sethna, Ryan N Gutenkunst, and Christopher R Myers. Sloppiness, robustness, and evolvability in systems biology. *Current Opinion in Biotechnology*, 19(4):389 – 395, 2008. Protein technologies / Systems biology.

[74] Karol Nienałtowski, Michał Włodarczyk, Tomasz Lipniacki, and Michał Komorowski. Clustering reveals limits of parameter identifiability in multi-parameter models of biochemical dynamics. *BMC Systems Biology*, 9(1):1–9, 2015.

[75] Duojia Pan. Hippo signaling in organ size control. *Genes & Development*, 21(8):886–897, 2007.

[76] Damian Szklarczyk, Andrea Franceschini, Stefan Wyder, Kristoffer Forslund, Davide Heller, Jaime Huerta-Cepas, Milan Simonovic, Alexander Roth, Alberto Santos, Kalliopi P Tsafou, Michael Kuhn, Peer Bork, Lars J Jensen, and Christian von Mering. String v10: protein-protein interaction networks, integrated over the tree of life. *Nucleic acids research*, 43(Database issue):D447–52, January 2015.

[77] F. C. Bernstein, T. F. Koetzle, G. J. Williams, E. F. Meyer, M. D. Brice, J. R. Rodgers, O. Kennard, T. Shimanouchi, and M. Tasumi. The P,rotein D,ata B,ank. A, computer-based archival file for macromolecular structures. *Eur J Biochem*, 80(2):319–324, November 1977.

[78] Minoru Kanehisa and Susumu Goto. Kegg: Kyoto encyclopedia of genes and genomes. *Nucleic Acids Research*, 28(1):27–30, 2000.

[79] Brian S. Robinson and Kenneth H. Moberg. Cell-cell junctions: α-catenin and e-cadherin help fence in yap1. *Current Biology*, 21(21):R890 – R892, 2011.

[80] Lisa Dietz and Albert Sickmann. *Protocols in In Vitro Hepatocyte Research*. Springer New York, New York, NY, 2015.

[81] Mohammad Fallahi-Sichani, Mohammed El-Kebir, Simeone Marino, Denise E. Kirschner, and Jennifer J. Linderman. Multiscale computational modeling reveals a critical role for tnf-α receptor 1 dynamics in tuberculosis granuloma formation. *The Journal of Immunology*, 2011.

[82] Thomas Höfer, Holger Nathansen, Max Löhning, Andreas Radbruch, and Reinhart Heinrich. Gata-3 transcriptional imprinting in th2 lymphocytes: A mathematical model. *Proceedings of the National Academy of Sciences*, 99(14):9364–9368, 2002.

[83] Helena Firczuk, Shichina Kannambath, Jürgen Pahle, Amy Claydon, Robert Beynon, John Duncan, Hans Westerhoff, Pedro Mendes, and John EG McCarthy. An in vivo control map for the eukaryotic mrna translation machinery. *Molecular Systems Biology*, 9(1), 2013.

[84] B. Hat, K. Puszynski, and T. Lipniacki. Exploring mechanisms of oscillations in p53 and nuclear factor-κb systems. *Systems Biology, IET*, 3(5):342–355, September 2009.

[85] Marina S Dietz, Franziska Fricke, Carmen L Krüger, Hartmut H Niemann, and Mike Heilemann. Receptor-ligand interactions: binding affinities studied by single-molecule and super-resolution microscopy on intact cells. *Chemphyschem*, 15(4):671–6, Mar 2014.

[86] Nicola C Martin, Christian T McCullough, Peter G Bush, Linda Sharp, Andrew C Hall, and David J Harrison. Functional analysis of mouse hepatocytes differing in dna content: volume, receptor expression, and effect of ifngamma. *J Cell Physiol*, 191(2):138–44, May 2002.

[87] Katerina Vlantis and Manolis Pasparakis. Role of tnf in pathologies induced by nuclear factor kappab deficiency. *Curr Dir Autoimmun*, 11:80–93, 2010.

[88] Harold P Erickson. Size and shape of protein molecules at the nanometer level determined by sedimentation, gel filtration, and electron microscopy. *Biol Proced Online*, 11:32–51, 2009.

[89] I. Dor, M. Namba, and J. Sato. Establishment and some biological characteristics of human hepatoma cell lines. *Gan*, 66(4):385–392, Aug 1975.

[90] Myo T. Tyn and Todd W. Gusek. Prediction of diffusion coefficients of proteins. *Biotechnology and Bioengineering*, 35(4):327–338, 1990.

[91] José Braga, James G. McNally, and Maria Carmo-Fonseca. A reaction-diffusion model to study {RNA}, motion by quantitative fluorescence recovery after photobleaching. *Biophysical Journal*, 92(8):2694 – 2703, 2007.

[92] Harvey F. Lodish, Arnold Berk, Lawrence Zipursky, Paul Matsudaira, David Balitmore, and James Darnell. *Molecular Cell Biology*. W.H. Freeman and Company, 2000.

[93] Kim Newton and Vishva M. Dixit. Signaling in innate immunity and inflammation. *Cold Spring Harbor Perspectives in Biology*, 4(3), 2012.

[94] Catherine Brenner, Lorenzo Galluzzi, Oliver Kepp, and Guido Kroemer. Decoding cell death signals in liver inflammation. *Journal of Hepatology*, 59(3):583 – 594, 2013.

[95] Maureen Shuh, Humberto Bohorquez, George E. Loss Jr., and Ari J. Cohen. Tumor necrosis factor-α: Life and death of hepatocytes during liver ischemia/reperfusion injury. *The Ochsner Journal*, 13(1):119–130, 2013.

[96] Markus F. Neurath and Susetta Finotto. Il-6 signaling in autoimmunity, chronic inflammation and inflammation-associated cancer. *Cytokine & Growth Factor Reviews*, 22(2):83 – 89, 2011.

[97] Pasquale Sansone and Jacqueline Bromberg. Targeting the interleukin-6/jak/stat pathway in human malignancies. *Journal of Clinical Oncology*, 30(9):1005–1014, 2012.

[98] Ute Albrecht, Xiangping Yang, Rosanna Asselta, Verena Keitel, Maria Luisa Tenchini, Stephan Ludwig, Peter C. Heinrich, Dieter HÃd'ussinger, Fred Schaper, and Johannes G. Bode. Activation of nf-κb by il-1β blocks il-6-induced sustained {STAT3}, activation and stat3-dependent gene expression of the human Îş-fibrinogen gene. *Cellular Signalling*, 19(9):1866 – 1878, 2007.

[99] Yasuhiro Yoshida, Arvind Kumar, Yoshinobu Koyama, Haibing Peng, Ahmet Arman, Jason A. Boch, and Philip E. Auron. Interleukin 1 activates stat3/nuclear factor-κb cross-talk via a unique traf6- and p65-dependent mechanism. *Journal of Biological Chemistry*, 279(3):1768–1776, 2004.

[100] Philippe Collas. The current state of chromatin immunoprecipitation. *Molecular Biotechnology*, 45(1):87–100, 2010.

[101] Ana Cuadrado and Angel R. Nebreda. Mechanisms and functions of p38 mapk signalling. *Biochemical Journal*, 429(3):403–417, 2010.

[102] Erwin F. Wagner and Angel R. Nebreda. Signal integration by jnk and p38 mapk pathways in cancer development. *Nat Rev Cancer*, 9(8):537–549, Aug 2009.

[103] Kazufumi Sujita, Fumio Okuno, Yoshiya Tanaka, Yoshiaki Hirano, Yoshito Inamoto, Sumiya Eto, and Masao Arai. Effect of interleukin 1 (il-1) on the levels of cytochrome p-450 involving il-1 receptor on the isolated hepatocytes of rat. *Biochemical and Biophysical Research Communications*, 168(3):1217 – 1222, 1990.

[104] Johannes Witt, Sandra Barisic, Oliver Sawodny, Michael Ederer, Dagmar Kulms, and Thomas Sauter. Modeling time delay in the nfκb signaling pathway following low dose il-1 stimulation. *EURASIP journal on bioinformatics & systems biology*, 2011(1):3, 2011.

[105] Iris Rajman. Pk/pd modelling and simulations: utility in drug development. *Drug Discovery Today*, 13(7-8):341 – 346, 2008.

[106] Eva Balsa-Canto and Julio R. Banga. Amigo, a toolbox for advanced model identification in systems biology using global optimization. *Bioinformatics*, 2011.

[107] A.E.C. Ihekwaba, D.S. Broomhead, R.L. Grimley, N. Benson, and D.B. Kell. Sensitivity analysis of parameters controlling oscillatory signalling in the nf-kbpathway: the roles of ikk and ikbalpha. *Systems Biology, IEE Proceedings*, 1(1):93–103, June 2004.

[108] Valentina Raia, Marcel Schilling, Martin BÃűhm, Bettina Hahn, Andreas Kowarsch, Andreas Raue, Carsten Sticht, Sebastian Bohl, Maria Saile, Peter MÃűller, Norbert Gretz, Jens Timmer, Fabian Theis, Wolf-Dieter Lehmann, Peter Lichter, and Ursula KlingmÃijller. Dynamic mathematical modeling of il13-induced signaling in hodgkin and primary mediastinal b-cell lymphoma allows prediction of therapeutic targets. *Cancer Research*, 71(3):693–704, 2011.

[109] E Wisse, R B De Zanger, K Charels, P Van Der Smissen, and R S McCuskey. The liver sieve: considerations concerning the structure and function of endothelial fenestrae, the sinusoidal wall and the space of disse. *Hepatology*, 5(4):683–92, 1985.

[110] G J Tangelder, D W Slaaf, A M Muijtjens, T Arts, M G oude Egbrink, and R S Reneman. Velocity profiles of blood platelets and red blood cells flowing in arterioles of the rabbit mesentery. *Circulation Research*, 59(5):505–14, 1986.

[111] K Krawczyk, P Szczesniak, A Kumor, A Jasinska, A Omulecka, M Pietruczuk, D Orszulak-Michalak, S Sporny, and E Malecka-Panas. Adipohormones as prognostric markers in patients with nonalcoholic steatohepatitis (nash). *J Physiol Pharmacol*, 60 Suppl 3:71–5, Oct 2009.

[112] Ainhoa Fernández-Yunquera, Cristina Ripoll, Rafael Bañares, Marta Puerto, Diego Rincón, Ismael Yepes, Vega Catalina, and Magdalena Salcedo. Everolimus immunosuppression reduces the serum expression of fibrosis markers in liver transplant recipients. *World J Transplant*, 4(2):133–40, Jun 2014.

[113] Paloma Sanz-Cameno, María Trapero-Marugán, María Chaparro, Evan Anthony Jones, and Ricardo Moreno-Otero. Angiogenesis: From chronic liver inflammation to hepatocellular carcinoma. *Journal of Oncology*, 2010:272170, 2010.

[114] Kai Breuhahn, Gregory Gores, and Peter Schirmacher. Strategies for hepatocellular carcinoma therapy and diagnostics: lessons learned from high throughput and profiling approaches. *Hepatology*, 53(6):2112–21, Jun 2011.

[115] Liang Qiao, Hongxia Zhang, Jun Yu, Rona Francisco, Paul Dent, Matthias P. A. Ebert, Christoph Röcken, and Geoffrey Farrell. Constitutive activation of nf-κb in human hepatocellular carcinoma: Evidence of a cytoprotective role. *Human Gene Therapy*, 17(3):280–290, Mar 2006.

[116] Michelle L Chaisson, John T Brooling, Warren Ladiges, Sophia Tsai, and Nelson Fausto. Hepatocyte-specific inhibition of nf-kappab leads to apoptosis after tnf treatment, but not after partial hepatectomy. *J Clin Invest*, 110(2):193–202, Jul 2002.

[117] Savas Tay, Jacob J. Hughey, Timothy K. Lee, Tomasz Lipniacki, Stephen R. Quake, and Markus W. Covert. Single-cell nf-κb dynamics reveal digital activation and analogue information processing. *Nature*, 466(7303):267–271, Jul 2010.

[118] Elfriede Friedmann, Andrea C. Pfeifer, Rebecca Neumann, Ursula Klingmüller, and Rolf Rannacher. *Model Based Parameter Estimation: Theory and Applications*, chapter Interaction Between Experiment, Modeling and Simulation of Spatial Aspects in the JAK2/STAT5 Signaling Pathway, pages 125–143. Springer Berlin Heidelberg, Berlin, Heidelberg, 2013.

[119] Daisuke Ohshima and Kazuhisa Ichikawa. Regulation of nf-κb oscillation by nuclear transport: Mechanisms determining the persistency and frequency of oscillation. *PLoS ONE*, 10(6):e0127633, 06 2015.

[120] Maria Anna Rapsomaniki, Eugenio Cinquemani, Nickolaos Nikiforos Giakoumakis, Panagiotis Kotsantis, John Lygeros, and Zoi Lygerou. Inference of protein kinetics by stochastic modeling and simulation of fluorescence recovery after photobleaching experiments. *Bioinformatics*, 31(3):355–362, 2015.

[121] Matthias Grell, Harald Wajant, Gudrun Zimmermann, and Peter Scheurich. The type 1 receptor (cd120a) is the high-affinity receptor for soluble tumor necrosis factor. *Proceedings of the National Academy of Sciences*, 95(2):570–575, 1998.

A Appendix

List of Figures

List of Tables

Abbreviations

TNF	tumor necrosis factor
TNFR	TNF receptor
LPS	lipopolysaccharide
TLR	toll-like-receptor
IL	interleukin
IL-1R	interleukin 1 receptor
NF-κB	B-cell nuclear factor κB
IκB	NF-κB inhibitor
IKK	IκB kinase
Nemo	NF-κB essential modulator
A20	Tumor necrosis factor alpha-induced protein 3
IAP	inhibitor of apoptosis protein
cIAP	cellular IAP
BRIC	Baculoviral IAP repeat-containing protein
TRADD	TNFR-associated death domain protein
FADD	Fas-associated death domain protein
TRAF	TNFR associated factor
RIPK1	receptor-interacting serine/threonine-protein kinase 1
TGF	transforming growth factor
TAK1	TGFβ-activated kinase 1
TAB	TAK1 associated binding protein
p38	Mitogen-activated protein kinase 14
JNK	c-Jun N-terminal kinase
MSK	mitogen- and stress-activated kinase
Ser	serine
PKC	protein kinase C
CK	caseine kinase
CREB	cyclic AMP-response element-binding protein
CBP	CREB-binding protein
HDAC	histone deacetylase
gp130	glycoprotein 130
JAK	canus kinase
STAT	signal transducer and activator of transcription
SOCS	suppressor of cytokine signalling
Hippo	serine/threonine-protein kinase hippo
YAP	Yes-associated protein
MST	Mammalian STE20-like protein kinase
Sav	salvador homolog
LATS	large tumor suppressor homolog
MOB	MPS one binder kinase activator-like
TAZ	Tafazzin
TEAD	TEA domain family member
SMAD	smad family protein
NF2	neurofirbromatosis type 2
Heps	hepatocytes
LSEC	liver sinusoidal endothelial cells

HSC	hepatocellular stellate cells
MC	liver marcrophages
EL	extra cellular lumen
RFP	red fluorescent protein
ODE	ordinary differential equation
PDE	partial differential equation
RT-qPCR	reverse transcription quantitative polymerase chain reaction
ELISA	enzyme-linked immunosorbent assay
ChIP	Chromatin immunoprecipitation
cyt	cytoplasm
nuc	nucleus
ass	association
diss	dissociation
exp	export
imp	import
degr	degradation
phos	phosphorylation
dephos	dephosphorylation
transc	transcription
transl	translation
transc_i	transcription initiation
transc_e	transcription elongation
mR	mRNA

A.1 Experimental Data

Table A.1: Western immunoblot measurements of the principal NF-κB pathway components from primary murine hepatocytes treated with 10 ng/ml TNF.

Time in min	p65 in arb. units	p-p65 in arb. units	IκBα in arb. units	p-IκBα in arb. units
0	100.00		131.82	152.31
5	79.79		100.72	161.04
10	104.71		74.64	380.29
20	73.22		25.18	168.16
40	90.88		48.31	250.30
60	104.29		107.49	358.91
120	75.37		128.37	248.22
180	105.54		109.63	226.91
240	57.61		94.96	231.43
0	56.59	42.73	99.89	
5	68.08	41.16	82.33	
10	73.95	610.54	36.25	
20	68.48	358.93	7.90	
40	60.17	168.82	23.24	
60	66.30	168.77	74.87	
120	44.80	113.59	126.00	
180	62.95	112.37	114.83	
240	72.53	68.30	49.02	
0	47.70	43.26	85.05	
5	42.96	77.20	95.68	
10	48.96	312.89	61.58	
20	80.43	358.04	19.32	
40	90.17	134.25	32.02	
60	63.04	88.02	78.59	
120	9.90	82.71	134.50	
180	32.76	73.94	94.50	
240				

Table A.2: Western immunoblot measurements of the principal NF-κB pathway components from primary murine hepatocytes treated with 10 ng/ml TNF, continued .

Time in min	p65 in arb. units	p-p65 in arb. units	IκBα in arb. units	p-IκBα in arb. units
0	43.36	83.66	71.16	
5	50.55	73.39	83.16	
10	74.67	291.99	66.77	
20	75.40	346.71	27.00	
40	72.77	162.77	25.11	
60	59.92	130.88	73.82	
120	37.20	94.11	129.08	
180	40.87	78.02	119.93	
240	37.19	155.95	106.49	
0	69.77	126.09	88.21	144.03
5	53.25	186.27	87.98	612.71
10	64.92	390.01	29.38	414.96
20	65.38	190.80	10.28	137.18
40	59.78	141.20	42.82	144.88
60	72.09	113.99	83.95	248.78
120	59.57	110.63	130.66	174.51
180	53.84	126.70	103.05	158.31
240	72.43	134.63	101.54	114.72
0	46.20	57.19	89.03	134.97
5	34.35	132.62	113.05	159.32
10	36.25	355.01	61.91	444.46
20	49.17	282.06	18.78	133.19
40	73.02	171.70	28.46	168.13
60	65.21	150.84	75.69	312.44
120	94.86	225.75	124.12	302.59
180	59.96	203.48	82.36	235.67
240	95.65	76.39	97.75	121.57
0	41.35	157.94	98.36	138.27
5	55.48	169.08	118.55	174.55
10	52.80	390.78	64.37	513.58
20	48.67	207.71	18.39	117.02
40	73.33	58.61	22.18	56.91
60	68.70	67.33	77.80	152.29
120	44.90	90.46	114.07	223.40
180	49.33	17.62	72.28	140.01
240				

Table A.3: Western immunoblot measurements of the principal NF-κB pathway components from primary murine hepatocytes treated with 10 ng/ml TNF, continued .

Time in min	p65 in arb. units	p-p65 in arb. units	IκBα in arb. units	p-IκBα in arb. units
0		105.51	77.80	55.65
5		204.26	75.30	275.05
10		316.43	59.00	532.52
20		213.33	23.28	98.43
40		187.12	28.23	120.58
60		173.17	76.62	150.10
120			127.26	201.91
180			121.89	210.13
240			132.68	140.86
0	65.15	123.40	81.63	187.13
5	68.33	138.77	93.50	368.36
10	60.34	411.77	47.89	411.55
20	61.64	177.53	30.95	241.55
40	54.28	82.59	40.04	167.06
60	84.89	154.34	118.85	400.54
120	61.18	116.12	107.66	165.40
180	42.83	60.60	84.13	168.28
240	46.03	22.53	70.09	329.27

Table A.4: Western immunoblot measurements of phospho-p38, phospho-JNK, and phospho-MSK1 from primary murine hepatocytes treated with 10 ng/ml TNF.

Time in min	p-MSK1 in arb. units	p-p38 in arb. units	p-JNK in arb. units
0			0.567531736
5			1.00863806
10			1.715031255
20			1.603915653
40			0.814274814
60			0.908020218
120			0.889970256
180			0.833002587
240			1.045993857
0	0.57593767	0.850443549	0.643737004
5	1.150723464	1.289479964	1.046253984
10	1.881588367	1.419104346	1.74080456
20	1.387433846	1.300109093	1.438627616
40	1.139204711	0.96957664	1.036920318
60	0.794793984	0.847606624	0.59758753
120	0.687669578	0.842222958	0.659065857
180	0.637563	0.599861535	0.716991354
240	0.793642109	0.954413725	0.740610256
0	0.726754954	0.795615538	0.834281982
5	0.906263428	1.361767847	0.902137282
10	1.492754676	1.57041044	1.551975182
20	0.901902898	1.077660313	0.853243123
40	0.702772041	0.880048592	0.830677533
60	1.219494813	0.822416451	0.911495542
120	0.872105945	0.708597005	0.936355724
180	0.930973096	0.874938637	1.027428104
240	1.198418919	0.835722361	1.14542291

Table A.5: Western immunoblot measurements from primary murine hepatocytes treated with 0.1, 1, 10, 20, 50 ng/ml TNF, Experiment 1.

Time in min	TNF in ng/ml	p-p65 in arb. units	IκBα in arb. units	p65 in arb. units	p-IκBα in arb. units
0	0.1	0.57	1.31	1.58	0.43
5	0.1	1.17	1.39	1.64	0.72
10	0.1	0.83	1.12	1.44	0.43
20	0.1	1.00	0.92	1.10	0.41
40	0.1	1.09	0.84	1.41	0.43
60	0.1	0.76	0.95	0.91	0.30
120	0.1	0.74	0.97	0.75	0.36
0	1	0.57	1.31	1.58	0.43
5	1	1.02	0.76	1.09	1.13
10	1	1.14	0.90	1.45	2.03
20	1	0.97	0.39	1.12	0.55
40	1	0.62	0.43	1.06	0.45
60	1	0.51	0.87	1.08	0.48
120	1	0.56	1.44	1.19	0.66
0	10	0.57	1.31	1.58	0.43
5	10	1.63	0.63	1.11	2.44
10	10	1.87	0.53	0.86	1.37
20	10	1.38	0.25	0.97	0.42
40	10	1.39	0.76	1.04	0.74
60	10	1.04	1.67	0.86	0.63
120	10	1.03	2.11	0.84	0.70
0	20	0.57	1.31	1.58	0.43
5	20	2.12	0.80	1.43	3.46
10	20	1.60	0.48	1.23	2.07
20	20	0.93	0.15	1.10	0.33
40	20	0.73	0.37	1.17	0.57
60	20	0.61	0.97	1.03	0.51
120	20	0.54	1.21	1.35	0.81
0	50	0.57	1.31	1.58	0.43
5	50	3.19	1.03	0.93	2.76
10	50	3.33	0.43	0.96	1.30
20	50	2.23	0.20	0.72	0.16
40	50	1.83	0.77	0.64	0.49
60	50	1.64	2.45	1.09	0.79
120	50	1.36	2.57	0.38	0.88

Table A.6: Western immunoblot measurements from primary murine hepatocytes treated with 0.1, 1, 10, 20, 50 ng/ml TNF, Experiment 2.

Time in min	TNF in ng/ml	p-p65 in arb. units	IκBα in arb. units	p65 in arb. units	p-IκBα in arb. units
0	0.1	0.60	1.43	1.16	0.44
5	0.1	1.03	1.46	1.28	1.00
10	0.1	0.67	1.50	1.28	0.45
20	0.1	0.94	1.23	1.52	0.73
40	0.1	0.50	1.12	1.34	0.54
60	0.1	0.73	1.30	1.39	
120	0.1	0.46	0.95	0.78	
0	1	0.60	1.43	1.16	0.44
5	1	1.14	0.76	0.86	1.20
10	1	1.40	0.81	0.89	1.26
20	1	1.48	0.40	1.40	0.61
40	1	0.94	0.56	1.38	0.65
60	1	0.76	0.86	0.94	
120	1	0.59	1.97	1.01	
0	10	0.60	1.43	1.16	0.44
5	10	2.99	0.62	1.10	2.93
10	10	2.43	0.33	0.82	1.43
20	10	0.94	0.13	1.15	0.46
40	10	0.62	0.60	1.18	0.97
60	10	0.53	1.37	1.09	
120	10	0.55	1.65	0.90	
0	20	0.60	1.43	1.16	0.44
5	20	1.92	0.85	1.27	2.85
10	20	2.66	0.40	1.02	1.99
20	20	0.96	0.16	1.18	0.42
40	20	0.70	0.44	0.98	0.86
60	20	0.53	1.10	0.91	
120	20	0.64	1.54	0.89	
0	50	0.60	1.43	1.16	0.44
5	50	2.38	0.65	1.06	2.74
10	50	1.99	0.22	0.81	0.99
20	50	0.74	0.10	1.13	0.30
40	50	1.06	0.48	1.22	0.83
60	50	0.56	1.47	1.01	
120	50	0.84	1.98	1.37	

Table A.7: Reverse transcription, quantitative PCR measurements of IκBα mRNA from primary murine hepatocytes treated with 10 ng/ml TNF.

Time in min	IκBα mRNA in arb. Units Exp. 1	Exp. 2	Exp. 3
0	1	1.25	0.95
5	1.24	1.15	1.15
10	1.10	1.14	1.34
20	1.14	1.43	1.99
40	4.76	5.53	5.61
60	6.489	6.22	6.63
120	3.88	3.68	2.87
180	4.56	3.41	2.82
240			3.342

Table A.8: Reverse transcription, quantitative PCR measurements from primary murine hepatocytes treated with 0.1, 1, 10, 20, 50 ng/ml TNF.

Time in min	TNF in ng/ml	IκBα mRNA in arb. units	TNFa in ng/ml	IκBα mRNA in arb. units	TNFa in ng/ml	IκBα mRNA in arb. units
0	0.1	0.25	1	0.25	10	0.25
5	0.1	0.14	1	0.20	10	0.29
10	0.1	0.14	1	0.26	10	0.26
20	0.1	0.20	1	0.29	10	0.41
40	0.1	0.39	1	0.65	10	1.66
60	0.1	0.74	1	1.30	10	2.60
120	0.1	0.52	1	3.57	10	1.12
180	0.1	0.48	1	0.69	10	1.07
240	0.1	0.37	1	0.54	10	0.80
0	20	0.25	50	0.25		
5	20	0.26	50	0.26		
10	20	0.20	50	0.19		
20	20	0.41	50	0.46		
40	20	1.66	50	2.15		
60	20	2.21	50	2.25		
120	20	1.32	50	1.39		
180	20	1.15	50	1.07		
240	20	1.21	50	0.87		

Table A.9: TNF LUMINEX measurements from primary murine liver sinusoidal endothelial cells treated with diverse LPS concentrations.

Time in min	LPS in ng/ml	TNF in ng/cell Exp. 1	TNF in ng/cell Exp. 2	TNF in ng/cell Exp. 3
180	0	3.29E-07	3.29E-07	1.17E-06
360	0	3.43E-07	7.43E-07	1.17E-06
720	0	7.43E-07	1.17E-06	7.43E-07
1080	0	0.00E+00	3.29E-07	2.03E-06
1440	0	3.29E-07	3.29E-07	0.00E+00
180	1	3.29E-07	3.29E-07	2.03E-06
360	1	3.29E-07	0.00E+00	1.17E-06
720	1	2.46E-06	8.67E-07	1.89E-06
1080	1	1.17E-06	1.17E-06	2.90E-06
1440	1	0.00E+00	3.29E-07	0.00E+00
180	10	3.29E-07	3.79E-06	2.46E-06
360	10	2.46E-06	3.54E-07	2.90E-06
720	10	4.08E-06	2.90E-06	5.59E-06
1080	10	4.69E-06	6.05E-06	5.59E-06
1440	10	6.05E-06	4.69E-06	4.69E-06
180	50	2.90E-06	5.59E-06	3.79E-06
360	50	5.59E-06	5.59E-06	6.03E-06
720	50	4.69E-06	6.94E-06	9.23E-06
1080	50	1.02E-05	6.98E-06	9.48E-06
1440	50	7.97E-06	7.40E-06	5.59E-06
180	100	2.90E-06	2.18E-06	2.90E-06
360	100	5.59E-06	5.05E-06	6.49E-06
720	100	5.80E-06	8.31E-06	9.23E-06
1080	100	6.49E-06	7.40E-06	6.49E-06
1440	100	8.61E-06	9.42E-06	1.11E-05

Table A.10: TNF LUMINEX measurements from primary murine hepatic stellate cells treated with diverse LPS concentrations.

Time in min	LPS in ng/ml	TNF in ng/cell Exp. 1	TNF in ng/cell Exp. 2	TNF in ng/cell Exp. 3
0	0	6.09E-06	5.69E-06	7.69E-06
120	0	5.84E-06	4.08E-06	8.76E-06
360	0	3.32E-06	3.02E-06	1.12E-05
1440	0	3.44E-06	3.44E-06	6.81E-06
0	10	2.22E-05	2.22E-05	2.22E-05
120	10	5.48E-06	5.12E-06	6.92E-06
360	10	3.93E-06	4.87E-06	8.12E-06
1440	10	5.94E-06	5.10E-06	1.50E-05
0	50	6.09E-06	5.69E-06	7.69E-06
120	50	4.42E-06	5.48E-06	8.02E-06
360	50	6.15E-06	8.12E-06	1.09E-05
1440	50	5.66E-06	6.53E-06	7.61E-05
0	100	6.09E-06	5.69E-06	7.69E-06
120	100	6.56E-06	5.12E-06	4.42E-06
360	100	4.55E-06	5.83E-06	3.18E-05
1440	100	1.20E-05	6.53E-06	3.64E-05

Table A.11: TNF LUMINEX measurements from primary murine bone marrow-derived macrophages treated with diverse LPS concentrations.

Time in min	LPS in ng/ml	TNF in ng/cell Exp. 1	TNF in ng/cell Exp. 2
0	10	3.41E-08	3.10E-08
120	10	1.06E-06	8.75E-07
180	10	2.05E-06	1.47E-06
240	10	3.26E-06	2.06E-06
360	10	3.95E-06	2.89E-06
420	10	3.80E-06	2.98E-06
480	10	3.74E-06	2.99E-06
960	10	7.77E-06	5.91E-06
1440	10	7.73E-06	8.09E-06
0	50	3.41E-08	3.10E-08
120	50	1.07E-06	8.54E-07
180	50	2.24E-06	1.98E-06
240	50	3.23E-06	2.62E-06
360	50	6.00E-06	4.18E-06
420	50	5.82E-06	4.31E-06
480	50	6.36E-06	4.90E-06
960	50	1.03E-05	1.09E-05
1440	50	1.21E-05	9.20E-06
0	100	3.41E-08	3.10E-08
120	100	1.12E-06	9.68E-07
180	100	2.05E-06	2.04E-06
240	100	2.98E-06	3.17E-06
360	100	7.04E-06	5.10E-06
420	100	8.09E-06	5.46E-06
480	100	7.81E-06	4.90E-06
960	100	1.07E-05	1.12E-05
1440	100	1.20E-05	1.03E-05

Table A.12: Western immunoblot measurements from Hep56 treated with 10 ng/ml TNF.

time in min	p65 in arb. u.	p-p65 in arb. u.	IkBa in arb. u.	p-IkBa in arb. u.	p38 in arb. u.	p-p38 in arb. u.	MSK in arb. u.	JNK in arb. u.	p-JNK in arb. u.
0	1.00	1.00	1.00	1.00	1.00	1.00	1.00	1.00	1.00
5	0.50	2.48	0.70	2.79	0.59	1.98	0.66	0.79	1.82
10	0.50	3.11	0.38	2.98	0.70	2.03	0.98	0.98	2.57
20	1.14	0.96	0.32	1.74	0.83	2.07	0.75	0.93	2.34
40	0.66	1.61	0.76	3.56	0.84	1.71	0.69	0.82	2.19
60	0.21	1.48	0.85	4.16	0.85	1.68	0.51	0.93	2.12
120	0.45	1.02	0.60	3.75	0.67	1.41	0.65	0.92	1.88
180	1.43	1.70	0.93	3.21	0.81	1.69	0.72	1.08	2.36
240	1.94	2.23	0.83	3.74	1.04	1.53	1.49	1.50	2.67
300	1.08	2.99	0.76	3.75	1.01	1.53	1.11	1.38	2.65
360	1.45	2.78	0.65	2.66	0.88	1.46	1.48	1.45	2.52
420	1.36	2.54	0.56	1.69	1.07	1.43	1.73	1.53	2.42
480	0.74	4.85	0.50	2.12	0.92	1.00	1.11	1.25	1.92
0	0.88	2.32	0.79	1.02	0.46	1.93	1.09	1.10	2.07
5	0.66	1.79	0.77	3.09	0.50	2.19	0.46	0.49	2.15
10	0.60	3.36	0.88	3.64	0.55	1.92	0.71	0.79	2.38
20	0.79	1.62	0.42	1.66	0.58	0.98	0.37	0.46	1.54
40	0.36	1.64	0.28	3.27	0.69	0.82	0.80	1.12	1.23
60	0.57	1.39	0.53	2.72	0.75	0.97	0.48	0.60	1.86
120	0.55	1.43	0.56	3.02	0.86	0.99	0.78	1.07	1.86
180	0.61	1.35	0.68	2.38	0.87	0.78	0.50	0.73	2.35
240	1.26	2.14	0.59	2.45	1.06	1.17	0.96	1.04	2.07
300	1.27	2.21	0.61	2.17	0.97	1.19	0.96	0.97	2.05
360	1.50	1.57	0.47	2.49	0.88	1.02	1.38	1.53	2.27
420	1.24	2.33	0.49	1.58	0.76	1.26	1.35	1.49	2.34
480	1.24	2.80	0.40	2.21	1.28	1.51	1.11	1.33	1.09

Table A.13: Western immunoblot measurements from Hep56 treated with 10 ng/ml TNF.

time in min	p65 in arb. u.	p-p65 in arb. u.	IkBa in arb. u.	p-IkBa in arb. u.	p38 in arb. u.	p-p38 in arb. u.	MSK in arb. u.	JNK in arb. u.	p-JNK in arb. u.
0	0.65	1.11	0.62	2.28	0.76	0.91	0.66	1.10	0.71
5	0.75	2.57	0.65	2.00	0.75	1.53	0.64	1.17	0.94
10	0.56	3.70	0.39	2.03	0.71	2.20	0.53	0.96	2.42
20	0.66	1.26	0.19	2.51	0.68	1.97	0.54	0.97	2.27
40	0.90	2.35	0.51	3.23	0.83	1.56	0.37	0.89	1.88
60	0.75	1.56	0.88	2.60	0.78	1.26	0.73	1.14	2.08
120	0.80	1.37	0.85	1.88	0.77	1.53	0.38	0.89	1.39
180	0.87	2.00	0.58	1.54	0.76	1.32	0.32	0.88	2.10
240	0.93	1.42	0.66	1.71	0.95	0.90	0.58	0.92	2.42
300	1.05	2.15	0.51	2.63	0.83	0.86	1.51	1.20	2.06
360	1.09	1.51	0.57	0.54	0.87	0.93	1.42	1.16	2.29
420	1.49	2.46	0.43	4.02	1.03	1.16	1.03	1.08	2.80
480	1.32	1.72	0.64	2.83	0.91	0.62	1.40	1.13	1.36
0		0.95	0.44		0.60	1.74	0.64	0.93	1.63
5		0.98	0.56		0.65	1.69	0.69	0.86	1.60
10		2.76	0.48		0.75	1.93	0.67	0.97	2.49
20		1.77	0.38		0.64	1.04	0.61	0.94	2.02
40		1.83	0.37		0.71	1.17	0.72	0.97	1.16
60		1.68	0.60		0.64	1.38	0.68	1.09	1.35
120		1.24	0.81		0.74	1.00	0.67	1.03	1.59
180		2.26	0.99		0.82	1.15	1.11	1.25	1.51
240		1.91	0.58		0.80	1.11	0.79	1.01	1.47
300		2.19	0.62		0.84	1.38	0.98	1.10	2.18
360		2.08	0.59		1.21	1.35	0.97	1.14	2.26
420		3.40	0.67		0.89	1.18	1.54	1.21	3.13
480		2.36	0.43		1.11	1.49	1.05	1.10	2.38

Table A.14: Reverse transcription, quantitative PCR measurements from Hep56 treated with 10 ng/ml TNF.

time in min	p65 mRNA in arb. units	IkBa mRNA in arb. units
0	1	1
5	0.75	0.79
10	0.83	1.11
20	0.81	5.59
40	1.39	17.14
60	1.22	13.48
120	1.19	6.35
180	0.85	4.49
240	1.56	5.71
300	1.31	4.89
360	1.2	4.49
420	1.32	4.57
480	1.19	3.89
0	1.05	1.02
5	0.80	0.76
10	0.84	1.02
20	0.82	1.14
40	0.92	8.33
60	1.00	14.48
120	1.17	5.40
180	1.37	7.52
240	1.28	6.46
300	1.16	4.31
360	1.37	5.74
420	1.23	5.22
480	1.34	5.58
0	0.84	0.85
5	0.80	0.78
10	0.80	0.84
20	0.74	3.02
40	1.05	13.98
60	1.13	10.17
120	1.17	8.45
180	1.35	5.92
240	1.31	6.08
300	1.34	5.61
360	1.23	3.41
420	1.40	5.15
480	1.18	4.80

Table A.15: Western immunoblot measurements from Hepa1-6 treated with 10 ng/ml TNF.

time min	p65 arb. u.	p-p65 arb. u.	IkBa arb. u.	p-IkBa arb. u.	p38 arb. u.	p-p38 arb. u.	MSK arb. u.	JNK arb. u.	p-JNK arb. u.
0	1.00	1.00	1.00	1.00	1.00	1.00	1.00	1.00	1.00
5	0.30	2.88	0.53	3.16	0.75	11.66	0.65	0.87	1.93
10	0.64	4.54	0.24	1.45	1.05	18.92	1.13	1.07	6.21
20	0.49	1.29	0.23	0.25	1.24	9.97	1.16	1.11	7.62
40	0.50	1.54	0.86	2.53	1.14	6.06	0.91	1.02	3.20
60	0.33	1.17	3.21	1.63	2.08	3.70	1.06	1.03	2.08
120	0.59	1.36	1.62	1.55	1.35	2.51	1.27	1.11	2.09
180	0.67	1.79	1.55	1.12	1.40	2.65	1.97	1.25	2.08
240	0.78	1.53	1.33	1.56	1.21	2.24	1.75	1.18	2.18
300	1.12	2.02	1.18	1.24	1.48	2.66	2.54	1.23	1.99
360	1.20	1.90	1.10	0.96	1.80	2.02	2.09	1.31	2.14
420	0.93	1.87	0.82	1.01	1.44	1.71	2.81	1.24	1.89
480	0.96	2.37	0.81	0.85	1.98	1.13	2.31	1.27	1.98
0	0.49	0.75	0.83	0.45	1.03	1.33	0.20	0.19	4.36
5	0.28	3.27	0.24	3.34	0.86	14.52	0.43	0.42	3.52
10	0.45	3.03	0.09	0.30	0.96	15.96	0.76	0.82	3.34
20	0.42	1.01	0.17	0.32	1.09	6.75	0.78	0.63	2.94
40	0.45	1.51	1.74	1.29	1.16	2.94	0.56	0.55	0.94
60	0.32	1.00	1.91	1.02	1.16	2.81	0.90	0.87	0.56
120	0.37	1.32	1.18	0.95	1.18	3.03	0.80	0.64	0.87
180	0.42	1.33	0.95	0.71	1.18	2.24	0.86	0.67	0.30
240	0.63	1.43	0.95	0.54	1.36	2.49	0.82	0.66	1.28
300	0.87	1.88	0.94	0.56	1.44	1.76	1.63	1.08	0.43
360	1.04	1.86	0.88	0.77	1.56	2.35	1.13	0.86	1.10
420	0.81	1.61	0.80	0.77	1.35	1.66	0.83	0.76	0.45
480	1.18	1.71	0.81	0.71	1.75	1.78	1.60	0.91	0.33

Table A.16: Western immunoblot measurements from Hepa1-6 treated with 10 ng/ml TNF.

time min	p65 arb. u.	p-p65 arb. u.	IkBa arb. u.	p-IkBa arb. u.	p38 arb. u.	p-p38 arb. u.	MSK arb. u.	JNK arb. u.	p-JNK arb. u.
0	0.55	1.12	1.33	0.96	1.43	0.96	1.35	0.84	1.09
5	0.52	4.19	0.27	1.65	1.35	16.51	0.92	0.72	2.93
10	0.44	2.74	0.06	0.47	1.39	14.08	1.14	0.72	5.50
20	0.44	0.83	0.17	0.51	1.36	5.18	0.76	0.66	4.06
40	0.37	1.32	1.79	2.43	1.28	3.17	1.15	0.72	1.61
60	0.31	0.76	1.86	1.73	1.15	2.66	0.78	0.58	0.98
120	0.47	1.02	1.25	0.98	1.38	2.93	1.04	0.69	1.16
180	0.61	1.25	1.05	1.06	1.41	2.38	0.89	0.67	1.05
240	0.60	1.14	0.82	0.76	1.16	2.27	0.95	0.82	1.62
300	0.68	0.90	0.64	1.02	0.99	1.91	0.96	0.79	0.98
360	0.82	1.32	0.76	0.64	0.70	2.02	0.74	0.81	1.19
420	0.96	1.95	0.78	0.96	0.60	1.66	1.04	0.93	2.03
480	1.21	1.57	0.65	1.20	1.23	1.76	0.72	0.89	1.29
0	0.34	2.06	2.33	0.93	1.18	0.88	2.24	1.76	0.97
5	0.34	3.66	0.14	1.60	0.93	12.58	0.27	0.25	1.74
10	0.42	1.28	0.06	0.42	1.25	18.73	0.93	0.63	6.13
20	0.60	0.97	0.10	0.96	1.09	5.41	0.18	0.22	3.05
40	0.29	0.92	0.92	1.89	0.98	1.78	0.41	0.43	1.11
60	0.55	1.20	1.99	1.76	1.10	1.39	0.17	0.22	1.45
120	0.99	0.69	0.62	1.28	0.95	1.35	0.18	0.21	1.98
180	0.49	1.31	0.58	1.16	1.24	0.88	0.57	0.35	1.53
240	0.31	1.04	0.44	0.72	0.92	0.77	0.25	0.19	1.06
300	0.38	1.56	0.48	0.66	1.32	0.61	0.60	0.44	0.80
360	0.62	1.40	0.42	0.78	1.62	0.60	0.22	0.24	0.55
420	0.67	2.19	0.48	0.97	1.68	0.50	0.56	0.74	2.39
480	1.30	2.15	0.48	1.55	1.64	0.45	0.17	0.25	0.42

Table A.17: Reverse transcription, quantitative PCR measurements from Hepa1-6 treated with 10 ng/ml TNF.

time min	p65 mRNA arb. u.	IkBa mRNA arb. u.
0	1.00	1.00
5	0.69	0.71
10	0.78	1.30
20	0.92	6.61
40	1.37	36.86
60	1.57	34.40
120	1.78	11.27
180	2.39	11.79
240	2.05	9.07
300	2.02	7.60
360	2.82	9.53
420	1.95	6.66
480	2.56	9.13
0	0.99	1.69
5	0.80	1.56
10	0.91	3.67
20	1.16	15.48
40	1.14	35.15
60	1.99	16.16
120	2.31	17.94
180	1.91	11.36
240	1.45	7.21
300	2.94	13.56
360	1.48	6.08
420	1.57	6.88
480	1.63	6.49
0	1.13	1.76
5	1.12	2.18
10	1.32	6.70
20	1.09	19.06
40	1.47	35.37
60	1.78	13.30
120	2.61	16.71
180	1.89	11.44
240	1.48	8.42
300	1.78	7.68
360	1.98	7.39
420	1.43	5.80
480	2.06	6.71

A.2 TNF/NF-κB and Hippo/YAP Crosstalk Found by Martin Zauser

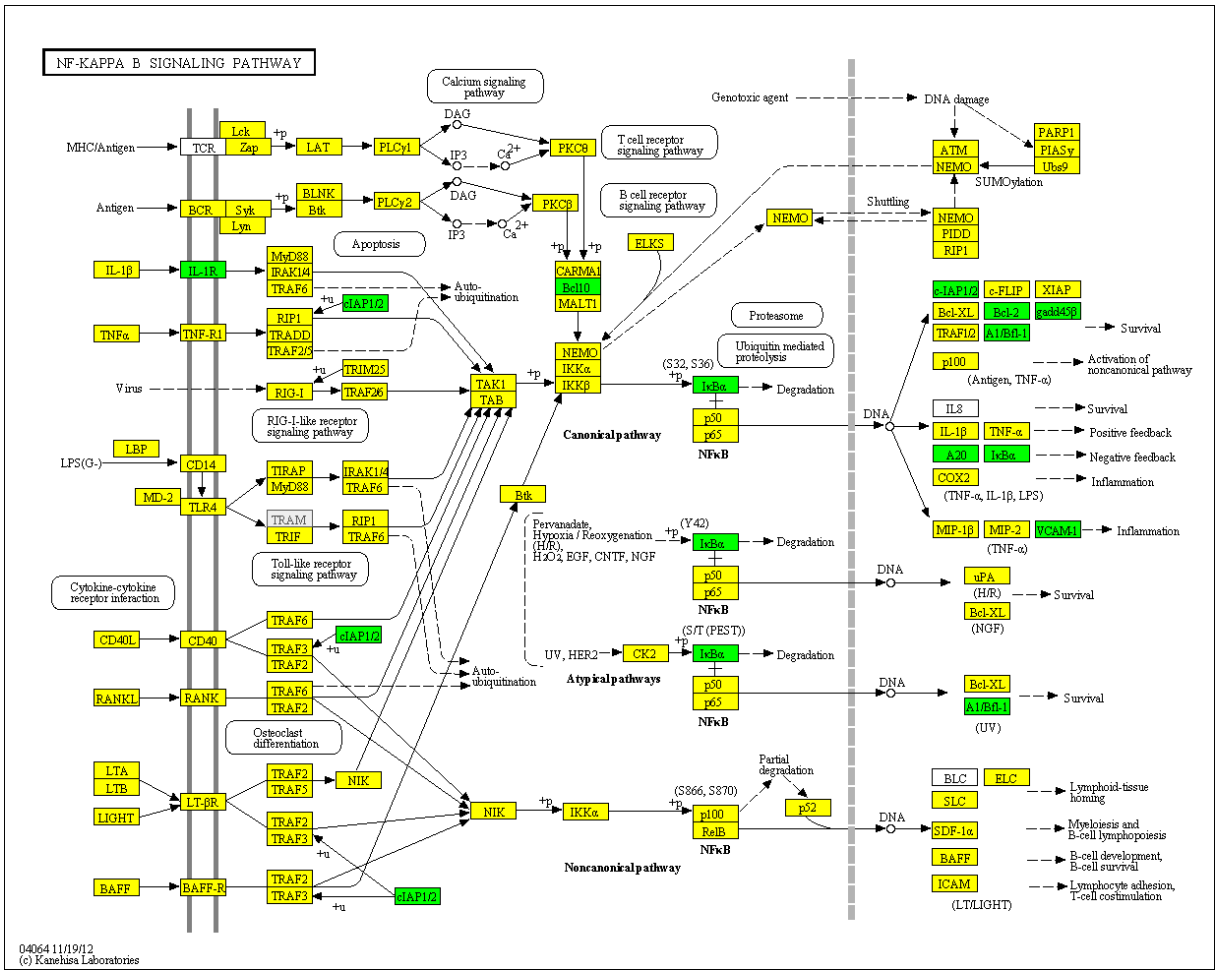

Figure A.1: NF-κB signalling pathway from the KEGG-pathway database. Species marked in green were found to be up regulated micro-array of YAP overexpression. When measuring the mRNA induction with RT-qPCR these findings could not be verified. Image and bioinformatic analysis by Martin Zauser, experimental experiments by Federico Pinna, micro-array analysis by the group of Fabian Theis.

A.3 ODE Model

Table A.18: Initial concentrations values of all species of the integrative liver model for LPS induced signalling. These values were used to calculate and the steady state values of the species, time course simulations were started from the steady state.

Species	Compartment	Inital Concentration in μM
p65_P	cytoplasm	0.004142097
IkBa_p	cytoplasm	0.058069182
IKKb	cytoplasm	0.3
IKKb_p	cytoplasm	0
p65-IkBa	cytoplasm	0.046678665
IkBa_mRNA	cytoplasm	0.158128991
IkBa	cytoplasm	0.447641581
p65_mRNA	cytoplasm	1
p65	cytoplasm	0.001541889
p38	cytoplasm	1
p38_P	cytoplasm	0
JNK	cytoplasm	1
JNK_P	cytoplasm	0
TNFR1	cytoplasm	3.00E-04
TNF:TNFR1	cytoplasm	0
p65_P	nucleus	0.207101584
IkBa	nucleus	0.895282942
p65-IkBa	nucleus	8.69E-01
IkBa_mRNA	nucleus	2.85E-07
IkBa_pre_mRNA_1	nucleus	2.357263853
p65	nucleus	0.077093694
p65_2P	nucleus	0.050685507
IkBa_pre_RNA_2	nucleus	2.357263853
MSK1_P	nucleus	0
MSK1	nucleus	15
TNF	EL	0
TNFR1	EL	0
TNF:TNFR1	EL	0
LPS	EL	0
TNF_mRNA	LSEC	0
TNF_pre_mRNA	LSEC	0
TNF_mRNA	MC	0
TNF_pre_mRNA	MC	0

[

ODE Model, Reactions I]Reactions of the integrative liver model for LPS induced signalling.

Reaction Name	Chemical Equation	Rate Law
LPS degradation LSCEs	LPS ->	mass action
LPS degradation MCs	LPS ->	mass action
TNF transcription initiation LSECs	->TNF_mRNA	see model file for details
TNF transcription termination LSECs	TNF_pre_mRNA ->TNF_mRNA	mass action
TNF translation LSECs	TNF_mRNA ->TNF_mRNA + TNF	mass action
TNF transcription initiation MCs	->TNF_pre_mRNA	see model file for details
TNF transcription termination MCs	TNF_pre_mRNA ->TNF_mRNA	mass action
TNF translation MCs	TNF_mRNA ->TNF_mRNA + TNF	mass action
TNF degradation	TNF ->	mass action
TNFR1 vesicle to outer membrane shuttle	TNFR1_cyt ->TNFR1_EL	mass action
TNFR1 outer membrane shuttle to vesicle shuttle	TNFR1_EL ->TNFR1_cyt	mass action
TNF TNFR1 association	TNF + TNFR1_EL ->TNF:TNFR1_EL	mass action
TNF TNFR1 dissociation	TNF:TNFR1_EL ->TNF + TNFR1_EL	mass action
TNF:TNFR1 complex internalisation	TNF:TNFR1_EL ->TNF:TNFR1_cyt	mass action
TNF internal degradation	TNF:TNFR1_cyt ->TNFR1_cyt	mass action
IKKbeta basal phosphorylation	IKKb ->IKKb_P	mass action
IKKbeta active phosphorylation	IKKb ->IKKb_P	michaelis menten
IKKbeta dephosphorylation	IKKb_P ->IKKb	mass action
IkBa:p65 complex phosphorylation	IkBa:p65_cyt ->IkBa_P + p65_P_cyt	michaelis menten
IkBa phosphorylation	IkBa_cyt ->IkBa_P	michaelis menten
IkBa_P degradation	IkBa_P ->	mass action
p65 dephosphorylation (cyt)	p65_P_cyt ->p65_cyt	mass action
p65_dephosphorylation (nuc)	p65_P_nuc ->p65_nuc	mass action
p65 nuclear import	p65_cyt ->p65_nuc	mass action
p65 nuclear export	p65_nuc ->p65_cyt	mass action
p65_P nuclear import	p65_P_cyt ->p65_P_nuc	mass action
p65_P nuclear export	p65_P_nuc ->p65_P_cyt	mass action
IkBa nuclear import	IkBa_cyt ->Ikba_nuc	mass action
IkBa nuclear export	IkBa_nuc ->IkBa_cyt	mass action

Reactions of the integrative liver model for LPS induced signalling, continued.

Reaction Name	Chemical Equation	Rate Law
complex nuclear import	IkBa:p65_cyt ->IkBa:p65_nuc	mass action
complex nuclear export	IkBa:p65_nuc ->IkBa:p65_cyt	mass action
complex association (cyt)	IkBa_cyt + p65_cyt ->IkBa:p65_cyt	mass action
complex dissociation (cyt)	IkBa:p65_cyt ->IkBa_cyt + p65_cyt	mass action
complex association (nuc)	IkBa_nuc + p65_nuc ->IkBa:p65_nuc	mass action
complex dissociation (nuc)	IkBa:p65_nuc ->IkBa_nuc + p65_nuc	mass action
p65 MSK1 phosphorylation 1	p65_nuc ->p65_P2	michaelis menten
p65 MSK1 phosphorylation 2	p65_P_nuc ->p65_P2	michaelis menten
p65 P2 dephosphorylation	p65_P2 ->p65_nuc	mass action
p38 basal phosphorylation	p38 ->p38_P	mass action
p38 active phosphorylation	p38 ->p38_P	michaelis menten
p38 dephosphorylation	p38_P ->p38	mass action
MSK1 phosphorylation	MSK1 ->MSK1_P	michaelis menten
MSK1 dephosphorylation	MSK1_P ->MSK1	mass action
JNK basal phosphorylation	JNK ->JNK_P	mass action
JNK active phosphorylation	JNK ->JNK_P	michaelis menten
JNK dephosphorylation	JNK_P ->JNK	mass action
IkBa transcription initiation	->IkBa_pre_mRNA1	see model file for details
IkBa transcription elongation	IkBa_pre_mRNA1 ->IkBa_pre_mRNA2	mass action
IkBa transcription termination	IkBa_pre_mRNA2 ->IkBa_mRNA_nuc	mass action
IkBa nuclear export	IkBa_mRNA_nuc ->IkBa_mRNA_cyt	mass action
IkBa translation	IkBa_mRNA_cyt ->IkBa_mRNA_cyt + IkBa_cyt	michaelis menten

Table A.19: Origins of the parameters of the integrative liver model for LPS induced signalling.

Parameters	fitted or assigned	References
k_LPS_LSEC_degradation	fitted	
kA_TNF_mRNA_LSEC_ transcription_initiation	fitted	
vA_TNF_mRNA_LSEC_ transcription_initiation	fitted	
k_TNF_mRNA_LSEC_ transcription_elongations	fitted	
k_TNF_mRNA_LSEC_degradation	fitted	
k_TNF_LSEC_translation	fitted	
k_LPS_KC_degradation	fitted	
kA_TNF_mRNA_KC_ transcription_initiation	fitted	
vA_TNF_mRNA_KC_ transcription_initiation	fitted	
k_TNF_mRNA_KC_ transcription_elongations	fitted	
k_TNF_mRNA_KC_degradation	fitted	
k_TNF_KC_translation	fitted	
k_TNF_degradation	fitted	
k_TNF:TNFR1_aassociation	set to lit. value ($16.833 \mu M^{-1} * s^{-1}$)	[121]
k_TNF:TNFR1_dissociation	set to k_TNF:TNFR1_association * Kd, $Kd = 1.9 * 10^{-5} \mu M$	[121]
k_TNFR1_vesicle2outer_membrane _shuttle	fitted	
k_TNFR1_outer_membrane2vesicle _shuttle	set to lit value ($1.8 * 10^{-5} s^{-1}$)	[60]
k_TNF:TNFR1_EL_internalisation	set to lit. value ($7.7 * 10^{-4} s^{-1}$	[60]
k_TNF_internal_degradation	fitted	
k_IKKb_dephosphorylation	fitted	
k_basal_IKKb_phosphorylation	fitted	
vmax_IKKb_phosphorlyation	fitted	
Km_IKKb_phosphorylation	fitted	
Ka_IKKb_phosphorylation	fitted	
k_IkBa:p65_association	set to lit. value ($0.31 \mu M^{-1} s^{-1}$)	[46]
k_IkBa:p65_dissociation	set to k_IkBa:p65_association*Kd, Kd=3 nM	[46]

Origins of the parameters of the integrative liver model for LPS induced signalling, continued.

Parameters	fitted or assigned	References
k_IkBa:p65_nuclear_export	fitted	
k_IkBa:p65_nuclear_import	fited	
kcat_IkBa:p65_phosphorylation	fitted	
Km_IkBa:p65_phosphorylation	fited	
k_IkBa_complex_cyt_degradation	mesured	[59]
k_p65_degradation	measured	[59]
k_IkBa_nuclear_export	set to k_IkBa_nuclear_import/2	[46]
k_IkBa_nuclear_import	fitted	
kcat_IkBa_phosphorylation	set to kcat_IkBa: p65_phosphorylation	
Km_IkBa_phosphorlyation	fitted	
k_IkBa_cyt_degradation	measured	[59]
Km_IkBa_translation	fitted	
vmax_IkBa_translation	fitted	
k_p65_nuclear_export	set to k_p65_nuclear_import/50	[46]
k_p65_nuclear_import	fitted	
k_p65_translation	set to $1.68 * 10^{-06} s^{-1}$	
	calculated from concentration p65 per cell / k_p65_degradation (60000 Molecules per Cell, V =13 pl)	[46]
k_p65_dephosphorylation	fitted	
k_IkBa_P_degradation	fitted	
k_IkBa_mRNA_cyt_degradation	fitted	
k_IkBa_mRNA_nuc_degradation	fitted	
k_IkBa_mRNA_nuclear_export	fitted	
k_basal_p38_phosphorlyation	set to $1 * 10^{-05} s^{-1}$	
kcat_p38_phosphorylation	fitted	
Km_p38_phosphorylation	fitted	
k_p38_dephosphorylation	fitted	

Origins of the parameters of the integrative liver model for LPS induced signalling, continued.

Parameters	fitted or assigned	References
k_basal_JNK_phosphorlyation	set to $1 * 10^{-05} s^{-1}$	
kcat_JNK_phosphorylation	fitted	
Km_JNK_phosphorylation	fitted	
k_JNK_dephosphorylation	fitted	
k_IkBa_complex_nuc_degradation	measured	[59]
k_IkBa_nuc_degradation	measured	[59]
kcat_p65_phosphorylation_MSK1	fitted	
Km_p65_phosphorylation_MSK1	fitted	
kcat_MSK1_phosphorylaiton	fitted	
Km_MSK1_phosphorylation	fitted	
k_MSK1_dephosphorylation	fitted	
Ka_p65_IkBa_transcription_initiation	fitted	
Ka_p65_P_IkBa_transcription_initiation	fitted	
Ka_p65_P2_IkBa_transcription_initiation	fitted	
kbasal_IkBa_transcription_initiation	set to $1.25 * 10^{-06} s^{-1}$	
k_IkBa_transcription_elongation	fitted	

Table A.20: Parameter values of the integrative liver model for LPS induced signalling for all 30 parameter sets of the model ensemble.

	kcat_IkBa_phos.	k_IkBa:p65_ass.	Km_IkBa_phos.	k_IkBa_nuc._import	k_IkBa_nuc._export	k_IkBa:p65_diss.
1	467.2027177	0.017946353	0.1	0.005	2.50E-03	5.38E-05
2	45.935676	0.00727705	0.1	0.005	2.50E-03	2.18E-05
3	40.38409802	0.024732262	0.1	0.005	2.50E-03	7.42E-05
4	12.18097498	0.1	0.5	0.005	2.50E-03	3.00E-04
5	86.52935483	0.012988275	0.1	0.005	2.50E-03	3.90E-05
6	428.7578213	0.007146764	0.1	0.005	2.50E-03	2.14E-05
7	12.29483239	0.1	0.5	0.005	2.50E-03	3.00E-04
8	76.40962068	0.018324346	0.1	0.005	2.50E-03	5.50E-05
9	55.02060641	0.018125004	0.1	0.005	2.50E-03	5.44E-05
10	1000	0.1	0.5	0.005	2.50E-03	3.00E-04
11	36.82269751	0.01773735	0.1	0.005	2.50E-03	5.32E-05
12	73.645074	0.018316983	0.1	0.005	2.50E-03	5.50E-05
13	736.2082262	0.023783952	0.1	0.005	2.50E-03	7.14E-05
14	34.87895202	0.006636416	0.195181213	0.005	2.50E-03	1.99E-05
15	999.9414605	0.069326274	0.1	0.005	2.50E-03	2.08E-04
16	60.36335637	0.007150419	0.1	0.005	2.50E-03	2.15E-05
17	69.39246781	0.007246717	0.1	0.005	2.50E-03	2.17E-05
18	307.3139827	0.023907962	0.1	0.005	2.50E-03	7.17E-05
19	13.59748752	0.1	0.5	0.005	2.50E-03	3.00E-04
20	16.53505852	0.018126017	0.1	0.005	2.50E-03	5.44E-05
21	9.353319035	0.018277378	0.1	0.005	2.50E-03	5.48E-05
22	65.1998415	0.017896688	0.1	0.005	2.50E-03	5.37E-05
23	119.4523092	0.017958188	0.1	0.005	2.50E-03	5.39E-05
24	49.4377608	0.007173585	0.1	0.005	2.50E-03	2.15E-05
25	71.77868887	0.024457449	0.1	0.005	2.50E-03	7.34E-05
26	392.9065615	0.013157803	0.1	0.005	2.50E-03	3.95E-05
27	12.08697202	0.1	0.5	0.005	2.50E-03	3.00E-04
28	35.46332988	0.032316731	0.109722104	0.005	2.50E-03	9.70E-05
29	23.78424907	0.033429659	0.141052341	0.005	2.50E-03	1.00E-04
30	66.17364879	0.021404127	0.1	0.005	2.50E-03	6.42E-05

Parameter values of the integrative liver model for LPS induced signalling for all 30 parameter sets of the model ensemble, continued.

	k_IkBa_transc._e.	k_p65_degr.	k_IkBa_com._cyt_degr.	vmax_IkBa_transl.	k_p65_transl.	Ka_p65_P_IkBa_transc._i.
1	0.002052611	1.33E-05	1.00E-05	8.42E-04	1.68E-06	1.00E-04
2	0.002476155	1.33E-05	1.00E-05	7.57E-04	1.68E-06	1.00E-04
3	0.00203816	1.33E-05	1.00E-05	3.74E-04	1.68E-06	1.00E-04
4	0.002542963	1.33E-05	1.00E-05	3.87E-04	1.68E-06	1.00E-04
5	0.002230905	1.33E-05	1.00E-05	5.27E-04	1.68E-06	1.00E-04
6	0.002481247	1.33E-05	1.00E-05	7.66E-04	1.68E-06	1.00E-04
7	0.002530753	1.33E-05	1.00E-05	3.90E-04	1.68E-06	1.00E-04
8	0.002041545	1.33E-05	1.00E-05	8.57E-04	1.68E-06	1.00E-04
9	0.002034178	1.33E-05	1.00E-05	8.71E-04	1.68E-06	1.00E-04
10	0.002378198	1.33E-05	1.00E-05	1.99E-04	1.68E-06	1.00E-04
11	0.002056322	1.33E-05	1.00E-05	8.45E-04	1.68E-06	1.00E-04
12	0.002035278	1.33E-05	1.00E-05	8.55E-04	1.68E-06	1.00E-04
13	0.002077978	1.33E-05	1.00E-05	3.76E-04	1.68E-06	1.00E-04
14	0.001009944	1.33E-05	1.00E-05	7.79E-04	1.68E-06	3.44E-04
15	0.002076947	1.33E-05	1.00E-05	3.40E-04	1.68E-06	1.00E-04
16	0.002485372	1.33E-05	1.00E-05	7.65E-04	1.68E-06	1.00E-04
17	0.002458427	1.33E-05	1.00E-05	7.67E-04	1.68E-06	1.00E-04
18	0.002071373	1.33E-05	1.00E-05	3.75E-04	1.68E-06	1.00E-04
19	8.20E-04	1.33E-05	1.00E-05	4.71E-04	1.68E-06	5.35E-02
20	0.002048133	1.33E-05	1.00E-05	8.49E-04	1.68E-06	1.00E-04
21	0.002032457	1.33E-05	1.00E-05	8.70E-04	1.68E-06	1.00E-04
22	0.002056966	1.33E-05	1.00E-05	8.41E-04	1.68E-06	1.00E-04
23	0.002040525	1.33E-05	1.00E-05	8.76E-04	1.68E-06	1.00E-04
24	0.002473728	1.33E-05	1.00E-05	7.65E-04	1.68E-06	1.00E-04
25	0.002049251	1.33E-05	1.00E-05	3.74E-04	1.68E-06	1.00E-04
26	0.002224471	1.33E-05	1.00E-05	5.26E-04	1.68E-06	1.00E-04
27	0.002553547	1.33E-05	1.00E-05	3.85E-04	1.68E-06	1.00E-04
28	0.002163517	1.33E-05	1.00E-05	8.30E-04	1.68E-06	1.00E-04
29	0.002297852	1.33E-05	1.00E-05	8.31E-04	1.68E-06	1.00E-04
30	9.42E-04	1.33E-05	1.00E-05	8.50E-04	1.68E-06	1.00E-04

Parameter values of the integrative liver model for LPS induced signalling for all 30 parameter sets of the model ensemble, continued.

	k_IkBa_mRNA_nuc._exp.	k_IkBa_mRNA_cyt._degr.	k_IkBa_mRNA_nuc._degr.	k_IkBa_cyt_degr.	vmax_IKKb_phos.
1	1.00E-04	2.39E-04	5.00E-05	1.00E-05	6.31E+01
2	1.00E-04	2.23E-04	5.00E-05	5.00E-05	9.94E+02
3	1.00E-04	2.18E-04	5.00E-05	3.97E-05	3.86E+02
4	1.00E-04	2.10E-04	5.00E-05	2.52E-05	4.28E+01
5	1.00E-04	2.18E-04	5.00E-05	5.00E-05	6.74E+02
6	1.00E-04	2.24E-04	5.00E-05	5.00E-05	1.20E+02
7	1.00E-04	2.10E-04	5.00E-05	2.63E-05	1.00E+03
8	1.00E-04	2.37E-04	5.00E-05	1.00E-05	7.53E+02
9	1.00E-04	2.39E-04	5.00E-05	1.00E-05	4.69E+01
10	1.00E-04	2.27E-04	5.00E-05	5.00E-05	8.89E+02
11	1.00E-04	2.39E-04	5.00E-05	1.00E-05	1.00E+03
12	1.00E-04	2.39E-04	5.00E-05	1.00E-05	1.00E+03
13	1.00E-04	2.19E-04	5.00E-05	3.16E-05	8.43E+02
14	1.00E-04	9.41E-04	5.00E-05	5.00E-05	2.01E+02
15	1.00E-04	2.56E-04	5.00E-05	5.00E-05	7.84E+02
16	1.00E-04	2.24E-04	5.00E-05	5.00E-05	1.00E+03
17	1.00E-04	2.25E-04	5.00E-05	5.00E-05	4.28E+02
18	1.00E-04	2.19E-04	5.00E-05	3.31E-05	6.48E+01
19	1.00E-04	1.00E-03	5.00E-05	5.00E-05	2.13E+02
20	1.00E-04	2.38E-04	5.00E-05	1.00E-05	4.21E+02
21	1.00E-04	2.38E-04	5.00E-05	1.00E-05	1.00E+03
22	1.00E-04	2.38E-04	5.00E-05	1.00E-05	1.00E+03
23	1.00E-04	2.39E-04	5.00E-05	1.00E-05	6.45E+02
24	1.00E-04	2.25E-04	5.00E-05	5.00E-05	1.00E+03
25	1.00E-04	2.18E-04	5.00E-05	3.72E-05	5.76E+02
26	1.00E-04	2.18E-04	5.00E-05	5.00E-05	6.43E+01
27	1.00E-04	2.10E-04	5.00E-05	2.42E-05	4.31E+02
28	1.00E-04	2.04E-04	5.00E-05	1.53E-05	9.92E+02
29	1.00E-04	2.04E-04	5.00E-05	4.52E-05	6.34E+01
30	1.00E-04	1.00E-03	5.00E-05	1.00E-05	1.00E+03

Parameter values of the integrative liver model for LPS induced signalling for all 30 parameter sets of the model ensemble, continued.

	k_IkBa_nuc._degr.	k_IkBa_com._nuc._degr.	k_IkBa:p65_nuc._exp.	Ka_IKKb_phos.	Km_IKKb_phos.
1	1.00E-05	1.00E-05	1.00E-04	0.001	5
2	1.00E-05	1.00E-05	1.00E-04	0.001	5
3	1.00E-05	1.00E-05	0.002	0.001	5
4	1.00E-05	1.00E-05	0.002	0.048	5
5	1.00E-05	1.00E-05	1.00E-04	0.004	5
6	1.00E-05	1.00E-05	1.00E-04	0.002	5
7	1.00E-05	1.01E-05	0.002	1.120	5
8	1.00E-05	1.00E-05	1.00E-04	0.001	5
9	1.00E-05	1.00E-05	1.00E-04	0.001	5
10	1.00E-05	1.00E-05	0.001910774	1.797	5
11	1.00E-05	1.00E-05	1.00E-04	0.001	5
12	1.00E-05	1.00E-05	1.00E-04	0.001	5
13	1.00E-05	1.00E-05	0.002	0.058	5
14	1.00E-05	1.00E-05	1.00E-04	0.164	5
15	1.00E-05	1.01E-05	0.002	1.763	5
16	1.00E-05	1.00E-05	1.00E-04	0.001	5
17	1.00E-05	1.00E-05	1.00E-04	0.002	5
18	1.00E-05	1.00E-05	0.001968836	0.001	5
19	1.00E-05	1.00E-05	7.23E-04	0.233	5
20	1.00E-05	1.00E-05	1.00E-04	0.001	5
21	1.00E-05	1.00E-05	1.00E-04	0.001	5
22	1.00E-05	1.00E-05	1.00E-04	0.005	5
23	1.00E-05	1.00E-05	1.00E-04	0.003	5
24	1.00E-05	1.00E-05	1.00E-04	0.001	5
25	1.00E-05	1.00E-05	0.002	0.001	5
26	1.00E-05	1.00E-05	1.00E-04	0.008	5
27	1.00E-05	1.00E-05	0.001999842	0.480	5
28	1.00E-05	1.00E-05	1.00E-04	0.720	5
29	1.00E-05	1.00E-05	1.00E-04	0.046	5
30	1.00E-05	1.00E-05	1.00E-04	0.002	5

Parameter values of the integrative liver model for LPS induced signalling for all 30 parameter sets of the model ensemble, continued.

	k_basal_IKKb_phos.	k_IKKb_dephos.	k_p65_nuc._exp.	k_TNF_degr.	Km_IkBa:p65_phos.	kcat_IkBa:p65_phos.
1	4.71E-06	3.047	5.00E-04	1.56E-04	0.500	467.20
2	8.44E-05	4.856	5.00E-04	1.22E-04	0.500	45.94
3	3.14E-05	2.885	5.00E-04	1.45E-04	0.500	40.38
4	1.00E-07	0.002	5.00E-04	1.08E-04	0.100	12.18
5	1.37E-05	1.988	5.00E-04	1.33E-04	0.347	86.53
6	6.27E-06	3.350	5.00E-04	1.23E-04	0.500	428.76
7	1.00E-07	0.002	5.00E-04	1.08E-04	0.100	12.29
8	5.61E-05	5.867	5.00E-04	1.55E-04	0.500	76.41
9	3.51E-06	0.259	5.00E-04	1.56E-04	0.500	55.02
10	1.27E-07	0.335	5.00E-04	1.00E-03	0.100	1000.00
11	7.53E-05	3.815	5.00E-04	1.55E-04	0.500	36.82
12	7.49E-05	7.570	5.00E-04	1.56E-04	0.500	73.65
13	1.17E-06	1.976	5.00E-04	1.44E-04	0.500	736.21
14	1.10E-07	0.004	5.00E-04	1.11E-04	0.499	34.88
15	1.25E-07	0.302	5.00E-04	1.00E-03	0.100	999.94
16	8.47E-05	6.371	5.00E-04	1.23E-04	0.500	60.36
17	1.50E-05	1.295	5.00E-04	1.23E-04	0.500	69.39
18	5.26E-06	3.690	5.00E-04	1.44E-04	0.500	307.31
19	1.11E-07	0.002	5.00E-04	1.10E-04	0.100	13.60
20	3.15E-05	0.716	5.00E-04	1.56E-04	0.500	16.54
21	7.51E-05	0.950	5.00E-04	1.55E-04	0.500	9.35
22	1.36E-05	1.230	5.00E-04	1.56E-04	0.500	65.20
23	1.62E-05	2.608	5.00E-04	1.55E-04	0.500	119.45
24	8.50E-05	5.240	5.00E-04	1.23E-04	0.500	49.44
25	4.69E-05	7.669	5.00E-04	1.44E-04	0.500	71.78
26	6.74E-07	0.444	5.00E-04	1.33E-04	0.347	392.91
27	1.00E-07	0.002	5.00E-04	1.08E-04	0.100	12.09
28	1.00E-07	0.004	5.00E-04	1.62E-04	0.500	35.46
29	1.00E-07	0.002	5.00E-04	1.65E-04	0.500	23.78
30	3.37E-05	3.417	5.00E-04	2.00E-04	0.500	66.17

Parameter values of the integrative liver model for LPS induced signalling for all 30 parameter sets of the model ensemble, continued.

	Ka_p65_IkBa_transc._i.	k_IkBa_P_degr.	k_p65_dephos.	Ka_p65_P2_IkBa_transc._i.	Km_p65_phos._MSK1
1	0.36	0.0028	5.61E-04	0.00010	1.073
2	0.22	0.0029	0.001100125	0.04555	9.999
3	0.61	0.0028	1.18E-03	0.00010	0.001
4	0.43	0.0100	0.004676856	1.00000	10.000
5	0.40	0.0028	1.12E-03	0.00010	10.000
6	0.29	0.0029	0.001101231	0.39917	10.000
7	0.61	0.0100	4.69E-03	0.00013	0.002
8	0.74	0.0028	5.52E-04	0.00010	1.005
9	0.19	0.0028	5.60E-04	0.00010	0.927
10	0.79	0.0064	1.00E-01	0.00010	0.001
11	0.27	0.0028	5.67E-04	0.00010	1.066
12	0.59	0.0028	5.52E-04	0.00010	1.002
13	0.42	0.0028	1.17E-03	0.00010	0.001
14	0.99	0.0037	1.67E-03	0.00010	0.001
15	0.69	0.0061	0.1	0.00023	0.001
16	0.23	0.0029	1.10E-03	0.03329	0.052
17	0.05	0.0029	0.00110344	0.00011	0.002
18	0.57	0.0028	1.17E-03	0.00010	0.001
19	1.00	0.0100	4.96E-03	0.01762	0.001
20	0.70	0.0028	5.58E-04	0.00010	1.013
21	0.64	0.0028	5.52E-04	0.00010	0.945
22	0.73	0.0028	5.61E-04	0.00010	1.070
23	0.63	0.0028	5.53E-04	0.00010	0.907
24	0.11	0.0029	1.10E-03	0.00035	0.002
25	0.59	0.0028	0.00117611	0.00771	0.001
26	0.20	0.0028	1.12E-03	0.00046	0.421
27	0.58	0.0100	4.66E-03	0.66931	9.738
28	0.89	0.0033	7.47E-04	0.00010	0.972
29	0.07	0.0039	9.96E-04	0.00010	0.723
30	0.08	0.0028	5.77E-04	0.00683	6.561

Parameter values of the integrative liver model for LPS induced signalling for all 30 parameter sets of the model ensemble, continued.

	kcat_p65_phos._MSK1	k_MSK1_dephos.	Km_MSK1_phos.	kcat_MSK1_phos.	k_IkBa:p65_nuc._imp.
1	6.93E+00	0.010	0.332	9.05E-04	2.00E-03
2	3.74E-04	0.010	0.332	1.00E-05	1.99E-03
3	1.00E-06	0.010	0.332	1.00E-05	1.00E-05
4	2.25E-05	0.010	0.332	1.00E-05	1.00E-05
5	1.87E-04	0.010	0.332	1.09E-05	2.00E-03
6	2.95E-05	0.010	0.332	2.38E-04	2.00E-03
7	5.72E-06	0.010	0.332	1.01E-05	1.06E-05
8	2.53E-02	0.009	0.332	1.00E-03	2.00E-03
9	2.08E-02	0.009	0.332	1.00E-03	2.00E-03
10	1.00E-06	0.010	0.332	1.00E-05	1.00E-05
11	1.50E-01	0.010	0.332	1.28E-04	2.00E-03
12	2.83E-02	0.009	0.332	9.35E-04	2.00E-03
13	1.00E-06	0.010	0.332	1.00E-05	1.00E-05
14	1.01E-06	0.010	0.332	1.03E-05	2.00E-03
15	1.00E-06	0.010	0.332	1.00E-05	1.00E-05
16	1.07E-06	0.010	0.332	1.00E-05	2.00E-03
17	1.51E-06	0.010	0.332	1.23E-05	2.00E-03
18	1.00E-06	0.010	0.332	1.00E-05	1.00E-05
19	1.00E-06	0.010	0.332	1.02E-05	1.00E-05
20	5.10E-02	0.010	0.332	1.00E-03	2.00E-03
21	1.36E-02	0.009	0.332	1.00E-03	2.00E-03
22	1.08E-01	0.010	0.332	1.00E-03	2.00E-03
23	2.57E-02	0.009	0.332	5.25E-04	2.00E-03
24	3.09E-06	0.010	0.332	1.21E-05	2.00E-03
25	1.00E-06	0.010	0.332	9.21E-04	1.00E-05
26	2.20E-05	0.010	0.332	1.77E-05	2.00E-03
27	1.38E-06	0.010	0.332	1.00E-05	1.00E-05
28	2.74E+00	0.010	0.332	1.07E-05	2.00E-03
29	8.53E-02	0.010	0.332	1.00E-03	2.00E-03
30	1.57E+01	0.010	0.332	1.90E-05	2.00E-03

Parameter values of the integrative liver model for LPS induced signalling for all 30 parameter sets of the model ensemble, continued.

6 k_p65_nuc._exp.	k_basal_IkBa_transc._i.	kcat_p38_phos.	Km_p38_phos.	k_basal_p38_phos.	
1	1.00E-05	1.00E-06	776.9485942	1.46E+00	9.56E-07
2	1.00E-05	1.00E-06	563785.5531	1.00E+01	1.44E-04
3	1.00E-05	1.00E-06	96118.13064	7.16E-01	1.68E-04
4	1.00E-05	1.00E-06	22962.77872	1.94E+00	2.65E-05
5	1.00E-05	1.00E-06	158456.2339	1.00E+01	4.64E-05
6	1.00E-05	1.00E-06	76703.93034	8.50E+00	2.72E-05
7	1.00E-05	1.00E-06	139948.7048	1.09E+00	1.93E-04
8	1.00E-05	1.00E-06	836139.6067	6.80E+00	2.10E-04
9	1.00E-05	1.00E-06	903645.1961	6.32E+00	2.31E-04
10	1.00E-05	1.00E-06	90404.29738	5.29E+00	6.64E-05
11	1.00E-05	1.00E-06	138790.2018	1.59E-01	3.05E-04
12	1.00E-05	1.00E-06	147328.5571	7.22E-01	2.07E-04
13	1.00E-05	1.00E-06	89220.46791	1.00E-02	3.00E-04
14	1.00E-05	1.00E-06	124043.6716	3.33E+00	9.47E-05
15	1.00E-05	1.00E-06	69204.73592	1.00E-02	3.32E-04
16	1.00E-05	1.00E-06	549742.8212	9.99E+00	1.42E-04
17	1.00E-05	1.00E-06	61662.87246	1.00E-02	2.12E-04
18	1.00E-05	1.00E-06	371488.5643	8.38E+00	1.15E-04
19	1.00E-05	1.00E-06	16277.63331	1.00E+01	5.26E-06
20	1.00E-05	1.00E-06	38215.45207	1.00E-02	1.15E-04
21	1.00E-05	1.00E-06	166798.1435	1.06E-01	3.70E-04
22	1.00E-05	1.00E-06	18434.53528	1.00E-02	5.54E-05
23	1.00E-05	1.00E-06	163666.7303	1.03E-01	3.68E-04
24	1.00E-05	1.00E-06	142404.4151	7.65E-01	2.31E-04
25	1.00E-05	1.00E-06	35903.29318	1.00E-02	1.21E-04
26	1.00E-05	1.00E-06	71762.6859	7.42E+00	2.82E-05
27	1.00E-05	1.00E-06	87400.24468	1.00E-02	2.98E-04
28	1.00E-05	1.00E-06	1000000	5.64E+00	2.55E-04
29	1.00E-05	1.00E-06	71235.27778	1.17E+00	8.54E-05
30	1.00E-05	1.00E-06	264913.8708	7.53E+00	7.25E-05

Parameter values of the integrative liver model for LPS induced signalling for all 30 parameter sets of the model ensemble, continued.

	k_p38_dephos.	kcat_JNK_phos.	Km_JNK_phos.	k_basal_JNK_phos.	k_JNK_dephos.
1	8.87E-04	40247.89728	1.00E-03	9.33E-05	6.68E-04
2	9.91E-04	415043.0373	1.00E+01	7.09E-05	6.40E-04
3	9.43E-04	20925.99385	1.78E+00	1.61E-05	6.90E-04
4	0.001121089	36990.90401	3.94E+00	1.61E-05	6.97E-04
5	0.001079286	119342.2196	1.00E-03	2.62E-04	4.51E-04
6	0.001127981	45535.77481	1.00E-03	1.02E-04	6.23E-04
7	9.36E-04	14242.27727	1.40E+00	1.29E-05	7.04E-04
8	6.63E-04	32031.63929	3.44E+00	1.63E-05	7.42E-04
9	6.47E-04	15458.14016	1.00E-03	3.59E-05	7.27E-04
10	0.001874858	37216.12152	1.00E+01	1.14E-05	0.001232786
11	5.61E-04	129582.4385	1.00E-03	3.00E-04	4.62E-04
12	6.72E-04	15412.23183	1.29E+00	1.53E-05	7.41E-04
13	8.29E-04	26162.29254	9.96E+00	5.18E-06	7.05E-04
14	0.001136963	153969.9816	2.87E+00	8.07E-05	6.80E-04
15	0.001627902	136953.445	1.00E-03	4.67E-04	7.80E-04
16	9.99E-04	81755.17568	3.65E+00	3.65E-05	6.81E-04
17	9.45E-04	47395.71057	1.00E+01	9.42E-06	7.13E-04
18	9.99E-04	46111.60543	8.48E+00	1.04E-05	6.98E-04
19	0.001191885	124825.9771	1.00E-03	2.85E-04	4.62E-04
20	7.78E-04	94631.91071	1.00E-03	2.19E-04	5.42E-04
21	4.99E-04	128223.2817	1.00E-03	2.97E-04	4.66E-04
22	8.35E-04	32930.61271	1.25E-03	7.63E-05	6.84E-04
23	5.00E-04	19378.06683	9.54E+00	4.24E-06	7.59E-04
24	9.07E-04	66609.2981	4.89E-01	9.15E-05	6.26E-04
25	0.001006143	38060.52567	1.00E-03	8.32E-05	6.26E-04
26	0.001099618	30433.81989	1.00E-03	6.69E-05	6.46E-04
27	8.47E-04	87809.24084	1.00E-03	1.94E-04	5.24E-04
28	5.99E-04	791828.5149	1.00E-03	1.00E-03	9.72E-04
29	7.30E-04	129397.2517	1.00E-03	2.88E-04	4.40E-04
30	6.78E-04	61012.89357	1.00E-03	1.43E-04	6.31E-04

Parameter values of the integrative liver model for LPS induced signalling for all 30 parameter sets of the model ensemble, continued.

	k_TNF:TNFR1_ass.	k_TNF:TNFR1_diss.	k_TNFR1_v.2o._m. _sh.	k_TNFR1_o._m.2v. _sh.	k_TNF:TNFR1_EL_int.
1	1.68E+01	3.20E-04	4.00E-04	1.80E-05	7.70E-04
2	1.68E+01	3.20E-04	4.00E-04	1.80E-05	7.70E-04
3	1.68E+01	3.20E-04	4.00E-04	1.80E-05	7.70E-04
4	1.68E+01	3.20E-04	4.00E-04	1.80E-05	7.70E-04
5	1.68E+01	3.20E-04	4.00E-04	1.80E-05	7.70E-04
6	1.68E+01	3.20E-04	4.00E-04	1.80E-05	7.70E-04
7	1.68E+01	3.20E-04	4.00E-04	1.80E-05	7.70E-04
8	1.68E+01	3.20E-04	4.00E-04	1.80E-05	7.70E-04
9	1.68E+01	3.20E-04	4.00E-04	1.80E-05	7.70E-04
10	1.68E+01	3.20E-04	4.00E-04	1.80E-05	7.70E-04
11	1.68E+01	3.20E-04	4.00E-04	1.80E-05	7.70E-04
12	1.68E+01	3.20E-04	4.00E-04	1.80E-05	7.70E-04
13	1.68E+01	3.20E-04	4.00E-04	1.80E-05	7.70E-04
14	1.68E+01	3.20E-04	4.00E-04	1.80E-05	7.70E-04
15	1.68E+01	3.20E-04	4.00E-04	1.80E-05	7.70E-04
16	1.68E+01	3.20E-04	4.00E-04	1.80E-05	7.70E-04
17	1.68E+01	3.20E-04	4.00E-04	1.80E-05	7.70E-04
18	1.68E+01	3.20E-04	4.00E-04	1.80E-05	7.70E-04
19	1.68E+01	3.20E-04	4.00E-04	1.80E-05	7.70E-04
20	1.68E+01	3.20E-04	4.00E-04	1.80E-05	7.70E-04
21	1.68E+01	3.20E-04	4.00E-04	1.80E-05	7.70E-04
22	1.68E+01	3.20E-04	4.00E-04	1.80E-05	7.70E-04
23	1.68E+01	3.20E-04	4.00E-04	1.80E-05	7.70E-04
24	1.68E+01	3.20E-04	4.00E-04	1.80E-05	7.70E-04
25	1.68E+01	3.20E-04	4.00E-04	1.80E-05	7.70E-04
26	1.68E+01	3.20E-04	4.00E-04	1.80E-05	7.70E-04
27	1.68E+01	3.20E-04	4.00E-04	1.80E-05	7.70E-04
28	1.68E+01	3.20E-04	4.00E-04	1.80E-05	7.70E-04
29	1.68E+01	3.20E-04	4.00E-04	1.80E-05	7.70E-04
30	1.68E+01	3.20E-04	4.00E-04	1.80E-05	7.70E-04

Parameter values of the integrative liver model for LPS induced signalling for all 30 parameter sets of the model ensemble, continued.

	k_TNF_int._degr.	Km_IkBa_transl.	k_LPS_LSEC_degr.	kA_TNF_mR_LSEC_ transc._i.	vA_TNF_mR_LSEC_ transc._i.
1	8.88E-05	4.90	2.36E-04	1.07E+00	1.22E-05
2	7.04E-05	4.80	2.88E-04	1.02E+00	1.19E-05
3	6.25E-05	10.00	2.51E-04	1.05E+00	1.20E-05
4	6.78E-05	7.05	3.34E-04	9.78E-01	1.20E-05
5	6.50E-05	7.23	2.68E-04	1.03E+00	1.20E-05
6	7.09E-05	6.35	2.87E-04	1.02E+00	1.19E-05
7	6.79E-05	9.86	3.34E-04	9.78E-01	1.20E-05
8	8.92E-05	10.00	2.38E-04	1.07E+00	1.22E-05
9	8.94E-05	2.54	2.37E-04	1.07E+00	1.22E-05
10	1.00E-03	6.05	1.42E-04	1.23E+00	1.92E-05
11	8.90E-05	3.67	2.38E-04	1.07E+00	1.22E-05
12	8.96E-05	7.95	2.36E-04	1.07E+00	1.22E-05
13	6.38E-05	7.45	2.52E-04	1.05E+00	1.20E-05
14	9.26E-05	9.05	3.20E-04	9.89E-01	1.20E-05
15	1.00E-03	3.00	1.41E-04	1.23E+00	1.92E-05
16	7.08E-05	5.12	2.86E-04	1.02E+00	1.19E-05
17	7.10E-05	1.05	2.87E-04	1.02E+00	1.20E-05
18	6.35E-05	10.00	2.52E-04	1.05E+00	1.20E-05
19	8.19E-05	4.47	3.24E-04	9.85E-01	1.20E-05
20	8.91E-05	9.45	2.37E-04	1.07E+00	1.22E-05
21	9.00E-05	8.62	2.38E-04	1.07E+00	1.22E-05
22	8.88E-05	9.99	2.38E-04	1.07E+00	1.22E-05
23	9.03E-05	8.54	2.38E-04	1.07E+00	1.22E-05
24	7.10E-05	2.53	2.87E-04	1.02E+00	1.19E-05
25	6.30E-05	10.00	2.51E-04	1.05E+00	1.20E-05
26	6.48E-05	3.57	2.68E-04	1.03E+00	1.20E-05
27	6.77E-05	9.56	3.34E-04	9.78E-01	1.20E-05
28	8.16E-05	9.80	2.31E-04	1.08E+00	1.22E-05
29	7.23E-05	0.67	2.27E-04	1.09E+00	1.22E-05
30	9.68E-05	0.56	2.04E-04	1.12E+00	1.25E-05

Parameter values of the integrative liver model for LPS induced signalling for all 30 parameter sets of the model ensemble, continued.

	k_TNF_mR_LSEC_ transc._e.	k_TNF_LSEC_transl.	k_TNF_mR_LSEC_degr.	k_LPS_MC_degr.	kA_TNF_mR_MC_transc._i.
1	1.00E-06	2.16E-05	0.59	1.20E-04	8.21E-01
2	1.00E-06	2.12E-05	0.61	1.35E-04	7.77E-01
3	1.00E-06	2.13E-05	0.59	1.24E-04	8.09E-01
4	1.00E-06	2.14E-05	0.61	1.45E-04	7.54E-01
5	1.00E-06	2.13E-05	0.60	1.29E-04	7.95E-01
6	1.00E-06	2.12E-05	0.61	1.35E-04	7.74E-01
7	1.00E-06	2.14E-05	0.61	1.45E-04	7.54E-01
8	1.00E-06	2.16E-05	0.60	1.20E-04	8.21E-01
9	1.00E-06	2.16E-05	0.59	1.20E-04	8.21E-01
10	1.00E-06	3.42E-05	0.37	8.52E-05	8.91E-01
11	1.00E-06	2.16E-05	0.60	1.20E-04	8.20E-01
12	1.00E-06	2.16E-05	0.59	1.20E-04	8.21E-01
13	1.00E-06	2.13E-05	0.59	1.24E-04	8.09E-01
14	1.00E-06	2.13E-05	0.61	1.42E-04	7.62E-01
15	1.00E-06	3.41E-05	0.37	8.52E-05	8.91E-01
16	1.00E-06	2.12E-05	0.61	1.34E-04	7.80E-01
17	1.00E-06	2.12E-05	0.60	1.34E-04	7.73E-01
18	1.00E-06	2.13E-05	0.59	1.24E-04	8.09E-01
19	1.00E-06	2.13E-05	0.61	1.42E-04	7.67E-01
20	1.00E-06	2.16E-05	0.59	1.20E-04	8.21E-01
21	1.00E-06	2.16E-05	0.60	1.20E-04	8.21E-01
22	1.00E-06	2.16E-05	0.59	1.20E-04	8.21E-01
23	1.00E-06	2.16E-05	0.59	1.20E-04	8.21E-01
24	1.00E-06	2.12E-05	0.61	1.34E-04	7.77E-01
25	1.00E-06	2.13E-05	0.59	1.24E-04	8.09E-01
26	1.00E-06	2.13E-05	0.60	1.29E-04	7.95E-01
27	1.00E-06	2.14E-05	0.61	1.45E-04	7.54E-01
28	1.00E-06	2.17E-05	0.59	1.18E-04	8.27E-01
29	1.00E-06	2.17E-05	0.59	1.17E-04	8.30E-01
30	1.00E-06	2.23E-05	0.56	1.09E-04	8.51E-01

Parameter values of the integrative liver model for LPS induced signalling for all 30 parameter sets of the model ensemble, continued.

	vA_TNF_mR_MC_transc._i.	k_TNF_mR_MC_transc._e.n	k_TNF_MC_transl.	k_TNF_mR_MC_degr.
1	5.86E-06	1.00E-06	2.15E-06	0.052
2	5.58E-06	1.00E-06	2.05E-06	0.054
3	5.76E-06	1.00E-06	2.11E-06	0.053
4	5.47E-06	1.00E-06	2.00E-06	0.056
5	5.67E-06	1.00E-06	2.08E-06	0.054
6	5.59E-06	1.00E-06	2.05E-06	0.054
7	5.47E-06	1.00E-06	2.00E-06	0.056
8	5.85E-06	1.00E-06	2.14E-06	0.052
9	5.85E-06	1.00E-06	2.15E-06	0.052
10	9.57E-06	1.00E-06	3.45E-06	0.028
11	5.85E-06	1.00E-06	2.14E-06	0.052
12	5.86E-06	1.00E-06	2.15E-06	0.052
13	5.76E-06	1.00E-06	2.11E-06	0.053
14	5.49E-06	1.00E-06	2.01E-06	0.055
15	9.48E-06	1.00E-06	3.46E-06	0.028
16	5.59E-06	1.00E-06	2.05E-06	0.054
17	5.59E-06	1.00E-06	2.05E-06	0.054
18	5.76E-06	1.00E-06	2.11E-06	0.053
19	5.49E-06	1.00E-06	2.01E-06	0.055
20	5.86E-06	1.00E-06	2.14E-06	0.052
21	5.85E-06	1.00E-06	2.14E-06	0.052
22	5.85E-06	1.00E-06	2.14E-06	0.052
23	5.85E-06	1.00E-06	2.14E-06	0.052
24	5.59E-06	1.00E-06	2.05E-06	0.054
25	5.76E-06	1.00E-06	2.11E-06	0.053
26	5.67E-06	1.00E-06	2.08E-06	0.053
27	5.47E-06	1.00E-06	2.00E-06	0.056
28	5.90E-06	1.00E-06	2.16E-06	0.051
29	5.93E-06	1.00E-06	2.17E-06	0.051
30	6.19E-06	1.00E-06	2.27E-06	0.049

Table A.21: ODEs of the integrative liver model for LPS induced signalling.

$$\frac{d([p65\_P_{cyt}]\cdot V_{cyt})}{dt} = -((k\_p65\_nuc\_imp\cdot[p65\_P_{cyt}] - k\_p65\_nuc\_exp\cdot[p65\_P_{nuc}])) - V_{cyt}\cdot(k\_p65\_degr\cdot[p65\_P_{cyt}]) + V_{cyt}\cdot\left(\frac{vmax\_IkBa{:}p65\_phos\cdot[\text{"}p65{-}IkBa_{cyt}\text{"}]}{Km\_IkBa{:}p65\_phos+[\text{"}p65{-}IkBa_{cyt}\text{"}]}\right) - V_{cyt}\cdot(k\_p65\_dephos\cdot[p65\_Pcyt])$$

$$\frac{d([IkBa\_P]\cdot V_{cyt})}{dt} = +V_{cyt}\cdot\left(\frac{vmax\_IkBa\_phos\cdot[IkBa_{cyt}]}{Km\_IkBa\_phos+[IkBa_{cyt}]}\right) - V_{cyt}\cdot(k\_IkBa\_P\_degr\cdot[IkBa\_P]) + V_{cyt}\cdot\left(\frac{vmax\_IkBa{:}p65\_phos\cdot[\text{"}p65{-}IkBa_{cyt}\text{"}]}{Km\_IkBa{:}p65\_phos+[\text{"}p65{-}IkBa_{cyt}\text{"}]}\right)$$

$$\frac{d([IKKb]\cdot V_{cyt})}{dt} = -V_{cyt}\cdot\left(\frac{vmax\_IKKb\_phos\cdot[IKKb]\cdot[TNF{:}TNFR1_{EL}]}{(Km\_IKKb\_phos+[IKKb])\cdot(Ka\_IKKb\_phos+[TNF{:}TNFR1_{EL}])}\right) - V_{cyt}\cdot(k\_basal\_IKKb\_phos\cdot[IKKb]) + V_{cyt}\cdot(k\_IKKb\_dephos\cdot[IKKb\_P])$$

$$\frac{d([IKKb\_P]\cdot V_{cyt})}{dt} = +V_{cyt}\cdot\left(\frac{vmax\_IKKb\_phos\cdot[IKKb]\cdot[TNF{:}TNFR1_{EL}]}{(Km\_IKKb\_phos+[IKKb])\cdot(Ka\_IKKb\_phos+[TNF{:}TNFR1_{EL}])}\right) + V_{cyto}\cdot(k\_basal\_IKKb\_phos\cdot[IKKb]) - V_{cyt}\cdot(k\_IKKb\_dephos\cdot[IKKb\_P])$$

$$\frac{d([\text{"}p65{-}IkBa_{cyt}\text{"}]\cdot V_{cyt})}{dt} = +((k\_IkBa:p65\_nuc\_exp\cdot[\text{"}p65-IkBa_{nuc}\text{"}] - k\_IkBa:p65\_nuc\_imp\cdot[\text{"}p65-IkBa_{cyt}\text{"}])) + V_{cyt}\cdot((k\_IkBa:p65\_ass\cdot[IkBa_{cyt}]\cdot[p65_{cyt}] - k\_IkBa:p65\_diss\cdot[\text{"}p65-IkBa_{cyt}\text{"}])) - V_{cyt}\cdot(k\_p65\_degradation\cdot[\text{"}p65-IkBacytoplasm\text{"}]) - V_{cytoplasm}\cdot(k\_IkBa\_complex\_cyt\_degradation\cdot[\text{"}p65-IkBacytoplasm\text{"}]) - V_{cytoplasm}\cdot\left(\frac{vmax\_IkBa{:}p65\_phosphorylation\cdot[\text{"}p65{-}IkBacytoplasm\text{"}]}{Km\_IkBa{:}p65\_phosphorylation+[\text{"}p65{-}IkBacytoplasm\text{"}]}\right)$$

ODEs of the integrative liver model for LPS induced signalling.

$$\frac{d([\text{IkBa\_mRNA}_{cyt}] \cdot V_{cyt})}{dt} = -V_{cyt} \cdot (\text{k\_IkBa\_mRNA\_cyt\_degr} \cdot [\text{IkBa\_mRNA}_{cyt}]) + (\text{k\_IkBa\_mRNA\_nuc\_exp} \cdot [\text{IkBa\_mRNA}_{nuc}])$$

$$\begin{aligned}\frac{d([\text{IkBa}_{cyt}] \cdot V_{cytoplasm})}{dt} = & -V_{cyt} \cdot (\text{k\_IkBa\_cyt\_degr} \cdot [\text{IkBa}_{cyt}]) \\ & -V_{cyt} \cdot \left(\frac{\text{vmax\_IkBa\_phos} \cdot [\text{IkBa}_{cyt}]}{\text{Km\_IkBa\_phos} + [\text{IkBa}_{cyt}]}\right) \\ & -V_{cyt} \cdot (\text{k\_IkBa : p65\_ass} \cdot [\text{IkBa}_{cyt}] \cdot [\text{p65}_{cyt}] - \text{k\_IkBa : p65\_diss} \cdot [\text{"p65} - \text{IkBa}_{cyt}\text{"}]) \\ & +V_{cyt} \cdot (\text{k\_p65\_degr} \cdot [\text{"p65} - \text{IkBa}_{cyt}\text{"}]) \\ & +V_{cyt} \cdot \left(\frac{\text{vmax\_IkBa\_transl} \cdot [\text{IkBa\_mRNA}_{cyt}]}{\text{Km\_IkBa\_transl} + [\text{IkBa\_mRNA}_{cyt}]}\right) \\ & -((\text{k\_IkBa\_nuc\_imp} \cdot [\text{IkBa}_{cyt}] - \text{k\_IkBa\_nuc\_exp} \cdot [\text{IkBa}_{nuc}]))\end{aligned}$$

$$\begin{aligned}\frac{d([\text{p65}_{cyt}] \cdot V_{cyt})}{dt} = & +V_{cyt} \cdot (\text{k\_p65\_transl} \cdot [\text{p65\_mRNA}]) \\ & -V_{cyt} \cdot (\text{k\_IkBa : p65\_ass} \cdot [\text{IkBa}_{cyt}] \cdot [\text{p65}_{cyt}] - \text{k\_IkBa : p65\_diss} \cdot [\text{"p65} - \text{IkBa}_{cyt}\text{"}]) \\ & +V_{cyt} \cdot (\text{k\_IkBa\_com\_cyt\_degr} \cdot [\text{"p65} - \text{IkBa}_{cyt}\text{"}]) \\ & -(\text{k\_p65\_nuc\_imp} \cdot [\text{p65}_{cyt}] - \text{k\_p65\_nuc\_exp} \cdot [\text{p65}_{nuc}]) \\ & +V_{cyt} \cdot (\text{k\_p65\_dephos} \cdot [\text{p65\_P}_{cyt}]) \\ & -V_{cyt} \cdot (\text{k\_p65\_degr} \cdot [\text{p65}_{cyt}])\end{aligned}$$

$$\begin{aligned}\frac{d([\text{p38}] \cdot V_{cyt})}{dt} = & -V_{cytoplasm} \cdot \left(\frac{\text{vmax\_p38\_phosphorlyation} \cdot [\text{p38}]}{\text{Km\_p38\_phosphorylation} + [\text{p38}]}\right) \\ & -V_{cytoplasm} \cdot (\text{k\_basal\_p38\_phosphorlyation} \cdot [\text{p38}]) \\ & +V_{cyt} \cdot (\text{k\_p38\_dephosphorylation} \cdot [\text{p38\_P}])\end{aligned}$$

ODEs of the integrative liver model for LPS induced signalling.

$$\frac{\mathrm{d}([\mathrm{p38\_P}]\cdot V_{\mathrm{cyt}})}{\mathrm{d}t} = +V_{\mathrm{cyt}}\cdot\left(\frac{\mathrm{vmax\_p38\_phos}\cdot[\mathrm{p38}]}{\mathrm{Km\_p38\_phos}+[\mathrm{p38}]}\right) + V_{\mathrm{cyt}}\cdot(\mathrm{k\_basal\_p38\_phos}\cdot[\mathrm{p38}]) - V_{\mathrm{cyt}}\cdot(\mathrm{k\_p38\_dephos}\cdot[\mathrm{p38\_P}])$$

$$\frac{\mathrm{d}([\mathrm{JNK}]\cdot V_{\mathrm{cyt}})}{\mathrm{d}t} = -V_{\mathrm{cyt}}\cdot\left(\frac{\mathrm{vmax\_JNK\_phos}\cdot[\mathrm{JNK}]}{\mathrm{Km\_JNK\_phos}+[\mathrm{JNK}]}\right) - V_{\mathrm{cyt}}\cdot(\mathrm{k\_basal\_JNK\_phos}\cdot[\mathrm{JNK}]) + V_{\mathrm{cyt}}\cdot(\mathrm{k\_JNK\_dephos}\cdot[\mathrm{JNK\_P}])$$

$$\frac{\mathrm{d}([\mathrm{JNK\_P}]\cdot V_{\mathrm{cyt}})}{\mathrm{d}t} = +V_{\mathrm{cyt}}\cdot\left(\frac{\mathrm{vmax\_JNK\_phos}\cdot[\mathrm{JNK}]}{\mathrm{Km\_JNK\_phos}+[\mathrm{JNK}]}\right) + V_{\mathrm{cyt}}\cdot(\mathrm{k\_basal\_JNK\_phos}\cdot[\mathrm{JNK}]) - V_{\mathrm{cyt}}\cdot(\mathrm{k\_JNK\_dephos}\cdot[\mathrm{JNK\_P}])$$

$$\frac{\mathrm{d}([\mathrm{TNFR1cyt}]\cdot V_{\mathrm{cyt}})}{\mathrm{d}t} = -\left((\mathrm{k\_TNFR1\_v2o\_m\_sh}\cdot[\mathrm{TNFR1_{cyt}}] - \mathrm{k\_TNFR1\_o\_m2v\_sh}\cdot[\mathrm{TNFR1_{EL}}])\right) + V_{\mathrm{cyt}}\cdot\left(\mathrm{k\_TNF\alpha\_int\_degr}\cdot[\mathrm{TNF:TNFR1_{cyt}}]\right)$$

$$\frac{\mathrm{d}([\mathrm{TNF{:}TNFR1_{cyt}}]\cdot V_{\mathrm{cyt}})}{\mathrm{d}t} = +(\mathrm{k\_TNF\alpha:TNFR1\_int}\cdot[\mathrm{TNF:TNFR1_{EL}}]) - V_{\mathrm{cyt}}\cdot\left(\mathrm{k\_TNF\alpha\_int\_degr}\cdot[\mathrm{TNF:TNFR1_{cyt}}]\right)$$

$$\frac{\mathrm{d}([\mathrm{p65\_P_{nuc}}]\cdot V_{\mathrm{nuc}})}{\mathrm{d}t} = +\left((\mathrm{k\_p65\_nuc\_imp}\cdot[\mathrm{p65\_P_{cyt}}] - \mathrm{k\_p65\_nuc\_exp}\cdot[\mathrm{p65\_P_{nuc}}])\right) - V_{\mathrm{nuc}}\cdot(\mathrm{k\_p65\_degr}\cdot[\mathrm{p65\_P_{nuc}}]) - V_{\mathrm{nuc}}\cdot(\mathrm{k\_p65\_dephos}\cdot[\mathrm{p65\_P_{nuc}}]) - V_{\mathrm{nuc}}\cdot\left(\frac{\mathrm{vmax\_p65\_phos\_MSK1}\cdot[\mathrm{p65\_Pnuc}]}{\mathrm{Km\_p65\_phos\_MSK1}+[\mathrm{p65\_P_{nuc}}]}\right)$$

ODEs of the integrative liver model for LPS induced signalling.

$$\frac{d([\text{IkBa}_{\text{nuc}}]\cdot V_{\text{nuc}})}{dt} = +V_{\text{nuc}}\cdot(\text{k\_p65\_degr}\cdot[\text{"p65-IkBa}_{\text{nuc}}\text{"}]) -V_{\text{nuc}}\cdot((\text{k\_IkBa:p65\_ass}\cdot[\text{p65}_{\text{nuc}}]\cdot[\text{IkBa}_{\text{nuc}}]-\text{k\_IkBa:p65\_diss}\cdot[\text{"p65-IkBa}_{\text{nuc}}\text{"}])) -V_{\text{nuc}}\cdot(\text{k\_IkBa\_nuc\_degr}\cdot[\text{IkBa}_{\text{nuc}}]) +((\text{k\_IkBa\_nuc\_imp}\cdot[\text{IkBa}_{\text{cyt}}]-\text{k\_IkBa\_nuc\_exp}\cdot[\text{IkBa}_{\text{nuc}}]))$$

$$\frac{d([\text{"p65-IkBa}_{\text{nuc}}\text{"}]\cdot V_{\text{nuc}})}{dt} = -((\text{k\_IkBa:p65\_nuc\_exp}\cdot[\text{"p65-IkBa}_{\text{nuc}}\text{"}]-\text{k\_IkBa:p65\_nuc\_imp}\cdot[\text{"p65-IkBa}_{\text{cyt}}\text{"}])) -V_{\text{nuc}}\cdot(\text{k\_p65\_degr}\cdot[\text{"p65-IkBa}_{\text{nuc}}\text{"}]) -V_{\text{nuc}}\cdot(\text{k\_IkBa\_complex\_nuc\_degr}\cdot[\text{"p65-IkBa}_{\text{nuc}}\text{"}]) +V_{\text{nuc}}\cdot((\text{k\_IkBa:p65\_ass}\cdot[\text{p65nuc}]\cdot[\text{IkBanuc}]-\text{k\_IkBa:p65\_diss}\cdot[\text{"p65-IkBa}_{\text{nuc}}\text{"}]))$$

$$\frac{d([\text{IkBa\_mRNA}_{\text{nuc}}]\cdot V_{\text{nuc}})}{dt} = -V_{\text{nuc}}\cdot(\text{k\_IkBa\_mRNA\_nuc\_degr}\cdot[\text{IkBa\_mRNA}_{\text{nuc}}]) -(\text{k\_IkBa\_mRNA\_nuc\_exp}\cdot[\text{IkBa\_mRNA}_{\text{nuc}}]) +V_{\text{nuc}}\cdot(\text{k\_IkBa\_transc\_e}\cdot[\text{IkBa\_pre\_mRNA\_2}])$$

$$\frac{d([\text{IkBa\_pre\_mRNA\_1}]\cdot V_{\text{nuc}})}{dt} = +V_{\text{nuc}}\cdot(\text{k\_basal\_IkBa\_transc\_i}+\text{Ka\_p65\_P\_IkBa\_transc\_i}\cdot[\text{p65\_P}_{\text{nuc}}] +\text{Ka\_p65\_IkBa\_transc\_i}\cdot[\text{p65}_{\text{nuc}}]+\text{Ka\_p65\_P2\_IkBa\_transc\_i}\cdot[\text{p65\_P2}]) -V_{\text{nuc}}\cdot(\text{k\_IkBa\_transc\_e}\cdot[\text{IkBa\_pre\_mRNA\_1}])$$

$$\frac{d([\text{p65}_{\text{nuc}}]\cdot V_{\text{nuc}})}{dt} = +V_{\text{nuc}}\cdot(\text{k\_IkBa\_complex\_nuc\_degr}\cdot[\text{"p65-IkBa}_{\text{nuc}}\text{"}]) +V_{\text{nuc}}\cdot(\text{k\_p65\_dephos}\cdot[\text{p65\_P}_{\text{nuc}}]) -V_{\text{nuc}}\cdot(\text{k\_p65\_degr}\cdot[\text{p65}_{\text{nuc}}]) -V_{\text{nuc}}\cdot\left(\frac{\text{vmax\_p65\_phos\_MSK1}\cdot[\text{p65}_{\text{nuc}}]}{\text{Km\_p65\_phos\_MSK1}+[\text{p65}_{\text{nuc}}]}\right) +V_{\text{nuc}}\cdot(\text{k\_p65\_dephos}\cdot[\text{p65\_P2}]) +((\text{k\_p65\_nuc\_imp}\cdot[\text{p65}_{\text{cyt}}]-\text{k\_p65\_nuc\_exp}\cdot[\text{p65}_{\text{nuc}}])) -V_{\text{nuc}}\cdot((\text{k\_IkBa:p65\_ass}\cdot[\text{p65}_{\text{nuc}}]\cdot[\text{IkBa}_{\text{nuc}}]-\text{k\_IkBa:p65\_diss}\cdot[\text{"p65-IkBa}_{\text{nuc}}\text{"}]))$$

ODEs of the integrative liver model for LPS induced signalling.

$$\frac{\mathrm{d}([\mathrm{p65\_P2}]\cdot V_{\mathrm{nuc}})}{\mathrm{d}t} = +V_{\mathrm{nuc}}\cdot\left(\frac{\mathrm{vmax\_p65\_phosp\_MSK1}\cdot[\mathrm{p65\_P_{nuc}}]}{\mathrm{Km\_p65\_phos\_MSK1}+[\mathrm{p65\_P_{nuc}}]}\right) + V_{\mathrm{nuc}}\cdot\left(\frac{\mathrm{vmax\_p65\_phos\_MSK1}\cdot[\mathrm{p65_{nuc}}]}{\mathrm{Km\_p65\_phos\_MSK1}+[\mathrm{p65_{nuc}}]}\right) - V_{\mathrm{nuc}}\cdot(\mathrm{k\_p65\_degr}\cdot[\mathrm{p65\_P2}]) - V_{\mathrm{nuc}}\cdot(\mathrm{k\_p65\_dephos}\cdot[\mathrm{p65\_P2}])$$

$$\frac{\mathrm{d}([\mathrm{IkBa\_pre\_mRNA\_2}]\cdot V_{\mathrm{nuc}})}{\mathrm{d}t} = +V_{\mathrm{nuc}}\cdot(\mathrm{k\_IkBa\_transc\_e}\cdot[\mathrm{IkBa\_pre\_mRNA\_1}]) - V_{\mathrm{nuc}}\cdot(\mathrm{k\_IkBa\_transc\_e}\cdot[\mathrm{IkBa\_pre\_mRNA\_2}])$$

$$\frac{\mathrm{d}([\mathrm{MSK1\_P}]\cdot V_{\mathrm{nuc}})}{\mathrm{d}t} = +V_{\mathrm{nuc}}\cdot\left(\frac{\mathrm{vmax\_MSK1\_phos}\cdot[\mathrm{MSK1}]}{\mathrm{Km\_MSK1\_phos}+[\mathrm{MSK1}]}\right) - V_{\mathrm{nuc}}\cdot(\mathrm{k\_MSK1\_dephos}\cdot[\mathrm{MSK1\_P}])$$

$$\frac{\mathrm{d}([\mathrm{MSK1}]\cdot V_{\mathrm{nuc}})}{\mathrm{d}t} = -V_{\mathrm{nuc}}\cdot\left(\frac{\mathrm{vmax\_MSK1\_phos}\cdot[\mathrm{MSK1}]}{\mathrm{Km\_MSK1\_phos}+[\mathrm{MSK1}]}\right) + V_{\mathrm{nuc}}\cdot(\mathrm{k\_MSK1\_dephos}\cdot[\mathrm{MSK1\_P}])$$

$$\frac{\mathrm{d}([\mathrm{TNF}]\cdot V_{\mathrm{EL}})}{\mathrm{d}t} = -V_{\mathrm{EL}}\cdot((\mathrm{k\_TNF\alpha:TNFR1\_ass}\cdot[\mathrm{TNFR1_{EL}}]\cdot[\mathrm{TNF}] - \mathrm{k\_TNF\alpha:TNFR1\_diss}\cdot[\mathrm{TNF:TNFR1_{EL}}])) + (\mathrm{k\_TNF\_LSEC\_transl}\cdot[\mathrm{TNF\_mRNA_{LSEC}}]) + (\mathrm{k\_TNF\_MC\_transl}\cdot[\mathrm{TNF\_mRNA_{MC}}]) - V_{\mathrm{EL}}\cdot(\mathrm{k\_TNF\_degr}\cdot[\mathrm{TNF}])$$

$$\frac{\mathrm{d}([\mathrm{TNFR1_{EL}}]\cdot V_{\mathrm{EL}})}{\mathrm{d}t} = +\left((\mathrm{k\_TNFR1\_v2o\_m\_sh}\cdot[\mathrm{TNFR1_{cyt}}] - \mathrm{k\_TNFR1\_o\_m2v\_sh}\cdot[\mathrm{TNFR1_{EL}}])\right) - V_{\mathrm{EL}}\cdot((\mathrm{k\_TNF\alpha:TNFR1\_ass}\cdot[\mathrm{TNFR1_{EL}}]\cdot[\mathrm{TNF}] - \mathrm{k\_TNF\alpha:TNFR1\_diss}\cdot[\mathrm{TNF:TNFR1_{EL}}]))$$

$$\frac{\mathrm{d}([\mathrm{TNF:TNFR1_{EL}}]\cdot V_{\mathrm{EL}})}{\mathrm{d}t} = +V_{\mathrm{EL}}\cdot((\mathrm{k\_TNF\alpha:TNFR1\_ass}\cdot[\mathrm{TNFR1_{EL}}]\cdot[\mathrm{TNF}] - \mathrm{k\_TNF\alpha:TNFR1\_diss}\cdot[\mathrm{TNF:TNFR1_{EL}}])) - (\mathrm{k\_TNF\alpha:TNFR1\_int}\cdot[\mathrm{TNF:TNFR1_{EL}}])$$

ODEs of the integrative liver model for LPS induced signalling.

$$\frac{\mathrm{d}([\mathrm{LPS}]\cdot V_{\mathrm{EL}})}{\mathrm{d}t} = -V_{\mathrm{EL}}\cdot(\mathrm{k\_LPS\_LSEC\_degr}\cdot[\mathrm{LPS}]) - V_{\mathrm{EL}}\cdot(\mathrm{k\_LPS\_MC\_degr}\cdot[\mathrm{LPS}])$$

$$\frac{\mathrm{d}([\mathrm{TNF\_mRNA_{LSEC}}]\cdot V_{\mathrm{LSEC}})}{\mathrm{d}t} = +V_{\mathrm{LSEC}}\cdot(\text{"k\_TNF\_mRNA\_LSEC\_transc\_e"}\cdot[\mathrm{TNF\_pre\_mRNA_{LSEC}}]) - V_{\mathrm{LSEC}}\cdot(\mathrm{k\_TNF\_mRNA\_LSEC\_degr}\cdot[\mathrm{TNF\_mRNA_{LSEC}}])$$

$$\frac{\mathrm{d}([\mathrm{TNF\_pre\_mRNA_{LSEC}}]\cdot V_{\mathrm{LSEC}})}{\mathrm{d}t} = +2\cdot V_{\mathrm{LSEC}}\cdot\left(\frac{\text{"vA\_TNF\_mRNA\_LSEC\_transc\_i"}\cdot[\mathrm{LPS}]}{[\mathrm{LPS}]+\text{"kA\_TNF\_mRNA\_LSEC\_transc\_i"}}\right) - V_{\mathrm{LSEC}}\cdot(\text{"k\_TNF\_mRNA\_LSEC\_transc\_e"}\cdot[\mathrm{TNF\_pre\_mRNA_{LSEC}}])$$

$$\frac{\mathrm{d}([\mathrm{TNF\_mRNA_{MC}}]\cdot V_{\mathrm{MC}})}{\mathrm{d}t} = +V_{\mathrm{MC}}\cdot(\text{"k\_TNF\_mRNA\_MC\_transcription\_e"}\cdot[\mathrm{TNF\_pre\_mRNA_{MC}}]) - V_{\mathrm{MC}}\cdot(\mathrm{k\_TNF\_mRNA\_MC\_degr}\cdot[\mathrm{TNF\_mRNA_{MC}}])$$

$$\frac{\mathrm{d}([\mathrm{TNF\_pre\_mRNAMC}]\cdot V_{\mathrm{MC}})}{\mathrm{d}t} = +2\cdot V_{\mathrm{MC}}\cdot\left(\frac{\text{"vA\_TNF\_mRNA\_MC\_ transcription\_initiation"}\cdot[\mathrm{LPS}]}{[\mathrm{LPS}]+\text{"kA\_TNF\_mRNA\_MC\_ transcription\_initiation"}}\right) - V_{\mathrm{MC}}\cdot(\text{"k\_TNF\_mRNA\_MC\_transc\_e"}\cdot[\mathrm{TNF\_pre\_mRNAMC}])$$

A.4 Fisher Information Results

Table A.22: Table showing results for repeated parameter estimations with the Levenberg-Marquardt algorithm starting from random start values. All parameters were fitted.

Target Function	kcat_JNK_phos	k_TNF_degr	Km_JNK_phos	k_basal_JNK_phos	k_dephos
1.46883	0.0345847	0.0013199	0.001	2.21E-06	0.0013192
1.46883	0.4473	0.00131769	0.001	2.86E-05	0.00129496
1.46883	0.137783	0.00132213	0.001	8.79E-06	0.0013104
1.46883	0.0573401	0.0013194	0.001	3.67E-06	0.00131823
1.46883	0.176104	0.00132255	0.001	1.12E-05	0.00130754
1.46883	0.293112	0.00132303	0.001	1.87E-05	0.00129961
1.46883	0.045642	0.00131937	0.001	2.92E-06	0.00131901
1.46883	0.0050307	0.00132049	0.33558	2.41E-07	0.00132056
1.46883	0.312638	0.00131787	0.001	2.00E-05	0.00130341
1.46883	0.485551	0.00131743	0.001	3.11E-05	0.00129276
1.46883	0.00458472	0.00132036	0.001	2.93E-07	0.00132066
1.46883	0.00718942	0.00132032	0.001	4.59E-07	0.00132052
1.46883	0.45276	0.00131766	0.001	2.90E-05	0.00129464
1.46883	0.00922753	0.0013203	0.001	5.89E-07	0.00132042
1.46883	0.0904466	0.00131926	0.001	5.78E-06	0.00131626
1.46883	0.0024859	0.00132071	0.001	1.59E-07	0.00132044
1.46883	0.323356	0.001323	0.001	2.06E-05	0.00129771
1.46883	0.0203724	0.00131998	0.001	1.30E-06	0.00132002
1.46883	0.0119759	0.00132065	0.001	7.65E-07	0.00131989
1.46883	0.0433938	0.0013197	0.001	2.77E-06	0.00131882
1.46883	0.00628392	0.00132032	0.001	4.01E-07	0.00132058
1.46883	0.0585966	0.00132168	0.001	3.74E-06	0.00131589
1.46883	0.079687	0.00131927	0.001	5.09E-06	0.00131693
1.46883	0.00328182	0.00132073	0.001	2.10E-07	0.00132037
1.46883	0.00417854	0.00132035	0.543973	1.73E-07	0.00132077
1.46883	0.0017309	0.00132049	0.001	1.11E-07	0.0013207
1.46883	0.0569166	0.00131941	0.001	3.64E-06	0.00131825

Table showing results for repeated parameter estimations with the Levenberg-Marquardt algorithm starting from random start values. All parameters were fitted.

Target Function	kcat_JNK_phos	k_TNF_degr	Km_JNK_phos	k_basal_JNK_phos	k_dephos
1.46883	0.322195	0.00132301	0.001	2.05E-05	0.00129778
1.46883	0.0102785	0.00132087	0.001	6.56E-07	0.00131979
1.46883	0.022664	0.00132114	0.001	1.45E-06	0.00131872
1.46883	0.344793	0.00132299	0.001	2.20E-05	0.00129636
1.46883	0.00532775	0.00132032	0.001	3.40E-07	0.00132064
1.46883	0.63723	0.00131639	0.001	4.08E-05	0.00128406
1.46883	0.0352835	0.00131988	0.001	2.25E-06	0.00131917
1.46883	0.0238077	0.00131998	0.001	1.52E-06	0.0013198
1.46883	0.0646185	0.00132178	0.001	4.12E-06	0.00131541
1.46883	0.453114	0.00132344	0.001	2.89E-05	0.00128902
1.46883	0.0343593	0.00132127	0.001	2.19E-06	0.00131785
1.46883	0.00515548	0.00132078	0.001	3.29E-07	0.0013202
1.46883	0.214213	0.00132295	0.001	1.37E-05	0.00130472
1.46883	0.102413	0.00132183	0.001	6.53E-06	0.00131296
1.46883	0.319128	0.00132301	0.001	2.03E-05	0.00129797
1.46883	0.0946245	0.00131925	0.001	6.05E-06	0.00131599
1.46883	0.0786372	0.00131927	0.001	5.03E-06	0.001317
1.46883	0.0191564	0.00131997	0.001	1.22E-06	0.0013201
1.46883	0.00832496	0.00132082	0.001	5.32E-07	0.00131995
1.46883	0.0383192	0.00131982	0.001	2.45E-06	0.00131904
1.46883	0.42192	0.00132324	0.001	2.69E-05	0.00129119
1.46883	0.665029	0.00132478	0.001	4.23E-05	0.00127423
1.46883	0.13603	0.00131899	0.001	8.70E-06	0.0013136
1.46883	0.151397	0.00131881	0.001	9.68E-06	0.0013128
1.46884	0.0124631	0.00132061	4.206	1.53E-07	0.00132051
1.46884	0.00792765	0.00132062	0.522783	3.33E-07	0.00132032

Table showing results for repeated parameter estimations with the Levenberg-Marquardt algorithm starting from random start values. All parameters were fitted.

Target Function	kcat_JNK_phos	k_TNF_degr	Km_JNK_phos	k_basal_JNK_phos	k_dephos
1.46884	0.00590697	0.0013204	1.34311	1.61E-07	0.00132072
1.46884	0.0083292	0.00132062	1.63166	2.02E-07	0.00132044
1.46884	0.0156242	0.0013206	5.57139	1.52E-07	0.00132051
1.46884	0.0145744	0.00132055	5.12526	1.52E-07	0.00132056
1.46884	1.49553	0.00132021	0.001	9.55E-05	0.00122553
1.46884	0.022571	0.00132059	11.3221	1.17E-07	0.00132057
1.46884	0.00835475	0.00132053	1.99828	1.78E-07	0.00132063
1.46884	0.00534709	0.0013203	1.13915	1.60E-07	0.00132083
1.46884	1.38752	0.0013255	0.001	8.83E-05	0.00122756
1.46884	0.0131504	0.00132062	4.95502	1.41E-07	0.00132051
1.46884	0.00988306	0.00132061	2.27862	1.93E-07	0.00132046
1.46884	0.0457147	0.0013206	28.2206	1.00E-07	0.00132058
1.46884	1.50663	0.00132597	0.001	9.58E-05	0.00121955
1.46884	0.0130391	0.00132061	4.59373	1.49E-07	0.00132051
1.46884	0.00936844	0.0013206	2.49411	1.71E-07	0.0013205
1.46884	1.01711	0.00131512	0.001	6.52E-05	0.00126092
1.46884	0.0128232	0.00132028	4.35392	1.53E-07	0.00132083
1.46884	0.0089255	0.00132062	4.70513	1.00E-07	0.00132056
1.46884	0.00474953	0.00132066	0.752037	1.73E-07	0.00132045
1.46884	1.17172	0.00132515	0.001	7.46E-05	0.00124162
1.46884	0.0061153	0.00132063	1.44567	1.60E-07	0.00132048
1.46884	0.00928782	0.00132062	4.38123	1.10E-07	0.00132055
1.46884	1.15947	0.00132022	0.001	7.41E-05	0.00124695
1.46884	0.00598656	0.00132063	1.4421	1.57E-07	0.00132049
1.46884	0.0501746	0.00132061	31.0711	1.00E-07	0.00132057
1.46884	1.16499	0.00131506	0.001	7.47E-05	0.00125149

Table showing results for repeated parameter estimations with the Levenberg-Marquardt algorithm starting from random start values. All parameters were fitted.

Target Function	kcat_JNK_phos	k_TNF_degr	Km_JNK_phos	k_basal_JNK_phos	k_dephos
1.46884	1.41947	0.00131495	0.001	9.10E-05	0.00123526
1.46884	0.0183075	0.00132041	6.69317	1.52E-07	0.0013207
1.46884	0.0107448	0.00132061	3.48365	1.53E-07	0.0013205
1.46884	0.00843744	0.00132066	0.701821	3.17E-07	0.00132028
1.46884	0.00761565	0.00132069	0.60267	3.04E-07	0.00132028
1.46884	0.0172039	0.00132037	6.27479	1.51E-07	0.00132075
1.46884	0.0103914	0.00132011	2.75074	1.77E-07	0.00132099
1.46884	0.0474251	0.00132029	21.9104	1.32E-07	0.00132084
1.46885	2.02529	0.00132806	0.001	0.000128596	0.00118471
1.46885	1.80642	0.00131377	0.001	0.000115954	0.00121151
1.46885	0.0115378	0.00132004	1.97022	2.48E-07	0.00132097
1.46885	1.61155	0.00132638	0.001	0.000102461	0.00121251
1.46885	2.03511	0.00131276	0.001	0.000130732	0.00119774
1.46887	2.78258	0.00133047	0.001	0.000176341	0.00113458
1.4689	3.78164	0.00133477	0.001	0.000238845	0.00106785
1.4689	0.991659	0.00132049	100	6.27E-07	0.00131999
1.4689	1.00608	0.00132048	100	6.36E-07	0.00131998
1.4689	3.8131	0.00133367	0.001	0.00024103	0.00106673
1.46891	4.07162	0.00133621	0.001	0.00025687	0.00104843
1.46892	0.171809	0.00131852	12.9867	7.86E-07	0.00132176
1.46892	0.0482643	0.00131678	1.5688	1.20E-06	0.00132315
1.46892	0.175285	0.00131888	13.3365	7.82E-07	0.00132129
1.46892	0.116316	0.00131854	8.06711	8.21E-07	0.0013217
1.46892	0.916758	0.00131553	78.233	7.42E-07	0.00132506
1.46892	0.227019	0.00131852	17.878	7.69E-07	0.00132178
1.46892	0.201057	0.00131398	15.513	7.81E-07	0.00132518
1.46892	0.0595629	0.00131668	2.85248	9.90E-07	0.00132347

Table showing results for repeated parameter estimations with the Levenberg-Marquardt algorithm starting from random start values. All parameters were fitted.

Target Function	kcat_JNK_phos	k_TNF_degr	Km_JNK_phos	k_basal_JNK_phos	k_dephos
1.46892	0.2181	0.00131852	17.061	7.72E-07	0.00132178
1.46892	4.31627	0.00133796	0.001	0.000271934	0.00103166
1.46892	1.16497	0.00132153	100	7.36E-07	0.00131881
1.46892	0.0942623	0.00131577	6.06736	8.55E-07	0.00132501
1.46894	1.45097	0.00132042	100	9.17E-07	0.00131967
1.46894	4.80402	0.00134077	0.001	0.000301996	0.000998867
1.46895	4.9417	0.00134152	0.001	0.000310467	0.000989667
1.46896	5.11123	0.00134273	0.001	0.000320811	0.000978144
1.46897	0.806133	0.00132013	41.1852	1.22E-06	0.00131957
1.46897	0.669726	0.00132095	33.8743	1.23E-06	0.00131875
1.46897	1.09226	0.00131773	56.3539	1.22E-06	0.00132194
1.46897	0.136126	0.00132021	5.08857	1.43E-06	0.00131928
1.46897	0.224941	0.0013208	9.93709	1.31E-06	0.00131881
1.46897	0.370214	0.00132015	17.7954	1.26E-06	0.00131951
1.46897	0.41763	0.00132222	20.383	1.24E-06	0.00131747
1.46897	0.578398	0.00132335	29.0301	1.23E-06	0.00131634
1.46897	1.90546	0.00132037	100	1.20E-06	0.00131933
1.46897	0.217485	0.0013213	9.57082	1.31E-06	0.00131694
1.46897	0.659477	0.00132039	33.3308	1.23E-06	0.0013193
1.46897	0.0750276	0.00132373	1.06479	2.31E-06	0.00131486
1.46897	0.213073	0.00132076	9.30142	1.32E-06	0.00131883
1.46897	0.557286	0.00132012	27.7975	1.24E-06	0.00131955
1.46897	1.10782	0.00132012	57.3134	1.21E-06	0.00131958
1.46897	0.0926428	0.00132029	2.5498	1.67E-06	0.00131896
1.46897	0.111225	0.00132024	3.66751	1.52E-06	0.00131915
1.46897	0.285105	0.00131819	13.1471	1.29E-06	0.00132137
1.46897	0.0790253	0.00131907	1.57349	1.96E-06	0.00131987
1.46897	0.81766	0.00132013	41.7828	1.22E-06	0.00131957

Table showing results for repeated parameter estimations with the Levenberg-Marquardt algorithm starting from random start values. All parameters were fitted.

Target Function	kcat_JNK_phos	k_TNF_degr	Km_JNK_phos	k_basal_JNK_phos	k_dephos
1.46897	1.60898	0.00132011	84.1024	1.21E-06	0.00131959
1.46897	0.354281	0.00131843	16.8871	1.27E-06	0.0013212
1.46897	0.251018	0.00132407	11.4203	1.29E-06	0.0013155
1.46897	0.509835	0.00132014	25.2728	1.24E-06	0.00131953
1.46897	0.0753669	0.00132081	0.9665	2.45E-06	0.00131765
1.46897	1.89494	0.00132009	99.5633	1.20E-06	0.00131962
1.46897	1.01078	0.0013199	52.1398	1.21E-06	0.00131978
1.46897	1.20283	0.00131849	62.3645	1.21E-06	0.0013212
1.46897	0.944487	0.00132012	48.5676	1.22E-06	0.00131958
1.46897	0.653019	0.0013201	32.9138	1.23E-06	0.00131959
1.46897	0.310955	0.00132014	14.5861	1.27E-06	0.0013195
1.46897	1.11063	0.00132396	57.7387	1.20E-06	0.00131563
1.46897	0.43664	0.00132231	21.3829	1.24E-06	0.0013174
1.46897	0.380302	0.00131843	18.2955	1.26E-06	0.0013212
1.46898	0.0777869	0.00132068	0.71172	2.90E-06	0.00131733
1.46898	0.0781506	0.00132109	0.689667	2.95E-06	0.00131687
1.46898	0.0779798	0.00132071	0.700988	2.93E-06	0.00131727
1.46898	1.98194	0.00132032	100	1.25E-06	0.00131932
1.46898	0.107637	0.0013212	0.302372	5.27E-06	0.00131404
1.46898	2.05471	0.00132031	100	1.30E-06	0.00131927
1.46901	2.37842	0.00132026	100	1.50E-06	0.00131906
1.46906	3.05851	0.00132014	100	1.93E-06	0.00131861
1.46906	3.032	0.00132014	100	1.91E-06	0.00131862
1.46908	6.38413	0.00135141	0.001	0.000397952	0.000892644
1.46911	3.64758	0.00131966	100	2.30E-06	0.00131879
1.46919	4.76565	0.00131985	100	3.01E-06	0.00131747
1.4692	4.93826	0.00131982	100	3.11E-06	0.00131736
1.46924	5.37603	0.00131972	100	3.39E-06	0.00131709

Table showing results for repeated parameter estimations with the Levenberg-Marquardt algorithm starting from random start values. All parameters were fitted.

Target Function	kcat_JNK_phos	k_TNF_degr	Km_JNK_phos	k_basal_JNK_phos	k_dephos
1.46935	7.67487	0.00136552	0.001	0.000473044	0.000804205
1.46946	8.25794	0.00131922	100	5.19E-06	0.0013152
1.46975	12.0761	0.00131856	100	7.57E-06	0.00131271
1.46982	12.9489	0.00131847	100	8.12E-06	0.00131208
1.68199	11.0195	0.00332145	0.001	0.000160088	0.000150937
1.83661	10.7308	0.00380317	0.0010291	8.44E-05	6.99E-05
1.91406	100	0.00992343	0.001	8.81E-05	7.15E-05
1.93407	21.9137	0.018247	0.00100006	6.26E-05	0.000204818
1.93481	4.12923	0.0326082	0.898909	2.94E-06	0.000217684
1.93486	0.754208	0.0399491	1.49246	3.36E-07	0.000219747
1.93487	12.049	0.0686213	36.3242	2.08E-07	0.000219928
1.93487	0.0943579	0.0406187	0.016239	1.01E-07	0.00021995
1.93488	63.8689	0.0942029	0.257596	2.30E-05	0.000197169
1.93488	2.48546	0.0979295	1.87977	3.90E-07	0.000219807
1.93488	84.6172	0.099895	0.207902	2.97E-05	0.000189946
1.93488	87.5	0.0911549	0.126745	3.64E-05	0.000183856
1.93488	0.247605	0.0542249	0.00187139	2.02E-07	0.000220092
1.93488	73.7814	0.0999763	0.205435	2.61E-05	0.00019333
1.93488	89.6255	0.0596469	0.0993818	5.72E-05	0.000162914
1.93489	1.10033	0.000220401	0.158248	0.000190876	0.1
1.9349	79.8085	0.0894826	0.0424196	3.70E-05	0.00018006
1.93494	3.00583	0.000221083	3.53155	0.00013295	0.1
1.95464	10.6128	0.00412107	0.00116198	5.33E-05	4.01E-05
2.06752	10.6641	0.00442464	0.0016028	3.64E-05	2.54E-05
2.24667	10.5938	0.00474754	0.00196607	1.90E-05	1.19E-05
2.41683	10.1502	0.004819	0.00248415	6.62E-06	3.75E-06
2.41947	10.3326	0.00495557	0.00230054	6.44E-06	3.64E-06

Table showing results for repeated parameter estimations with the Levenberg-Marquardt algorithm starting from random start values. All parameters were fitted.

Target Function	kcat_JNK_phos	k_TNF_degr	Km_JNK_phos	k_basal_JNK_phos	k_dephos
2.4442	10.124	0.00487221	0.00233531	4.81E-06	2.69E-06
2.45898	9.87908	0.00473212	0.00251236	3.86E-06	2.14E-06
2.46546	9.88066	0.00475408	0.00244604	3.44E-06	1.90E-06
2.4795	9.68655	0.00465075	0.00250576	2.54E-06	1.39E-06
2.47976	9.6833	0.00465007	0.0025488	2.52E-06	1.38E-06
2.48312	9.64554	0.00463351	0.00255259	2.31E-06	1.26E-06
3.60273	0.00293253	1.00E-06	0.001	2.63E-06	0.034096
3.9263	0.0059575	1.00E-06	0.001	6.70E-06	0.0361335
4.59804	0.0292215	1.00E-06	0.001	5.96E-05	0.0467708
5.327	30.244	0.0465899	0.828147	1.63E-07	0.0420533
5.327	17.7636	0.0444068	0.00692619	1.00E-07	0.0489692

Table A.23: Table showing results for repeated parameter estimations with the Levenberg-Marquardt algorithm starting from random start values. Only three parameters were fitted, after the Fisher information was employed to reduce the number of fit parameters.

Target Function	k_TNF_degr	k_basal_JNK_phos	k_dephos
1.46898	0.00132099	1.41E-06	0.00131851
1.46898	0.00132101	1.41E-06	0.00131849
1.46898	0.00132101	1.41E-06	0.00131849
1.46898	0.00132099	1.41E-06	0.00131851
1.46898	0.00132104	1.41E-06	0.00131846
1.46898	0.00132099	1.41E-06	0.00131851
1.46898	0.00132101	1.41E-06	0.00131849
1.46898	0.00132101	1.41E-06	0.00131849
1.46898	0.00132101	1.41E-06	0.00131849
1.46898	0.00132101	1.41E-06	0.00131849
1.46898	0.00132103	1.41E-06	0.00131846
1.46898	0.00132099	1.41E-06	0.00131851
1.46898	0.00132103	1.41E-06	0.00131847
1.46898	0.00132103	1.41E-06	0.00131846
1.46898	0.00132099	1.41E-06	0.0013185
1.46898	0.001321	1.41E-06	0.0013185
1.46898	0.00132105	1.41E-06	0.00131845
1.46898	0.00132104	1.41E-06	0.00131845
1.46898	0.00132101	1.41E-06	0.00131849
1.46898	0.00132103	1.41E-06	0.00131847
1.46898	0.00132105	1.41E-06	0.00131845
1.46898	0.00132103	1.41E-06	0.00131847
1.46898	0.00132105	1.41E-06	0.00131845
1.46898	0.001321	1.41E-06	0.0013185
1.46898	0.00132101	1.41E-06	0.00131849
1.46898	0.00132105	1.41E-06	0.00131845

Table showing results for repeated parameter estimations with the Levenberg-Marquardt algorithm starting from random start values. Only three parameters were fitted, after the Fisher information was employed to reduce the number of fit parameters.

Target Function	k_TNF_degr	k_basal_JNK_phos	k_dephos
1.46898	0.00132104	1.41E-06	0.00131846
1.46898	0.00132101	1.41E-06	0.00131849
1.46898	0.00132105	1.41E-06	0.00131845
1.46898	0.00132105	1.41E-06	0.00131845
1.46898	0.00132105	1.41E-06	0.00131845
1.46898	0.00132105	1.41E-06	0.00131845
1.46898	0.00132105	1.41E-06	0.00131845
1.46898	0.00132104	1.41E-06	0.00131846
1.46898	0.00132101	1.41E-06	0.00131849
1.46898	0.00132104	1.41E-06	0.00131846
1.46898	0.00132101	1.41E-06	0.00131849
1.46898	0.00132105	1.41E-06	0.00131845
1.46898	0.00132105	1.41E-06	0.00131845
1.46898	0.00132101	1.41E-06	0.00131849
1.46898	0.00132105	1.41E-06	0.00131845
1.46898	0.00132099	1.41E-06	0.0013185
1.46898	0.00132101	1.41E-06	0.00131849
1.46898	0.00132105	1.41E-06	0.00131845
1.46898	0.00132105	1.41E-06	0.00131845
1.46898	0.00132101	1.41E-06	0.00131848
1.46898	0.00132101	1.41E-06	0.00131849
1.46898	0.00132105	1.41E-06	0.00131845
1.46898	0.00132105	1.41E-06	0.00131845
1.46898	0.00132101	1.41E-06	0.00131849
1.46898	0.00132104	1.41E-06	0.00131846
1.46898	0.00132101	1.41E-06	0.00131849

Table showing results for repeated parameter estimations with the Levenberg-Marquardt algorithm starting from random start values. Only three parameters were fitted, after the Fisher information was employed to reduce the number of fit parameters.

Target Function	k_TNF_degr	k_basal_JNK_phos	k_dephos
1.46898	0.001321	1.41E-06	0.0013185
1.46898	0.00132101	1.41E-06	0.00131849
1.46898	0.001321	1.41E-06	0.0013185
1.46898	0.00132101	1.41E-06	0.00131849
1.46898	0.00132101	1.41E-06	0.00131849
1.46898	0.00132103	1.41E-06	0.00131847
1.46898	0.00132103	1.41E-06	0.00131846
1.46898	0.00132104	1.41E-06	0.00131846
1.46898	0.00132099	1.41E-06	0.00131851
1.46898	0.00132104	1.41E-06	0.00131846
1.46898	0.001321	1.41E-06	0.00131849
1.46898	0.00132101	1.41E-06	0.00131849
1.46898	0.00132105	1.41E-06	0.00131845
1.46898	0.001321	1.41E-06	0.0013185
1.46898	0.00132103	1.41E-06	0.00131846
1.46898	0.00132103	1.41E-06	0.00131846
1.46898	0.00132105	1.41E-06	0.00131845
1.46898	0.00132101	1.41E-06	0.00131849
1.46898	0.00132104	1.41E-06	0.00131846
1.46898	0.00132105	1.41E-06	0.00131845
1.46898	0.00132101	1.41E-06	0.00131849
1.46898	0.00132105	1.41E-06	0.00131845
1.46898	0.00132105	1.41E-06	0.00131845
1.46898	0.00132104	1.41E-06	0.00131846
1.46898	0.00132101	1.41E-06	0.00131849

Table showing results for repeated parameter estimations with the Levenberg-Marquardt algorithm starting from random start values. Only three parameters were fitted, after the Fisher information was employed to reduce the number of fit parameters.

Target Function	k_TNF_degr	k_basal_JNK_phos	k_dephos
1.93488	0.000220413	4.45E-06	0.1
1.46898	0.001321	1.41E-06	0.0013185
1.46898	0.00132105	1.41E-06	0.00131845
1.46898	0.00132105	1.41E-06	0.00131845
1.46898	0.00132104	1.41E-06	0.00131846
1.46898	0.00132103	1.41E-06	0.00131847
1.46898	0.001321	1.41E-06	0.00131849
1.46898	0.00132104	1.41E-06	0.00131846
1.46898	0.00132105	1.41E-06	0.00131845
1.46898	0.00132105	1.41E-06	0.00131845
1.46898	0.001321	1.41E-06	0.00131849
1.46898	0.00132099	1.41E-06	0.00131851
1.46898	0.00132105	1.41E-06	0.00131845
1.46898	0.001321	1.41E-06	0.0013185
1.46898	0.00132101	1.41E-06	0.00131849
1.93488	0.00022041	4.45E-06	0.1
1.46898	0.00132101	1.41E-06	0.00131849
1.46898	0.00132104	1.41E-06	0.00131845
1.46898	0.00132101	1.41E-06	0.00131849
1.46898	0.00132099	1.41E-06	0.00131851
1.46898	0.00132099	1.41E-06	0.00131851
1.46898	0.00132105	1.41E-06	0.00131845
1.46898	0.00132105	1.41E-06	0.00131845
1.46898	0.00132104	1.41E-06	0.00131846

Table showing results for repeated parameter estimations with the Levenberg-Marquardt algorithm starting from random start values. Only three parameters were fitted, after the Fisher information was employed to reduce the number of fit parameters.

Target Function	k_TNF_degr	k_basal_JNK_phos	k_dephos
1.46898	0.00132099	1.41E-06	0.00131851
1.46898	0.00132103	1.41E-06	0.00131847
1.46898	0.00132101	1.41E-06	0.00131849
1.46898	0.00132099	1.41E-06	0.00131851
1.46898	0.00132103	1.41E-06	0.00131847
1.46898	0.00132103	1.41E-06	0.00131846
1.46898	0.00132101	1.41E-06	0.00131849
1.46898	0.00132101	1.41E-06	0.00131849
1.46898	0.00132101	1.41E-06	0.00131849
1.46898	0.00132101	1.41E-06	0.00131849
1.46898	0.00132101	1.41E-06	0.00131849
1.46898	0.00132104	1.41E-06	0.00131846
1.46898	0.00132101	1.41E-06	0.00131849
1.46898	0.00132101	1.41E-06	0.00131849
1.46898	0.00132104	1.41E-06	0.00131846
1.46898	0.00132105	1.41E-06	0.00131845
1.46898	0.00132101	1.41E-06	0.00131849
1.46898	0.00132105	1.41E-06	0.00131845
1.46898	0.00132101	1.41E-06	0.00131849
1.46898	0.00132099	1.41E-06	0.0013185
1.46898	0.00132101	1.41E-06	0.00131848
1.46898	0.00132101	1.41E-06	0.00131848
1.46898	0.00132105	1.41E-06	0.00131845
1.46898	0.001321	1.41E-06	0.0013185

Table showing results for repeated parameter estimations with the Levenberg-Marquardt algorithm starting from random start values. Only three parameters were fitted, after the Fisher information was employed to reduce the number of fit parameters.

Target Function	k_TNF_degr	k_basal_JNK_phos	k_dephos
1.46898	0.00132101	1.41E-06	0.00131849
1.93488	0.000220411	4.45E-06	0.1
1.46898	0.00132104	1.41E-06	0.00131846
1.46898	0.00132101	1.41E-06	0.00131849
1.46898	0.00132105	1.41E-06	0.00131845
1.46898	0.00132105	1.41E-06	0.00131845
1.46898	0.00132101	1.41E-06	0.00131849
1.46898	0.00132101	1.41E-06	0.00131849
1.46898	0.00132101	1.41E-06	0.00131849
1.46898	0.00132105	1.41E-06	0.00131845
1.46898	0.00132105	1.41E-06	0.00131845
1.46898	0.00132103	1.41E-06	0.00131846
1.46898	0.00132104	1.41E-06	0.00131846
1.46898	0.00132101	1.41E-06	0.00131849
1.46898	0.001321	1.41E-06	0.0013185
1.46898	0.00132099	1.41E-06	0.00131851
1.46898	0.00132099	1.41E-06	0.00131851
1.46898	0.00132101	1.41E-06	0.00131849
1.46898	0.00132101	1.41E-06	0.00131849
1.46898	0.00132103	1.41E-06	0.00131847
1.46898	0.00132105	1.41E-06	0.00131845
1.46898	0.00132099	1.41E-06	0.00131851
1.46898	0.00132099	1.41E-06	0.00131851
1.46898	0.00132105	1.41E-06	0.00131845

Table showing results for repeated parameter estimations with the Levenberg-Marquardt algorithm starting from random start values. Only three parameters were fitted, after the Fisher information was employed to reduce the number of fit parameters.

Target Function	k_TNF_degr	k_basal_JNK_phos	k_dephos
1.46898	0.00132101	1.41E-06	0.00131849
1.46898	0.001321	1.41E-06	0.0013185
1.46898	0.00132101	1.41E-06	0.00131849
1.46898	0.001321	1.41E-06	0.0013185
1.46898	0.001321	1.41E-06	0.0013185
1.46898	0.00132101	1.41E-06	0.00131849
1.46898	0.00132105	1.41E-06	0.00131845
1.46898	0.00132103	1.41E-06	0.00131847
1.46898	0.00132105	1.41E-06	0.00131845
1.46898	0.00132099	1.41E-06	0.00131851
1.46898	0.00132105	1.41E-06	0.00131845
1.46898	0.00132101	1.41E-06	0.00131849
1.46898	0.001321	1.41E-06	0.0013185
1.46898	0.00132103	1.41E-06	0.00131846
1.46898	0.00132104	1.41E-06	0.00131846
1.46898	0.00132103	1.41E-06	0.00131846
1.46898	0.001321	1.41E-06	0.0013185
1.46898	0.00132103	1.41E-06	0.00131847
1.46898	0.00132101	1.41E-06	0.00131849
1.46898	0.00132099	1.41E-06	0.0013185
1.46898	0.00132099	1.41E-06	0.00131851
1.46898	0.00132101	1.41E-06	0.00131849
1.46898	0.00132104	1.41E-06	0.00131846
1.46898	0.00132101	1.41E-06	0.00131849
1.46898	0.00132101	1.41E-06	0.00131849

Table showing results for repeated parameter estimations with the Levenberg-Marquardt algorithm starting from random start values. Only three parameters were fitted, after the Fisher information was employed to reduce the number of fit parameters.

Target Function	k_TNF_degr	k_basal_JNK_phos	k_dephos
1.46898	0.00132104	1.41E-06	0.00131846
1.46898	0.00132101	1.41E-06	0.00131849
1.46898	0.00132104	1.41E-06	0.00131846
1.46898	0.00132104	1.41E-06	0.00131846
1.46898	0.00132103	1.41E-06	0.00131846
1.46898	0.00132101	1.41E-06	0.00131849
1.46898	0.00132103	1.41E-06	0.00131847
1.46898	0.00132105	1.41E-06	0.00131845
1.46898	0.001321	1.41E-06	0.0013185
1.46898	0.00132104	1.41E-06	0.00131846
1.46898	0.00132099	1.41E-06	0.0013185
1.46898	0.00132101	1.41E-06	0.00131848
1.46898	0.00132103	1.41E-06	0.00131847
1.46898	0.00132101	1.41E-06	0.00131849
1.46898	0.00132101	1.41E-06	0.00131849
1.46898	0.00132099	1.41E-06	0.00131851
1.46898	0.00132104	1.41E-06	0.00131846
1.46898	0.00132104	1.41E-06	0.00131846
1.46898	0.00132104	1.41E-06	0.00131846
1.46898	0.00132099	1.41E-06	0.00131851
1.46898	0.00132099	1.41E-06	0.00131851
1.46898	0.00132105	1.41E-06	0.00131845
1.46898	0.00132099	1.41E-06	0.00131851
1.46898	0.00132101	1.41E-06	0.00131848
1.46898	0.00132104	1.41E-06	0.00131846
1.46898	0.00132101	1.41E-06	0.00131849

A.5 Supplementary DVD contents

1. PDF copy of this thesis
2. Supplementary Videos
   (a) Single cell microscopy images form HLE cells with transiently transfected RelA-RFP
   (b) PDE simulations of the complete NκB model
3. Supplementary Scripts
   (a) Cell-Profiler script to analyze microscopy images
   (b) R script to analyze Cell-Profiler results